

**DESIGN RESTORATION METHOD FOR EXISTING
REINFORCED CONCRETE SLAB BRIDGES**

ABRHAM GEBRE TAREKEGN

September, 2013

**DESIGN RESTORATION METHOD FOR EXISTING
REINFORCED CONCRETE SLAB BRIDGES**

(既設 RC スラブ橋の復元設計法)

by

ABRRHAM GEBRE TAREKEGN

A Dissertation
Submitted to
The Department of Civil Engineering
Yokohama National University

In Partial Fulfillment of the Requirements
for the Degree of
Doctor of Philosophy

Graduate School of Engineering
Yokohama National University
Yokohama, Japan
September, 2013

This dissertation is dedicated to:

My beloved Family

and

Alula Demoz

**DESIGN RESTORATION METHOD FOR EXISTING
REINFORCED CONCRETE SLAB BRIDGES**

ACKNOWLEDGEMENTS

Thanks to the Almighty God and St. Mary for each and every success in my life and for their endless blessings. They have endowed me courage and strength as well as precious health throughout my life.

My deepest gratitude goes to my research advisor Prof. Tatsuya TSUBAKI for his professional, genuine guidance and valuable advice to accomplish the dissertation on time. It is a privilege to work with him. I am grateful to thank Prof. Yamada, Prof. Katsuchi, Associate Prof. Akira HOSODA and Associate Prof. Nishio for their guidance and support in reviewing this research work. I wish to thank the former Research Associate, Dr. Kazuhiko HAYASHI and to my friends in the Concrete Laboratory for their support.

I would like to extend my special appreciation to my beloved family for their encouragement and being with me in all ups and downs. They have been in my side in every aspect. Had it not been your genuine co-operation, it would have not been possible to conduct this research. Special thanks to my father, Gebre Tarekegn, and my mother, Legesech W/Gebriel, for their deepest concern and for all their help and support they have provided me to realize my dream. Really, they sacrificed a lot.

I also extend my acknowledgement to the Ministry of Education, Culture, Sports, Science and Technology of Japan (Monbukagakusho) for the financial grant to conduct this research.

I would like to express my profound heartfelt thanks to my relatives, friends and to those people who have collaborated with me.

ABSTRACT

Bridges constructed several decades ago have been deteriorated due to many reasons and hence their capacity is reduced. Capacity performance assessment is one of the major tasks to be performed in bridge management and should be exercised with care. Original design documents, drawings and plans are important to perform such an activity. In cases of older bridges, assessing as much design information as possible is difficult. In the absence of these data, assessing bridge's performance will be a common problem bridge engineers face.

For bridges where necessary details, such as reinforcement in the concrete bridge, are not available, design restoration should be performed. Design restoration is a process of accurately describing the initial condition (design values) of a structure from its current condition (actual values). On the other hand, if deflection is used as additional data, it reflects the present actual values.

A literature review on distributions of Ethiopian bridges shows that reinforced concrete bridges are dominant, which comprises 84% of the country's bridge and they are in various state of deterioration. Almost 46% of the bridges are found in fair and bad conditions, about 44% of them are constructed before 40-110 years ago and considerable numbers of bridges were constructed in the years 1935-1945, by Italians. For restoration of initial conditions of bridges constructed in the specified period of time, detailed study on the Italian and AASHTO LRFD Bridge Design Specifications were carried out.

For capacity assessment of RC bridges, classification and identification of damages are of great importance. Wide variety of failures is due to old bridge failures and design deficiency leading to bridge collapse. The literature survey also shows that the principal causes of the major defects of RC bridges in Ethiopia are excessive loading, poor design and aging.

Concrete testing with a test hammer and from core test and detection of position of reinforcing bars using a magnetic device are the most frequently used non-destructive testing methods. For multi-layer reinforcement arrangement, however, if the gap between the reinforcement layers is small, only the first layer of the reinforcement can be detected

using the radar method.

In this study, a design restoration method for RC slab bridges is proposed. In the method, the unknown parameters are computed using a nonlinear deflection equation. Moreover, using this method, reinforcing area and position of any layer can be estimated. In the computation, variations in the neutral axis depth profile and the moment of inertia expression with parabolic functions are assumed. In line with this, new closed-form explicit equations for the computation of slope and deflection of RC beams by considering variation in neutral axis depth profile are proposed.

For the probabilistic design restoration, a Latin Hypercube Sampling (LHS) of random variables and experimental investigations under a control of achieved concrete cover thickness and dimensions for RC slab bridges is presented to take into account the statistical variations in the design parameters and to obtain the mean values and the confidence limits for mean of the restored design data. This LHS method is used to improve the computational efficiency in the estimation of actual values. The confidence interval to the mean tells us the accuracy (reliability) of the design restoration.

With the present method, the current values can be obtained using the dimensional data and the deflections by load test only. In considering the statistical variations, the allowable limits of dimensional measurements by AASHTO Bridge Construction Specification are considered.

A standard RC slab bridge is designed as per AASHTO LRFD Bridge Design Specification and simulated using FEM. In the simulation, the mesh consists of rectangular elements of 0.05m in size with 4 nodes and SBETA material model is used. The FEM simulation helps to predict deflection of bridges. For the derivation of empirical formula for the estimation of yield strength of steel by considering the effects of material constants and dimensional data is considered. Based on the FEM simulation results, current and initial conditions are restored. The design restoration results of the present method give better accuracy than the conventional method.

The verification of the present method is shown using the experimental data. Test specimens of RC slab and beam are used to verify analytical results. For these test specimens, the coefficients of variations for dimensions obtained from experimental

investigation are used. In addition, the result which is obtained from FEM simulation is verified by using the proposed method.

Uncertainty and sensitivity analysis of random variables affecting the design restoration are performed. Cross-sectional area of steel bar and cover thickness are the most influencing factors in the estimation process.

Based on the current results obtained, the initial condition of bridges; material strengths, dimensions, cross-sectional area of steel bar and position of reinforcing bars are estimated. The performance rating of RC bridge is performed and the probabilistic distributions of the rating factors for inventory loadings and posting analysis based on the current values are shown.

The present design restoration scheme proposed for RC slab bridges can be extended for RC T-girder bridges, arch bridges and composite structures. By using sufficiently accurate displacement transducers, the present design restoration method can also be applicable to restore RC sections with multi-layer reinforcement arrangement.

TABLE OF CONTENTS

ACKNOWLEDGEMENTS	i
ABSTRACT	ii
LIST OF FIGURES	x
LIST OF TABLES	xv
NOMENCLATURE.....	xvii
1. INTRODUCTION.....	1
1.1 Background	1
1.2 Objectives	4
1.3 Methodology	4
1.4 Outline of the Dissertation	5
1.5 Application of Results	7
1.6 Summary	7
References	7
2. LITERATURE SURVEY.....	9
2.1 Introduction	9
2.2 Bridge Management	10
2.3 Types and Classification of Bridges	11
2.3.1 Structural Types of Bridges.....	11
2.3.2 Classification of Bridges.....	12
2.3.2.1 Slab Bridges	12
2.3.2.2 Girder Bridges.....	14
2.3.3 Bridge Span Survey	15
2.4 Bridge Design Specifications	16
2.4.1 Italian Bridge Design Specification	17
2.4.2 AASHTO LRFD Bridge Design Specification	17
2.5 Design Restoration for Reinforced Concrete Bridges	17
2.5.1 Bridges without Design Drawings	19
2.5.2 Bridges with Unknown Structural Components	19
2.6 Assessment and Evaluation	20
2.7 Types of Defects of RC Bridges	21

2.8 Testing Methods	23
2.8.1 Visual Inspection.....	23
2.8.2 Load Testing.....	23
2.8.2.1 Supplementary Load Tests	24
2.8.2.2 Proving Load Testing	24
2.9 Summary	25
References	25
3. DESIGN RESTORATION FOR RC SLAB BRIDGES.....	27
3.1 Introduction	27
3.2 Design Restoration	28
3.2.1 Method of Design Restoration	28
3.2.2 Deterministic Design Restoration	30
3.2.3 Probabilistic Design Restoration.....	30
3.2.4 Computation of Moment of Inertia at a Section	32
3.3 Estimation of Actual Yield Strength of Steel	37
3.3.1 Single-Layer Reinforcement Arrangement	38
3.3.2 Multi-Layer Reinforcement Arrangement	42
3.4 Sensitivity Analysis	44
3.5 Probabilistic Analysis	45
3.6 Summary	47
References	47
4. NUMERICAL MODELING AND EXPERIMENTAL INVESTIGATIONS.....	49
4.1 Introduction	49
4.2 Constitutive Model	50
4.2.1 Material Model of Concrete.....	50
4.2.2 Stress-Strain Relationships for Concrete	50
4.2.3 Material Stiffness Matrices	51
4.2.4 Material Model of Steel	51
4.2.5 Bond Model of Steel and Concrete.....	51
4.2.6 Material Stiffness of Composite Material	51
4.3 FEM Simulation of RC Slab Bridges.....	52
4.4 Experimental Investigations	57

4.4.1 Distribution of Dimensions and Cover Thickness	57
4.4.2 Load Test of RC Slab Specimen	60
4.4.3 Load Test of RC Beam Specimen-1	62
4.4.4 Load Test of RC Beam Specimen-2	63
4.5 Summary	65
References	65
5. ESTIMATION OF CURRENT VALUES, RESTORING INITIAL VALUES AND VERIFICATION OF PROPOSED METHOD	67
5.1 Introduction	67
5.2 Estimation of Current Values.....	68
5.2.1 Bridges with Two Unknowns (Case 1 and 2)	68
5.2.2 Bridges with Three Unknowns (Case 3)	72
5.3 Restoring Initial Design Values	79
5.3.1 Material Strengths	79
5.3.2 Bridge Dimensions.....	80
5.3.3 Cross-sectional Area of Steel	81
5.3.4 Effective Depth	81
5.4 Verification of Proposed Method.....	83
5.4.1 Design Restoration for Test Specimens	83
5.4.1.1 RC Slab Specimen	83
5.4.1.2 RC Beam Specimen-1	87
5.4.1.3 RC Beam Specimen-2.....	91
5.4.2 Design Restoration for Numerical Model.....	93
5.5 Summary	93
References	94
6. PERFORMANCE ASSESSMENT OF BRIDGES.....	95
6.1 Introduction	95
6.2 Bridge Load Rating	96
6.2.1 Live Load Rating	96
6.2.2 Sufficiency Rating	97
6.2.3 Rating Aspects for Existing Bridges	97
6.2.4 Legal Rating Loads	97

6.3 Rating Method	98
6.4 Posting Analysis	99
6.5 Probabilistic Performance Analysis of RC Bridges	100
6.6 Summary	101
References	102
7. CONCLUSIONS AND RECOMMENDATIONS.....	103
7. 1 Conclusions	103
7. 2 Recommendations	104
APPENDIX A – CONVENTIONAL NON-DESTRUCTIVE MEASUREMENT TECHNIQUES	105
A.1 Introduction	105
A.2 Summary of Non-Destructive Tests’ Accuracy	106
References	110
APPENDIX B - ITALIAN BRIDGE DESIGN STANDARDS	111
B.1 Introduction.....	111
B.2 Live Loads	112
B.3 Positive Permanent Loads.....	116
B.4 Horizontal External Forces	116
B.5 Summary.....	117
References	117
APPENDIX C - INFLUENCE FUNCTION FOR DEFLECTION OF RC BEAMS CONSIDERING VARIATION IN NEUTRAL AXIS DEPTH PROFILE.....	118
C.1 Introduction.....	118
C.2 Computation of Neutral Axis Depth and Effective Moment of Inertia	120
C.2.1 Neutral Axis Profile for New Structures	120
C.2.2 Neutral Axis Depth Profile for Old Structures	124
C.3 Moment Distributions for Various Boundary Conditions.....	125
C.4 Slope and Deflection Calculations.....	126
C.5 Summary.....	131
References	132

APPENDIX D – THREE-DIMENSIONAL INFLUENCE FUNCTION FOR DEFLECTION OF RC SLABS	133
D.1 Introduction	133
D.2 Influence of 3D Deflections of RC Slabs	135
D.3 Three-Dimensional FEM Simulation	136
D.4 Analysis of Results	139
D.5 Summary.....	139
References	139
APPENDIX E – SUMMARY OF TEST RESULTS OF RC BEAM SPECIMEN - 2	140
E.1 Introduction.....	140
E.2 Loading Pattern.....	142
E.3 Load below Cracking Load.....	142
E.4 Load above Cracking Load.....	147
E.5 Crack Pattern.....	156
E.6 Summary	156
APPENDIX F – DESIGN RESTORATION FLOW FOR PRACTICAL APPLICATION	157

LIST OF FIGURES

Fig. 1.1 Research framework	5
Fig. 2.1 Critical stages in the life of a bridge.....	10
Fig. 2.2 Bridge management cycle	11
Fig. 2.3 Typical cross section of a standard RC slab bridge	13
Fig. 2.4 RC slab bridge	14
Fig. 2.5 Typical cross section of a standard RC T-girder bridge.....	14
Fig. 2.6 RC T-girder bridge.....	15
Fig. 2.7 Distribution of bridges by material type.....	15
Fig. 2.8 Distribution of bridges by year of construction.....	16
Fig. 2.9 Distribution of bridges by span length	16
Fig. 2.10 Design vehicular loads: (a) truck and (b) tandem.....	17
Fig. 2.11 Flow of design restoration for PC bridges.....	18
Fig. 3.1 Flow of design restoration of RC slab bridges	29
Fig. 3.2 Input and output in design restoration	30
Fig. 3.3 Flow of estimating d^a , A_s^a and $f_c'^a$	31
Fig. 3.4 Distribution of objective function.....	32
Fig. 3.5 Variation of neutral axis depth of new RC beam.....	32
Fig. 3.6 Concept of variation in neutral axis profile at different loading conditions.....	34
Fig. 3.7 Temperature - elastic modulus relationship of asphalt concrete.....	36
Fig. 3.8 RC section and strain diagram.....	38
Fig. 3.9 RC T-section and strain diagram	41
Fig. 3.10 Multi-layer reinforcement arrangement.....	42
Fig. 3.11 Arrangement of sampling intervals and sampling of random variables	46
Fig. 4.1 Material model of concrete.....	50
Fig. 4.2 Material model of steel	51
Fig. 4.3 Material data for concrete.....	53
Fig. 4.4 Material data for reinforcement.....	53
Fig. 4.5 Geometrical modeling of mesh.....	53
Fig. 4.6 FEM model of RC slab bridge.....	54
Fig. 4.7 Detail of FEM mesh and reinforcing bar.....	54
Fig. 4.8 Position of reinforcing bar	55

Fig. 4.9 Load- mid span deflection curves of mean values	56
Fig. 4.10 Cross section of RC beam	57
Fig. 4.11 Effective depth distribution	58
Fig. 4.12 Top width distribution.....	58
Fig. 4.13 Distribution of beam depth	59
Fig. 4.14 Probability distribution of achieved cover thicknesses of main bars	59
Fig. 4.15 Probability distribution of achieved beam widths (top width)	60
Fig. 4.16 Probability distribution of achieved beam depth.....	60
Fig. 4.17 Longitudinal section of specimen.....	61
Fig. 4.18 Load-mid span deflection diagram.....	61
Fig. 4.19 Load-mid span deflection diagram.....	63
Fig. 4.20 Longitudinal section of RC test beam 2	64
Fig. 4.21 Cross section of RC test beam 2.....	64
Fig. 4.22 Load- mid span deflection diagram (top surface).....	65
Fig. 4.23 Crack pattern at the end of loading of 300kN	65
Fig. 5.1 Design restoration scheme.....	68
Fig. 5.2 Probabilistic distribution of A_s^a (Case 1 and 2).....	70
Fig. 5.3 Probabilistic distribution of f_y^a (Case 1 and 2).....	71
Fig. 5.4 Distribution of cover thickness (Case 1 and 2).....	72
Fig. 5.5 Probabilistic distribution of f_c^a (Case 3).....	74
Fig. 5.6 Probabilistic distribution of A_s^a (Case 3).....	74
Fig. 5.7 Probabilistic distribution of d^a (Case 3).....	75
Fig. 5.8 Probabilistic distribution of f_y^a (Case 3).....	75
Fig. 5.9 Compressive strength development curve of concrete.....	80
Fig. 5.10 Probabilistic distribution of A_s (Case 3)	82
Fig. 5.11 Distribution of initial effective depth, d (Case 3)	82
Fig. 5.12 Distribution of moment	83
Fig. 5.13 Longitudinal section of specimen.....	84
Fig. 5.14 Load- mid span deflection diagram.....	84
Fig. 5.15 Probabilistic distribution of A_s^a and A_{s2}^a	85
Fig. 5.16 Probabilistic distribution of f_c^a	85
Fig. 5.17 Probabilistic distribution of d^a	86

Fig. 5.18 Probabilistic distribution of f_y^a	86
Fig. 5.19 Cross section of RC test beam.....	88
Fig. 5.20 Load- mid span deflection diagram	88
Fig. 5.21 Probabilistic distribution of A_s^a and A_{s2}^a	89
Fig. 5.22 Probabilistic distribution of f_c^a	89
Fig. 5.23 Probabilistic distribution of d^a	90
Fig. 5.24 Probabilistic distribution of f_y^a	90
Fig. 5.25 Load- mid span deflection diagram (top surface).....	92
Fig. 6.1 Distribution of inventory rating factor.....	100
Fig. 6.2 Distribution of rating factor for load posting.....	101
Fig. A.1 Concrete test hammer	105
Fig. A.2 Rebar detection device	106
Fig. B.1 Truck weighing 12tons.....	112
Fig. B.2 18tons steam roller.....	113
Fig. B.3 Vehicles weighing up to 40tons	113
Fig. B.4 Design tandem load.....	114
Fig. B.5 Undefined column of trucks weighing 12tons.....	114
Fig. B.6 Towing tractor and two trailers	114
Fig. B.7 Towing consists of a roller of 18 tons and UDL.....	115
Fig. B.8 Towing consists of two rollers and UDL	115
Fig. B.9 Uniformly distributed load of 400kgf/m.....	115
Fig. B.10 Roller weighing 17.5tons.....	115
Fig. B.11 Maximum bending moments	117
Fig. C.1 Variation of neutral axis depth of new RC beam	120
Fig. C.2 Concept of variation in neutral axis depth profile	122
Fig. C.3 Neutral axis depth envelope.....	124
Fig. C.4 Variation of neutral axis depth of existing RC beam	125
Fig. C.5 Influence Line for Bending Moment at C.....	126
Fig. D.1 Plan view and NA depth profiles	134
Fig. D.2 Plan view and deflection curves	135
Fig. D.3 3D FEM model of RC slab bridge.....	136
Fig. D.4 Loading grids.....	136
Fig. D.5 Deflection diagram with load applied at y=0 line	137

Fig. D.6 Deflection diagram with load applied at $y=0$ line	137
Fig. D.7 Deflection diagram with load applied at $y=1.0$ line	138
Fig. D.8 Deflection diagram with load applied at $y=2.5$ line	138
Fig. E.1 Longitudinal section of RC test beam 2.....	140
Fig. E.2 Cross section of RC test beam 2	141
Fig. E.3 Locations of LVDTs	141
Fig. E.4 Locations of strain gauges.....	141
Fig. E.5 Load deflection diagram of Position-1 (bottom surface)	142
Fig. E.6 Deflection diagrams (at pts. 2, 64 and 67)	143
Fig. E.7 Stain distribution (Position-1).....	143
Fig. E.8 Load deflection diagram of Position-2 (bottom surface)	144
Fig. E.9 Deflection diagrams (at pts. 2, 64 and 67)	144
Fig. E.10 Stain distribution (Position-2).....	145
Fig. E.11 Load deflection diagram of Position-3 (bottom surface)	145
Fig. E.12 Deflection diagrams (at pts. 2, 64 and 67)	146
Fig. E.13 Stain distribution (Position-3).....	146
Fig. E.14 Load deflection diagram of pt. 1 (top surface).....	147
Fig. E.15 Load deflection diagram of pt. 5 (bottom surface)	147
Fig. E.16 Mid span deflection diagram (Position-3).....	148
Fig. E.17 Deflection diagrams (at pts. 2, 64 and 67)	148
Fig. E.18 Stain distribution at $P=300\text{kN}$ (Position-3).....	149
Fig. E.19 Mid span deflection diagram (Position-2).....	149
Fig. E.20 Deflection diagrams (at pts. 2, 64 and 67)	150
Fig. E.21 Stain distribution at $P=300\text{kN}$ (Position-2).....	150
Fig. E.22 Mid span deflection diagram (Position-1).....	151
Fig. E.23 Deflection diagrams (at pts. 2, 64 and 67)	151
Fig. E.24 Stain distribution at $P=300\text{kN}$ (Position-1).....	152
Fig. E.25 Mid span deflection diagram (Position-2).....	152
Fig. E.26 Deflection diagram (at pts. 2, 64 and 67).....	153
Fig. E.27 Stain distribution at $P=300\text{kN}$ (Position-2).....	153
Fig. E.28 Mid span deflection diagram (Position-3).....	154
Fig. E.29 Deflection diagram (at pts. 2, 64 and 67).....	154
Fig. E.30 Stain distribution at $P=300\text{kN}$ (Position-3).....	155
Fig. E.31 Load- mid span deflection diagram (top surface)	155

Fig. E.32 Crack pattern at the end of loading of 300kN	156
Fig. E.33 Total surface crack width	156
Fig. F.1 Design restoration flow for practical application	158

LIST OF TABLES

Table 1.1 Comparison of conventional and present method.....	3
Table 2.1 Major defects of bridges	22
Table 4.1 Parameters of constitutive model of concrete	52
Table 4.2 Input variables	54
Table 4.3 Tolerances on effective depth and cover thickness	55
Table 4.4 Two cases of FEM simulation.....	56
Table 4.5 Achieved measurements of dimensions	58
Table 4.6 Experimental data of RC slab specimen	61
Table 4.7 Experimental data of RC beam specimen	62
Table 4.8 Loading positions of RC beam test specimen.....	64
Table 5.1 Statistical parameters of random variables (Case 1 and 2)	68
Table 5.2 Sampling of random variables (Case 1 and 2).....	69
Table 5.3 Results of statistical analysis (Case 1 and 2)	70
Table 5.4 Confidence intervals for f_y^a and A_s^a (Case 1 and 2)	71
Table 5.5 Statistical parameter of random variables (Case 3)	72
Table 5.6 Sampling of random variables (Case 3).....	73
Table 5.7 Confidence intervals of variables (Case 3)	76
Table 5.8 Comparison of results (Case 3).....	76
Table 5.9 Summary of tolerances.....	77
Table 5.10 Summary of design restoration results.....	77
Table 5.11 Uncertainty analysis of random variables	78
Table 5.12 Rank correlation coefficient r_p	78
Table 5.13 Discrete nominal yield strength, f_y	79
Table 5.14 Steel properties in JSCE Standard Specifications.....	80
Table 5.15 Confidence intervals of variables of RC slab test specimen.....	87
Table 5.16 Estimation of design data of RC slab specimen.....	87
Table 5.17 Confidence intervals of variables of RC beam test specimen.....	91
Table 5.18 Estimation of design data of RC beam test specimen	91
Table 5.19 Output of results and confidence intervals of RC beam specimen-2.....	92
Table 5.20 Estimation of design data of RC slab specimen (Case 1 and 2).....	93
Table 5.21 Estimation of design data of RC beam specimen (Case 3)	93

Table 6.1 Reinforcing steel yield stresses	99
Table A.1 Non-destructive tests' accuracy for cross-sectional shape of main girder	107
Table A.2 Non-destructive tests' accuracy for investigation of PC tendons and shear reinforcement	109
Table C.1 Variations in neutral axis depth and moment of inertia of different types of beams	128
Table C.2 Values of M_a , M_s and M_b (moment ordinates) for different types of beams....	129
Table C.3 Values of c_1 , c_2 , c_3 and c_4 for different types of beams	129
Table D.1 Summary of design restoration results	139
Table E.1 Loading positions of RC beam test specimen	142

NOMENCLATURE

Abbreviation

AASHTO	American Association of State Highway and Transportation Officials
COV	Coefficient of Variation
ERA	Ethiopian Roads Association
FEM	Finite Element Method
JIS	Japan Industrial Standards
JSCE	Japan Society of Civil Engineers
LHS	Latin Hypercube Sampling
LRFD	Load Resistance Factor Design
NA	Neutral Axis depth
NDT	Non Destructive Test
PC	Prestressed Concrete
RC	Reinforced Concrete

Symbols

A_s	Cross-sectional area of steel per unit width
A_s^a	Actual area of tensile steel per unit width
A_{sli}^a	Actual area of tensile steel of layer i per unit width
A_{s2}^a	Actual area of compression steel per unit width
a_1	Empirical constant
b	Beam width
b^a	Actual width
b_e^a	Actual effective width of flange
b_w^a	Actual web thickness
C_E	Coefficient used to compute E_c^a
COV_i	Coefficient of variation for random variable i
c_1, c_2, c_3, c_4	Empirical constants for deflection
D	Total depth
D^a	Actual total depth
D_i	Effect of dead loads

DE_i	Deflection equation i
d	Initial effective depth
d^a	Actual effective depth
d_2^a	Actual position of compression steel, measured from top fiber
d_{11}^a	Actual effective depth corresponding to layer 1 from the bottom
d_{ii}^a	Actual effective depth corresponding to layer i
E	Live load strip width
E_l	Interior strip width for one lane loaded
E_m	Interior strip width for multiple lanes loaded
E_c^a	Actual Young's modulus of concrete
E_s^a	Actual Young's modulus of steel
F	Function with statistical variations
F_h	Horizontal force
\bar{F}	Mean of F_i
f_c'	Compressive strength of concrete
$f_c'^a$	Actual concrete strength
f_y	Yield strength of steel
f_y^a	Actual yield strength of steel
g_1	Bridges with wooden floor
g_2	Bridges with roadbed
I	Impact factor for the live-load effect
\bar{I}_{cr}	Modified moment of inertia of the cracked section
$I(x)$	Moment of inertia
I_{cr}	Moment of inertia of cracked section
I_{unc}	Moment of inertia of uncracked section
k	Number of live-loads
L	Length of beam
L_i	Nominal live-load effect of rating vehicle
M_{DL}	Dead load moment
M_{LL}	Live load moment
M_{Tr}	Live load moment due to truck load

M_{lm}	Live load moment due to truck load
M_{ln}	Moment due to lane load
M_a, M_b	Support moments
M_s	Span moment
M^a	Actual allowable flexural moment of section per unit width
M_c^a	Actual bending moment carried by concrete per unit width
M_s^a	Actual bending moment carried by tensile steel, A_s^a , per unit width
M_{si}^a	Actual bending moment carried by tensile steel of the i^{th} layer per unit width
M_{s2}^a	Actual bending moment carried by compression steel per unit width
m	Number of dead-load components
n	Ratio of E_s^a to E_c^a
P	Maximum pressure
P_i	Applied load
P_x	Average value of attack penetration
q	Weight of a row of wagons
R	Total roadway width
r	Number of reinforcement layers
r_p	Partial coefficient of correlation
RF	Rating factor
S	Modified span length
t_f^a	Actual thickness of top slab
$U_{x.F}$	Contributions of the uncertainty of random variable i
u	Residual deflection
V	Maximum allowable speed
W	Roadway width
w	Total crack width
x	Distance measured from left support of beam
\bar{x}_i	Mean of x_i
x_l	Location of load position, measured from left support of beam

x_i	Random variable i
\bar{y}	Neutral axis depth at section, measured from top fiber
y^a	Actual neutral axis depth, measured from top fiber
y_0	Neutral axis depth of cracked section
y_l	Neutral axis depth of uncracked section
\bar{y}_0	Modified neutral axis depth of cracked section, measured from top fiber

Greek Symbols

α_i	Sensitivity factor of random variable i
α_T	Coefficient of thermal expansion
β	Ratio of A_{s2}^a to A_s^a
γ_c	Unit weight of concrete
γ_{DL}, γ_{LL}	Factor of safety for dead and live loads
$\gamma_{Di}, \gamma_{Li}, \gamma_L$	Dead- and live load factors
δ	Decrease in steel bar diameter
$\delta_o, \delta_x, \delta_{xi}, \Delta_i$	Deflections
δ_{xT}	Deflection of a beam due to thermal effect
ϵ_c^a	Actual compressive strain in concrete
ϵ_s^a	Actual tensile strain in steel
ϵ_{s1}^a	Actual tensile strain in steel of layer 1 from the bottom
ϵ_{s2}^a	Actual tensile strain in steel
ϵ_{si}^a	Actual tensile strain in steel of layer i
η	Ratio of M_a to M_{cr}
μ	Mean value
θ_x	Slope of beam
σ	Standard deviation
σ_c^a	Actual compressive strain in concrete
σ_{s2}^a	Actual stress in compression steel
σ_{sa}^a	Actual allowable stress of steel

σ_{si}^a	Actual tensile stress of steel of layer i
ϕ_t	Residual diameter of reinforcing bar at time t
ϕ_0	Nominal diameter of reinforcing
ϕR_n	Nominal resistance
ΔT	Temperature gradient
Δx	Increment of each random variable

1. INTRODUCTION

1.1 Background

Bridges are constructed primarily to carry communication routes, such as railways, over an obstacle like road, river etc. In terms of railway and roadway infrastructure, bridges play a crucial role for the surface transport. From an economic point of view and general industrial development, bridges make the communication much easier and faster [1.1].

The most common approach to assess the safety of a bridge in bridge management is the determination of its load carrying capacity and it is an important task that needs more attention and to be exercised with care. In case the bridges damaged, their loading capacities can be reduced and it requires considerable amount of time and money to reconstruct.

The problems of aging and rapid deterioration of bridges lead to decrease in the capacity of the structural member [1.2]. Moreover, overloading of bridges is one of worldwide problems most countries are facing to maintain a fully functioning transportation system. In order to inform the public of load limits and to develop freight

policies and truck routes, capacity performance of the bridge should be done [1.3].

To assess condition of bridges, original design documents, drawings and plans are important. In the absence of these data, assessing bridge's performance will be a common problem. In case of difficulties to get design information about the bridges, design restoration should be performed. Design restoration is a method of estimating initial condition of structures and it is affected by current measurements. Since measurements are inexact and contain errors of unknown magnitude, their effects on the design restoration have to be investigated [1.4].

Concrete testing with a test hammer is the most frequently used method worldwide for non-destructive testing of concrete and structural components [1.5]. Moreover, determination of compressive strength of concrete from core test is commonly used. Position of reinforcing bars can be detected by using a magnetic device [1.6]. For multi-layer reinforcement arrangement, if the gap between the reinforcement layers is small, only the first layer of the reinforcement can be detected using radar method.

Experience of applying design restoration for PC structures is reported [1.7]. The report provides detailed information on design restoration of PC bridges and different conventional non-destructive measurement techniques. A Summary of conventional non-destructive measurement techniques is attached in **APPENDIX A**.

A design restoration of RC slab bridges mainly from measurements and observations is the scope of this research. In this study, compressive strength of concrete, position of reinforcing bars and cross-sectional area of reinforcing bars are estimated from measurements and dimensions by using load test only (deflections as primary input). Using this method, area of reinforcing bar and position of any layer can be estimated. The method can also be practically used in cases where measuring devices are not available. Moreover, bond degradation between concrete and steel bar is reflected in excessive deflection and the reduced cross-sectional area of steel bars can be easily obtained from this method. Comparison of design restoration using the conventional and the present method is shown in **Table 1.1**.

Table 1.1 Comparison of conventional and present method

Conventional Method	Present Method
<ul style="list-style-type: none"> • Applicable and effective for reinforcement positions up to 450mm, if radar method is used [1.8]. • For multi-layer reinforcement arrangement, if the gap between the reinforcement layers is small, only the first layer of the reinforcement can be detected. • Accuracy: for bar position is 10mm (radar method), for concrete cover is 5mm (radar method), for bar diameter is 1-2mm (electro-magnetic induction method) and for compressive strength of concrete $\pm 10\%$. 	<ul style="list-style-type: none"> • Uses only outside data (mainly measurements of dimensions and deflection) • Any position of rebar can be estimated. • By using sufficiently accurate displacement transducers, the method can be applicable for RC sections with multi-layer reinforcement arrangement. • It can be used in cases where measuring devices are not available. • Better accuracy than the conventional method.

The design mean values and the confidence interval of a mean are obtained using probabilistic analysis. These confidence intervals are important to know how closely the estimated values to the actual ones and they tell us how good the estimated values are. Moreover, the confidence limits give a certain range of information to search an optimal result.

As the confidence interval of a mean value gets smaller and smaller, the more precise the restored value be [1.9]. This gives the reliability of the design restoration results. The initial design values are obtained using empirical relationships.

The current condition of the bridges may be estimated from load test and the initial condition can be estimated using a design restoration scheme. In the process of design restoration, the statistical variations of the design parameters influence the restored data. Since no study has been found on design restoration of RC bridges to take into account

the scatter in the design parameters, in this study, a new probabilistic design restoration and an alternative method of estimating initial conditions of existing RC bridges are presented.

The probabilistic distribution and the influence of random variables on the statistical variation of the estimated design restoration results are investigated. Moreover, based on the statistical variation of random variables, sensitivity analysis in the vicinity of mean values is conducted. As verification, experimental results of RC test specimens and simulation of RC slab bridges with FEM were carried out. Finally, the capacity of the bridge is rated based on the current restored data.

1.2 Objectives

The objective of this dissertation is to propose a complete methodology for design restoration and evaluation of load capacity of reinforced concrete highway and road bridges. Thus, the objectives are:

1. to establish a design restoration flow and scheme for the capacity performance assessment of existing RC slab bridges
2. to develop a rational analytical system for design restoration method of existing RC slab bridges to take into account the statistical variations in the design parameters and to obtain the mean values and the confidence limits
3. to verify the proposed method using experimental and FEM simulation results of RC beam specimens
4. to investigate the uncertainty and sensitivity of statistical random variables affecting the design restoration process
5. to analyze load capacity of RC bridge structures and recommend bridge load restrictions, if necessary

1.3 Methodology

Framework of the present research is shown in **Fig. 1.1**.

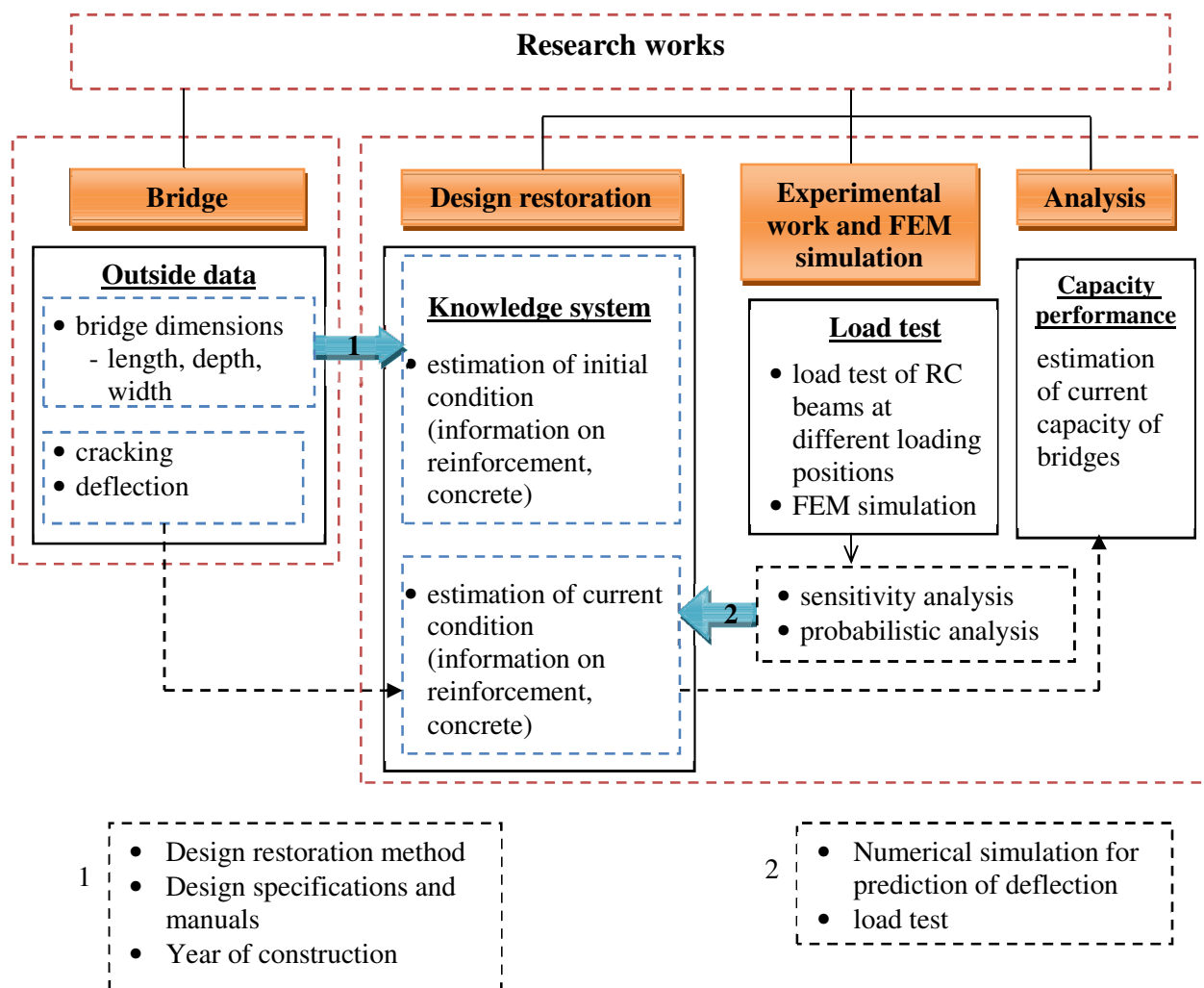


Fig. 1.1 Research framework

1.4 Outline of the Dissertation

The dissertation comprises of seven chapters. In chapter 1, general introduction, objectives and outline of the research are presented. Experience of applying design restoration for PC structures and conventional non-destructive measurement techniques are also discussed in this chapter.

Chapter 2 presents the literature survey made on types and classification of bridges, bridge management, types of defects of RC bridges and testing methods. The literature survey shows that major problems of bridges are aging, overloading and poor design. Inspection of the bridge is one of the most important tasks in the operation of a sound bridge management system and load testing of bridges can be of great benefit to know the

behavior of bridges. For capacity assessment of RC bridges, classification and identification of damages are of great importance. Wide variety of failures is due to old bridge failures and design deficiency leading to bridge collapse. The literature survey also shows that the principal causes of major defects of RC bridges in Ethiopia are excessive loading, poor design and aging. Bridge Design Specifications of Italy and AASHTO are reviewed in this chapter.

A new design restoration method for existing RC slab bridges based on the existing measurements of dimensions, observations and load test are presented under chapter 3. Flow of design restoration and a probabilistic design restoration scheme for reinforced concrete slab bridges are presented. Furthermore, empirical formula for the estimation of yield strength of steel by considering the effects of material constants and dimensional data, for single and multi-layer reinforcement arrangement, is obtained.

In chapter 4, numerical modeling of RC slab bridges using FEM simulation and results on experimental investigation of RC test specimens are discussed. FEM simulation of bridges for different cases is shown. Experimental investigation under the achieved dimensions and concrete cover of RC beam specimens has been performed. Load test on RC test specimens are conducted to restore the design values and to verify the proposed method.

A probabilistic design restoration of RC slab bridges by considering statistical variation of design parameters are performed in chapter 5. For sampling of random variables, a Latin Hypercube Sampling (LHS) method is used. Estimation of current values for six FEM simulation cases and for three test specimens are performed. From the results, mean values and confidence limits to the mean are obtained. Estimation of initial values and verification of the proposed method are also discussed in this chapter. Sensitivity and uncertainty analysis for the simulated bridges are performed. A comparison result of design restoration using the conventional and the present methods is presented in this chapter.

Chapter 6 presents a probabilistic load capacity assessment of RC bridge based on accepted standards and specifications. Performance evaluation of bridges is one of the most and important process in bridge management cycle and hence, using the design

restoration scheme, load rating of RC slab bridge is performed.

The last chapter includes conclusions drawn from this study and suggestions for further directions of investigation.

1.5 Application of Results

Once compressive strength of concrete, position of reinforcing bars and cross-sectional area of reinforcing bars are estimated from measurements and dimensions by using load test, the initial design values can be restored. Thus, the research helps to know the existing and initial conditions of RC slab bridges. From the estimated current condition, the capacity assessment of the bridge can easily be performed and it helps to manage and plan the most probable timing of damaged bridges to be replaced on time. It also helps for the life time prediction of bridges.

1.6 Summary

- General background about bridges and design restoration method are discussed.
- Comparison of design restoration technique using the conventional and the present methods is shown.
- Detailed objectives, methodology and outline of the research are presented.

References

- [1.1] Maciej M.: Evaluation of Load Capacity of Concrete Railway Slab Spans with Defects, Civil Engineering Department, University of Minho, Doctoral Thesis, 4800-058 Guimaraes, Portugal, Feb. 2008.
- [1.2] Mohiuddin A. Khan: Bridge and Highway Structure Rehabilitation and Repair, The McGraw-Hill Companies, Inc., 2010.
- [1.3] AASHTO: American Association of State Highway and Transportation Officials, Manual for Condition Evaluation of Bridges, Washington D.C, 20001, 1994.
- [1.4] Tarekegn, A.G. and Tsubaki, T.: Restoration Design for RC Slab Bridges by AASHTO LRFD, The 21st PC Symposium on Developments in Prestressed Concrete, JPCA, pp. 29-34, Oct. 2012.

- [1.5] Compressive Strength Measurement and Damage Assessment: Retrieved from <http://www.concretex-ray.com.au/strength-measurement?format=pdf>
- [1.6] Profometer: Rebar Detection System, Retrieved from http://www.proceq.com/fileadmin/documents/proceq/products/Concrete/Profometer_5_/English/Proceq_Brochure_Profometer_5__E.pdf
- [1.7] JPCEA, Report of the Technical Committee on Design Restoration of Prestressed Concrete, Japan Prestressed Concrete Engineering Association, March 2010.
- [1.8] SIR-EZ brochure, GSSI, Geophysical Survey Systems, Inc., 2012.
- [1.9] Confidence Interval for a Population Mean, Retrieved from <http://www.kean.edu/~fosborne/bstat/06amean.html>

2. LITERATURE SURVEY

2.1 Introduction

Design of bridge structure is a complex engineering problem which includes design of structural systems, selection of design manuals and standards. During design of bridges, an internationally accepted manuals and standards have to be referred. Most bridges in the world are constructed several decades ago and they have been deteriorated due to many reasons. The problem of aging, overloading and rapidly deteriorated bridges is an issue most countries are facing [2.1].

Maintenance of transportation facilities is a major industry. Transportation is an important requirement in people's daily lives. Both urban and rural areas are linked by highways and bridges. Global civilization is now dependent upon the use of automobiles and the public transport system. This giant industry maintains infrastructure for safe travel on roads, highways, and interstate highways [2.2].

In line with this, performance evaluation of bridges is one of the most and important process in bridge management cycle. Current bridge management systems rate them using various methodologies and approaches [2.3].

2.2 Bridge Management

Bridge management is the means by which a bridge stock is cared for from conception to the end of its useful life [2.4]. In practice, bridge management is necessary to coordinate and implement the tasks associated with the care of our bridges, such as:

- Collection of inventory data
- Regular inspection
- Assessment of condition and strength
- Repair, strengthening or replacement
- Prioritizing allocation of funds
- Safety

The six critical stages in the life of a bridge are shown in **Fig.2.1** [2.4].

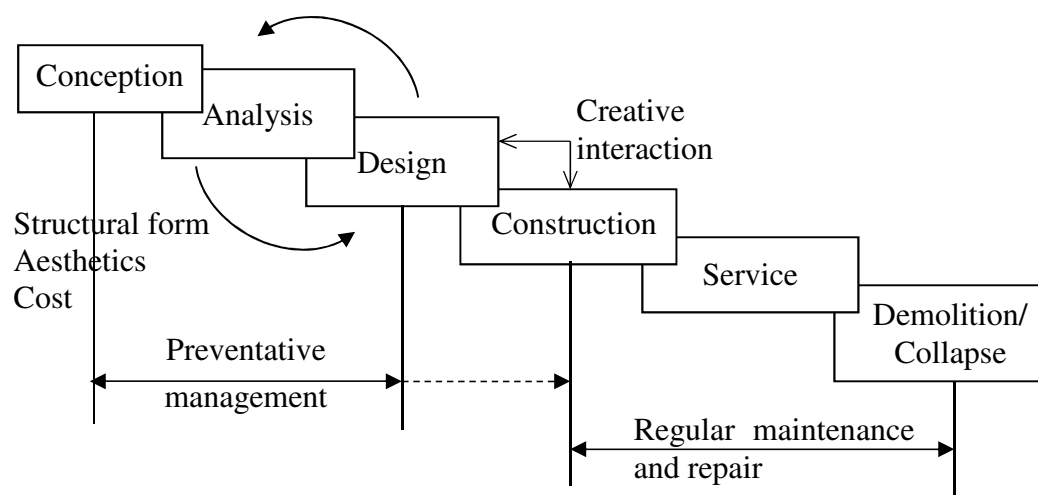


Fig. 2.1 Critical stages in the life of a bridge [2.4]

One of the most important tasks in the operation of a sound bridge management system is inspection of the bridge. It is ‘the keystone of our knowledge’ of the bridge. Apart from initial recording of the basic bridge data, regular reporting of a bridge’s condition provides a way of alerting bridge engineers to deterioration of the bridge from whatever cause, be it damage from vehicles; fracture, or material breakdown, and enables a bridge engineer to assess maintenance requirements. A great deal of experience and technical understanding is required in order to expedite an inspection in a methodical and systematic way [2.4]. Bridge management cycle is shown in **Fig. 2.2** [2.5].

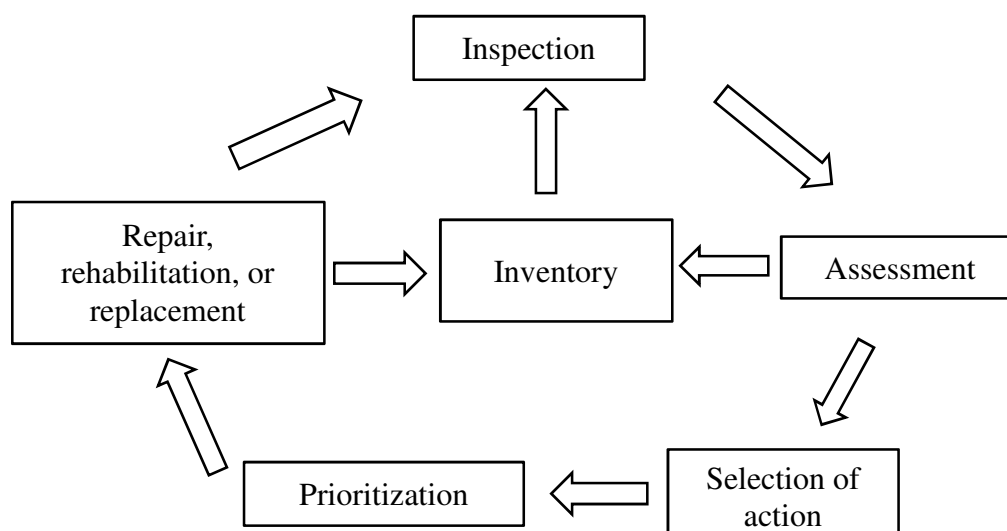


Fig. 2.2 Bridge management cycle [2.5]

The superstructure is subjected to greater wear and tear from traffic while the substructure is less affected. As a result, substructures are not replaced as often as superstructures. Hence, the life cycle costs and rehabilitation efforts are greater for the superstructure components. [2.2] Maintenance applies to:

- Existing concrete deck repairs
- Deck protective systems
- Deck drainage
- Bearings retrofit
- Concrete structure repairs
- Steel girders rehabilitation.

2.3 Types and Classification of Bridges

Some units of bridge construction are similar to those of building construction and serve similar purposes. These include footings, piers, caissons, walls, columns, beams, slabs, girders etc. However, the bridge designer has somewhat more freedom than the building designer in combining these units in the finished bridge structure.

2.3.1 Structural Types of Bridges

There are numerous types of bridges where for a particular site condition, more than

one type of bridge may be equally proposed on the basis of cost, time of construction or resource available. The type of bridge most suitable for a particular site can be selected after rough calculation results are estimated based on costs of construction and maintenance [2.6]. The types of bridges for general use fall under the following category.

- i. Simply supported bridges, suitable for short spans.
- ii. Balanced cantilever bridges, good for increased span and are mostly of reinforced concrete and/ or prestressed concrete construction.
- iii. Multiple but simple spans in series, used for medium or long span bridges.
- iv. Continuous beams: advantageous over simple spans for reduced weight, greater stiffness (smaller deflection), and less number of bearings. Continuous spans also provide redundancy and hence greater overload capacity than simple spans.
- v. Arch bridges: suitable for large spans.
- vi. Rigid frame bridges: horizontal deck slabs are made monolithic with vertical abutment walls and are economically suitable for moderate-medium span lengths.

2.3.2 Classification of Bridges

Bridges can be classified on the basis of the following characteristics [2.7].

1. Construction material as steel, concrete, timber or combination of any two or more.
2. Span length as short, medium or large.
3. Structural forms as slab, T-girder, box girder, arch, suspension etc.
4. Span type as single or multi-span.

Concrete can be used in many different ways and often many different configurations are feasible. However, market forces, projects and site conditions affect the relative economy of each option and this leads to selecting the different forms of bridge as slab, T or box girder, arch etc.

2.3.2.1 Slab Bridges

Single span slab bridges are perhaps the most common forms of bridges. It is indicated in design manual that they can be economical for spans from 6 m to 15 m.

However above 15 m they should preferably be ribbed [2.8]. Slab bridge has the following advantages [2.2]:

- Low construction height;
- Facility of supports' distribution;
- Simple formwork;
- Facility of reinforcement construction;
- Easy cementation, consolidation and curing of the fresh concrete;
- Elimination of the classical deck construction (slab, stringers and floor beams) and bracings;
- High rigidity (flexural and torsional) of the slab girder, which ensures good transmission of non-symmetrical as well as dynamic loads;
- Smooth bottom of the span surface allows much easier ventilation.

A typical cross section of a standard RC slab bridge [2.8] is shown in **Fig. 2.3**. A picture of slab bridge of multi spans are shown in **Fig. 2.4** [2.9].

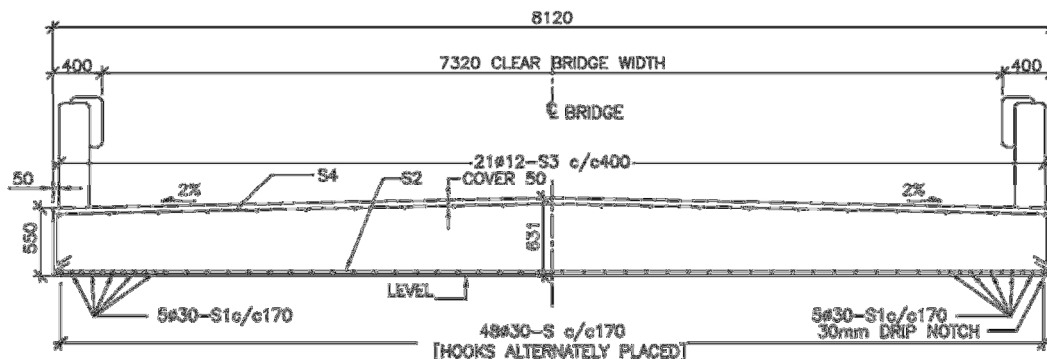


Fig. 2.3 Typical cross section of a standard RC slab bridge [2.8]



Fig. 2.4 RC slab bridge [2.9]

2.3.2.2 Girder Bridges

Girder bridges are usually used for single span bridges, or non-continuous girders in multi-span bridges, simple span in series. They shall be used for span lengths between 10 – 25 m [2.8], ranges from 10 – 20 m [2.7] and as of AASHTO LRFD Design Specification [2.9], T- girders are used for bridges spanning from about 10-25m. In accordance with the LRFD design method, materials used are minimized when the numbers of girders/beams are less in number [2.9]. A typical cross section of a standard RC T-girder bridge [2.8] and a picture of RC T-Girder bridge [2.9] are shown in **Fig. 2.5** and **Fig. 2.6** respectively.

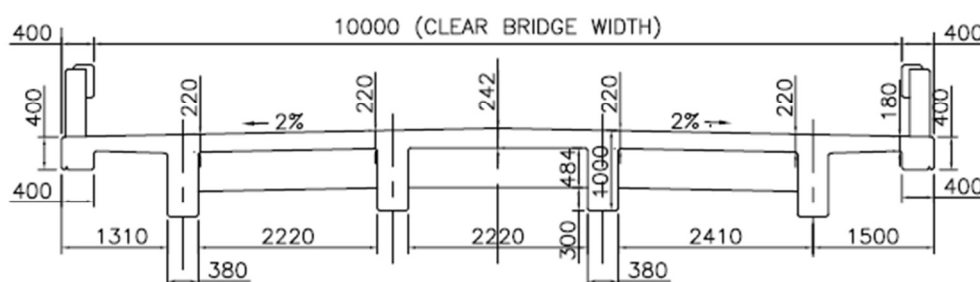


Fig. 2.5 Typical cross section of a standard RC T-girder bridge [2.8]



Fig. 2.6 RC T-girder bridge [2.9]

2.3.3 Bridge Span Survey

According to the results of the inspection and inventory of bridges data in Ethiopia [2.9], reinforced concrete bridges are dominant, which comprises 84% of the country's bridge and about 44% of them are constructed before 40-110 years ago. Almost 46% of the bridges are found in fair and bad conditions [2.10]. Based on the data [2.9], distributions of bridges by material type, year of construction and span-length are plotted and shown in **Figs. 2.7-2.9**.

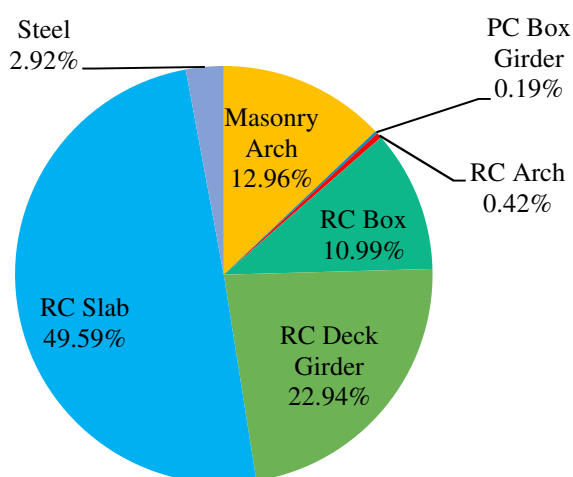


Fig. 2.7 Distribution of bridges by material type

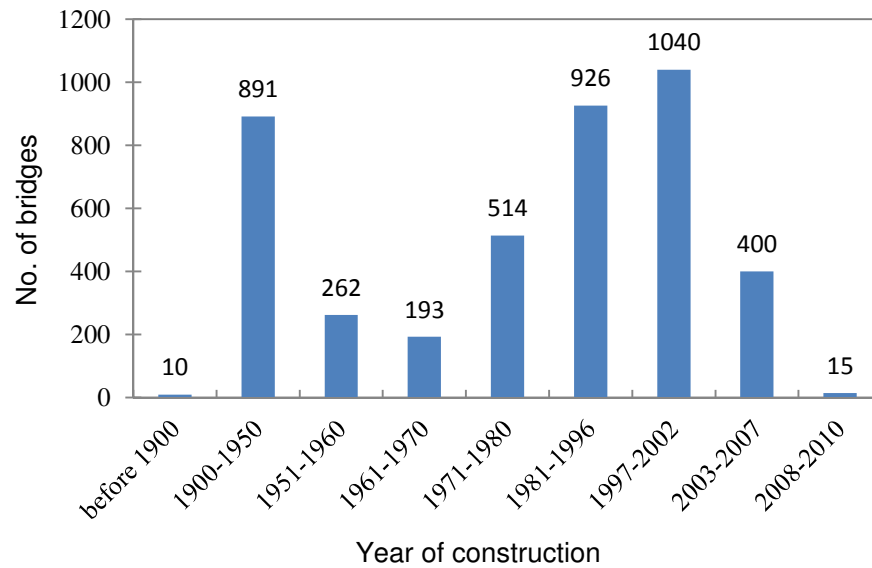


Fig. 2.8 Distribution of bridges by year of construction

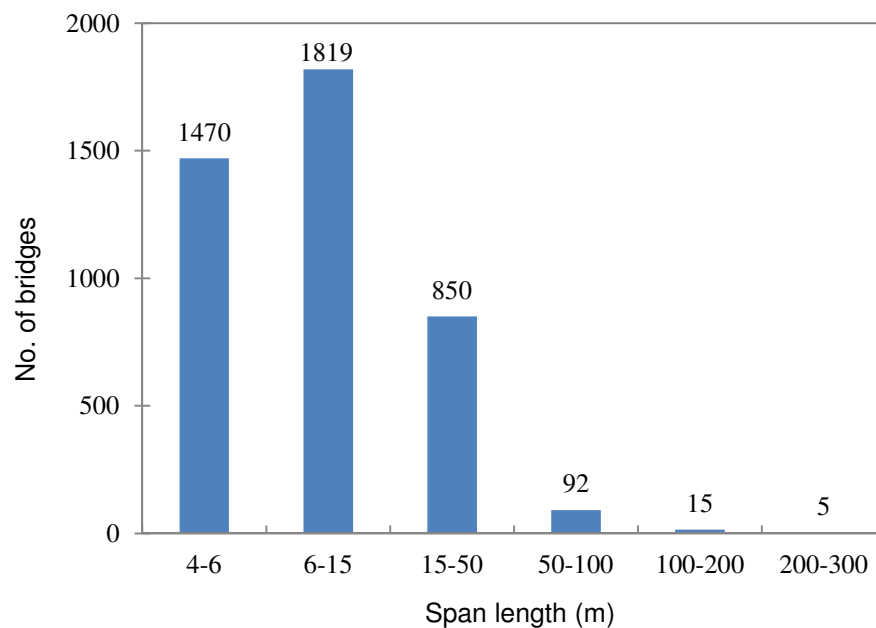


Fig. 2.9 Distribution of bridges by span length

2.4 Bridge Design Specifications

In Ethiopia, considerable numbers of bridges were constructed in the years 1935-1945. To assess performance of these bridges, it is difficult to obtain design data, plans and the kind of design manuals they used for the design of bridges as well. They might use their own standards. After that period, AASHTO LRFD Bridge Design Specification has been used.

2.4.1 Italian Bridge Design Specification

According to Italian Bridge Design Standards [2.11], roads are subdivided in relation to traffic as busy roads (Type-1), medium traffic (Type-2) and roads of small traffic (Type-3). The live loads to be taken in the calculation are discussed in **APPENDIX B**.

2.4.2 AASHTO LRFD Bridge Design Specification

Vehicular live loading on the roadways of bridges or incidental structures based on AASHTO LRFD bridge design specification, designated HL-93, and is used for the computation of live load force effects. It consists of a combination of the design truck or design tandem, and design lane load. A lane load of 9.3kN/m uniformly distributed in the longitudinal direction is used [2.12].

The equivalent live load width of longitudinal strips per lane for both shear and moment may be determined in accordance with AASHTO bridge design specifications. For the calculation of live load effects on the bridge, the concept of influence line is used and the maximum effect is selected for further analysis. To estimate the ultimate design moment, load factors of 1.25 for dead load, 1.75 for live loads and an impact factor of 1.33 are used. The design vehicular truck and tandem loads are shown in **Fig 2.10**.

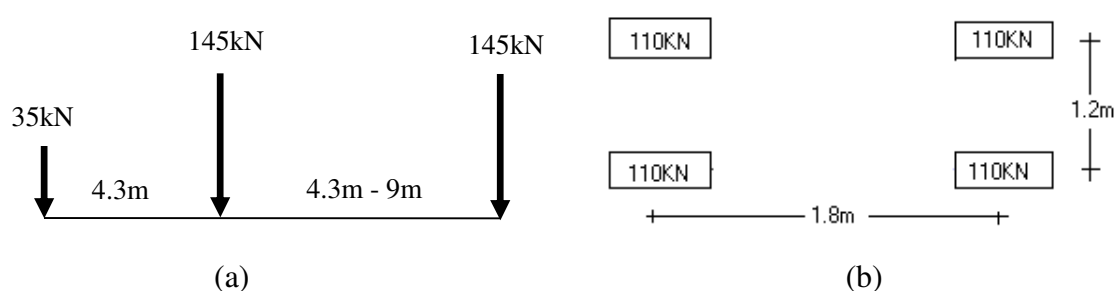


Fig. 2.10 Design vehicular loads: (a) truck and (b) tandem [2.12]

2.5 Design Restoration for Reinforced Concrete Bridges

Original design documents, drawings and plans are important for capacity performance assessment of bridges. In the absence of these data, assessing bridge's performance will be a common problem bridge engineers facing. In such cases, design

restoration should be performed and it is substantial. In line with this, initial and current conditions of bridges are of great importance. The current condition may be estimated from load test and the initial condition can be estimated using a design restoration scheme. Design restoration is a method of estimating initial condition of structures and it is affected by current measurements [2.1].

Experience of applying design restoration for PC structures is reported [2.13]. The report provides detailed information on design restoration of PC bridges and different conventional non-destructive measurement techniques. Flow of design restoration for a prestressed concrete bridge [2.14] is shown in **Fig. 2.11**. For steel structures, model validation and verification for structural analysis using FEM were carried out [2.15, 2.16]. Design restoration for RC slab bridges will be discussed in detail under Chapter 3.

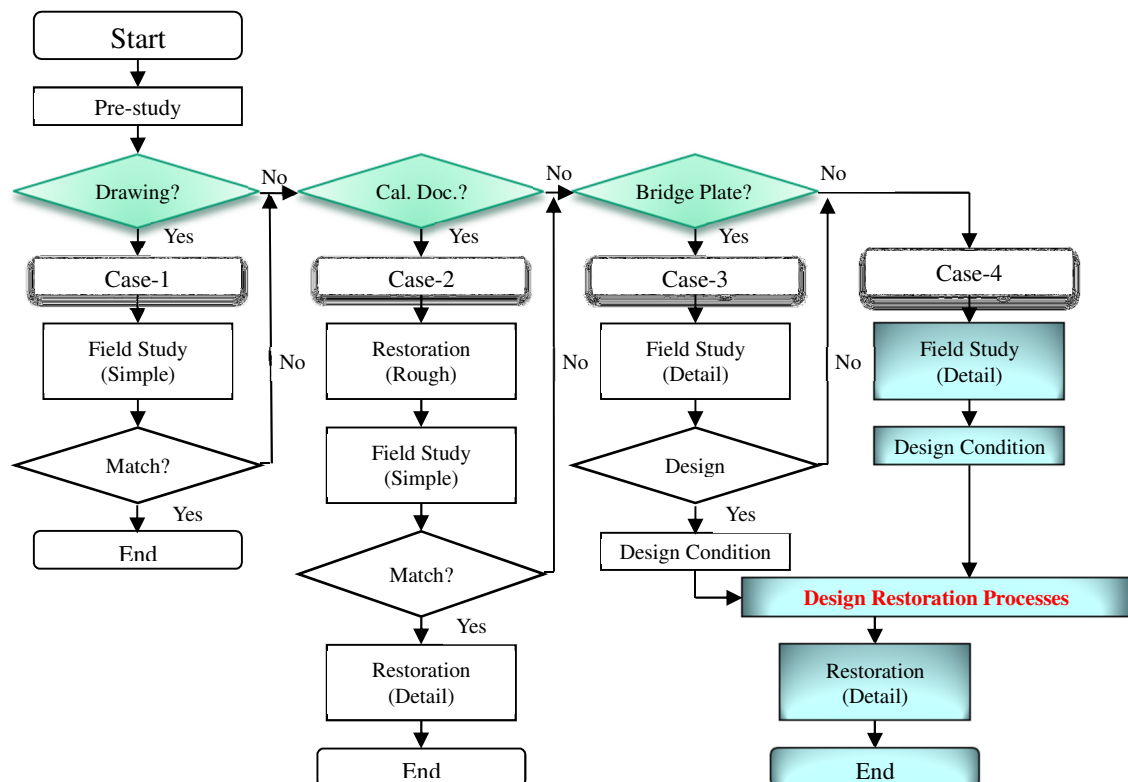


Fig. 2.11 Flow of design restoration for PC bridges [2.14]

As shown in **Fig. 2.11**, getting the method for Case-4 includes all cases. The construction year of the bridge and other required information can be obtained from field study.

2.5.1 Bridges without Design Drawings

There are some old bridges in service without plans. Establishing safe live-load-carrying capacity is essential to have a complete bridge document. When an inspector comes across a bridge without plans, sufficient field physical dimensions of each member and overall bridge geometry should be taken and recorded. In addition, information such as design year, design vehicle, designer, live-load history, and field condition of the bridge needs to be collected and recorded. This information will be very helpful to determine the safe live-load-carrying capacity. Also, bridge inspectors need to establish the material strength either using the design year or coupon testing [2.7].

In concrete girder bridges, field dimensions help to estimate the dead loads on the girders. Since the area of reinforcing steels is not known or is difficult to establish, determining the safe live load poses challenges to bridge owners. The live-load history and field condition of a bridge could be used to establish the safe load capacity of the bridge. For example, if a particular bridge has been carrying several heavy vehicles for years without damaging the bridge, this bridge could be left open for all legal vehicles [2.7].

2.5.2 Bridges with Unknown Structural Components

For bridges where necessary details, such as reinforcement in the concrete bridge, are not available from plans or field measurements, a physical inspection of the bridge by a qualified inspector and evaluation by a qualified engineer may be sufficient to approximate inventory and operating ratings. Load tests may be helpful in establishing the load carrying of such structures [2.17].

The yield stresses used for determining ratings should depend on the type of steel used in the structural members. When specifications of steel are not available, yield strengths should be taken from the applicable “Date Built” tables [2.17]. If there is no information about size and yield strength of steel bars, the method proposed in this study is important to restore the initial and current conditions of RC bridges.

2.6 Assessment and Evaluation

The strength assessment or evaluation of an existing road bridge becomes necessary for three main reasons [2.4].

- It is required to carry greater traffic loads than designed for, due to a general increase in traffic weights (principally from heavy lorries or trucks); increased traffic densities (with trucks occupying more lanes than the statutory limits) or from the passage of a single abnormal vehicle transporting, for example, a piece of heavy equipment.
- The structure has seriously deteriorated or suffered substantial damage resulting in a decrease in strength.
- There has been a change in design codes which may mean a reduction in acceptable safety levels.

The aim of an assessment is to establish the safe load carrying capacity of the bridge and most (if not all) national bridge management systems allow for this eventuality at particular intervals of time [2.4].

Performance assessment of bridges can be expressed in terms of load rating. Load rating is the process of ascertaining the capacity of each existing bridge in the nation's diverse inventory in order to inform the public of load limits and to develop freight policies and truck routes. Bridge load rating and design are two different business processes, yet they have much in common. Both have similar philosophical and mathematical approaches to structural analysis, load behavior, and resistance actions, and both require similar sets of detailed data describing each bridge. Both activities benefit from visualization [2.18].

Bridge load-ratings provide several useful results [2.19]:

- Confirm a bridge has adequate design for normal operations capacity
- Identify those bridges that do not have adequate capacity for normal operations and consider such bridges for posting
- Provide bridge capacity information and models for routing overload permit vehicles

- Identify unused capacity in existing bridges
- Support examination of structurally deficient bridges
- Provide a review on new bridge design

2.7 Types of Defects of RC Bridges

The proper evaluation of load capacity of damaged RC highway bridges requires a consistent methodology of defects classification and identification. The problem is even more significant, when the assessment procedure is carried out by more than one person [2.20]. The followings are the basic defect types of RC highway slab bridges.

- Contamination – Dirtiness or not designed plant vegetation
- Deformation – Geometry changes incompatible with the project, with changes of mutual distances of structure element points
- Deterioration – Physical and/or chemical changes of structural features against designed values
- Discontinuity – Inconsistent with a project break of material continuity
- Displacement – Change (or restriction) of location of a structure or its part incompatible with the project but without its deformation
- Loss of material – Decrease of designed amount of structure material

Damage is defined as changes to the material and/or geometric properties of these systems, including changes to the boundary conditions and system connectivity. Damage affects the current or future performance of these systems [2.3]. The damage identification process is generally structured into the following levels.

- Damage detection, where the presence of damage is identified.
- Damage location, where the location of the damage is determined.
- Damage typification, where the type of damage is determined.
- Damage extent, where the severity of damage is assessed.

Common concrete member defects include cracking, scaling, delamination, spalling, efflorescence, popouts, wear or abrasion, collision damage, scour, and overload [2.7]. Brief descriptions of common damages are given in this section.

The wide variety of failures is due to old bridge failures and design deficiency leading to bridge collapse [2.2]. The major defects and principal causes of RC bridges in Ethiopia are shown in **Table 2.1** [2.21].

Table 2.1 Major defects of bridges

No.	Damage/Defects	Principal causes
1	Flexural crack Shear crack	<ul style="list-style-type: none"> • Excessive load • Poor design
2	Concrete peel off/ Delamination	<ul style="list-style-type: none"> • Excessive load • Insufficient cover
3	Rebar exposure	<ul style="list-style-type: none"> • Insufficient cover • Concrete deterioration
4	Material deterioration Honeycomb	<ul style="list-style-type: none"> • Poor construction
5	Abrasion Potholes	<ul style="list-style-type: none"> • Poor construction • Aging

The damage/defects of bridges are important in estimating the current condition of RC bridges. In this study, the deterioration condition and loss in cross-sectional area of the bridge is taken into account for the design restoration process.

Several factors in the identification and prioritization of bridge rehabilitation should be considered [2.22]. These include:

- bridge sufficiency rating,
- historical significance,
- traffic volumes,
- bridge load capacity posting,
- bridge condition, including emergency repairs,
- length of detour, and
- economic analysis considering
 - repair,
 - rehabilitation,
 - replacement, and
 - life-cycle costs

2.8 Testing Methods

To obtain required information on the material properties, various tests should be performed. Among these, visual inspection and load testing are an important input for design restoration.

2.8.1 Visual Inspection

Visual inspection, as a preliminary step of bridge assessment, involves gathering of data from existing bridge via regular visual control based on various standards. Results of inspection are saved in the records (bridge book, sheets and digital files as well) for further analysis. This type of bridge examination gives a basis for taking decision on the use of some particular testing methods such as NDT (Non-Destructive Test) techniques. The information derived from the investigation will enable the residual capacity of a structure or element to be assessed and will enable an appropriate repair strategy to be selected [2.20].

Once a bridge has been inspected for its overall visual condition, it is often necessary to carry out non-destructive tests in order to further extend the diagnostic process if it is suspected that the bridge has been weakened in some way [2.17].

2.8.2 Load Testing

The load testing of bridges can be of great benefit to engineers in aiding their understanding of the behavior of bridges at both serviceability and the ultimate limit states under the action of live load [2.20].

The load testing of bridges can be of enormous benefit to engineers in aiding their understanding of the behavior of bridges at both the serviceability and the ultimate limit states under the action of live loads. After a bridge has been constructed it is quite usual to carry out a live load test to measure the response of the structure by the use of appropriate strain and displacement devices. This will confirm (or otherwise) the assumptions made in the original analysis regarding load distribution; stress levels and deflections [2.4]. There are three types of static load test that can be used on bridge superstructures:

- Supplementary load testing
- Proving load testing
- Collapse load testing

2.8.2.1 Supplementary Load Tests

This type of test is supplementary to the assessment process and is preferred by most engineers because it involves applying a known load to the bridge which is no greater than the existing traffic load and therefore should be safe with no damage or risk of collapse. It is therefore essentially a diagnostic performance test. Before the test load is specified it is essential to carry out a pre-test analysis based on a full material and dimensional survey of the bridge in order to establish the allowable maximum load which can safely be applied. The decision on whether to undertake a supplementary test is dependent on factors such as:

- The type of bridge
- The condition of the bridge
- The presence of structural actions not normally considered in analysis and providing a degree of hidden strength

2.8.2.2 Proving Load Testing

This type of test is the ideal one from an assessment point of view since it involves applying loads incrementally up to a value equivalent to the assessment loads factored for the ultimate limit state and in some ways is an extension of the supplementary load test.

The effect of aging related to bond deterioration can be reflected in excessive deflection of the bridges. From load test, if the measured deflections due to symmetrical loads and positions at the mid span are different, the damaged or deteriorated portion of the bridge can easily be identified/ detected. During load test, if uplift of the slab at the supports occurred, edge to edge of the support is taken as the span of the bridge. Thus, in the design restoration method, the span of the bridge should be adjusted.

2.9 Summary

- Literature survey on related topics has been made. It shows:
 - Major problems of bridges are aging, overloading and poor design
 - Inspection of the bridge is one of the most important tasks in the operation of a sound bridge management system
 - Load testing of bridges can be of great benefit to know the behavior of bridges
 - Experience of applying design restoration for PC structures is reported. The report provides detailed information on design restoration of PC bridges and different conventional non-destructive measurement techniques.
- Bridge Design Specifications of Italy and AASHTO has been reviewed.

References

- [2.1] Tarekegn, A.G. and Tsubaki, T.: Restoration Design for RC Slab Bridges by AASHTO LRFD, The 21st PC Symposium on Developments in Prestressed Concrete, JPCA, pp. 29-34, Oct. 2012.
- [2.2] Mohiuddin A. Khan: Bridge and Highway Structure Rehabilitation and Repair, The McGraw-Hill Companies, Inc., New York, 2010.
- [2.3] Wenzel, H.: Health Monitoring of Bridges, John Wiley & Sons, Ltd, VCE Holding GmbH, Vienna, Austria, 2009.
- [2.4] M. J. Ryall: Bridge Management, Butterworth-Heinemann, Linacre House, Jordan Hill, A division of Reed Educational and Professional Publishing Ltd, 2001.
- [2.5] JICA: Japan International Cooperation Agency Capacity Development Project on Bridge Management (CDBM), Bridge Inspection Manual, Addis Ababa, 2008.
- [2.6] M.G. Aswani: Design of Concrete Bridges, 2nd edition, Nai Sarak, KHANNA Publishers, 1995.
- [2.7] Chen, W. F.: Bridge Engineering Handbook, CRC Press LLC, Washington, D. C., 2000.
- [2.8] ERA: Ethiopian Roads Authority, Bridge Design Manual, Addis Ababa, 2002.
- [2.9] ERA: Ethiopian Roads Authority Bridge Management System, ERA BMS, Addis Ababa, 2010.

- [2.10] ERA: Ethiopian Roads Authority, Bridge Management in Ethiopia, Retrieved from <http://www.era.gov.et/portals/0/About%20Bridges%20for%20ERA-WebSite.pdf>
- [2.11] Ministero Dei Lavori Pubblici: Direzione General Dei Servizi Tecnici, Roma, 1945.
- [2.12] AASHTO: American Association of State Highway and Transportation Officials, LRFD Bridge Design Specifications, 4th edition, Washington, 2007.
- [2.13] JPCEA, Report of the Technical Committee on Design Restoration of Prestressed Concrete, Japan Prestressed Concrete Engineering Association, March 2010.
- [2.14] Uomoto, T. et al.: Report of the Technical Committee on Design Restoration of Prestressed Concrete - Systematization of Structural Restoration Design and Utilization of Various Sensing Technologies, J. of Prestressed Concrete, Japan, Japan Prestressed Concrete Engineering Association (JPCEA), Vol.52, No.5, pp.74-81, 2010.
- [2.15] Jonathan Desombre et al. : Experimentally Validated FEA Models of HF2V Damage Free Steel Connections for Use in Full Structural Analyses, Structural Engineering and Mechanics, Vol. 37, No. 4, 2011.
- [2.16] Kayser, T.H. and Binkhorst, J.: Computer Calculations of a Complex Steel Bridge Verified by Model Investigations, Rijkswaterstaat, DWW, The Hague, 1975.
- [2.17] AASHTO: American Association of State Highway and Transportation Officials, Manual for condition evaluation of bridges, Washington D.C, 20001, 1994.
- [2.18] Thompson, P.D. et al.: The Application of Object Technology in AASHTO's New Bridge Load Rating and Design Systems, Michael Baker Jr., Inc., USA, Retrieved from, <http://www.pdth.com/images/brware.pdf>
- [2.19] NMDOT: Bridge Procedures and Design Guide, The New Mexico Department of Transportation, January 2010.
- [2.20] Maciej M.: Evaluation of Load Capacity of Concrete Railway Slab Spans with Defects, Civil Engineering Department, University of Minho, Doctoral Thesis, 4800-058 Guimaraes, Portugal, Feb. 2008.
- [2.21] ERA: Ethiopian Roads Authority, Bridge Inspection Manual, Publication 1996:036(E), 2005.
- [2.22] DelDOT Bridge Design Manual: Rehabilitation of Existing Bridges, May 2005.

3. DESIGN RESTORATION FOR RC SLAB BRIDGES

3.1 Introduction

Nowadays constructed bridges are subjected to increasingly heavy traffic loads than expected. This together with deterioration due to external and environmental factors led to decrease in its capacity. Capacity performance assessment is one of the major tasks to be performed in bridge management and should be exercised with care [3.1].

To assess their conditions, original design documents, drawings and plans are important and must be available. If the design data is lost, inaccessible or a change exists in the design specification used, performance assessment is a difficult task. In the absence of these data, assessing bridge's performance will be a common problem bridge engineers face. It is mainly due to the absence of readymade bridge information or a change in design specification. In this case, design restoration should be performed and it is substantial [3.1].

Thus, a method of design restoration for existing RC slab bridges is important to estimate initial condition of bridges (steel and concrete strengths used, reinforcement size and spacing, etc.) and it is a necessary tool to estimate current condition of bridges.

3.2 Design Restoration

Design restoration is a process of accurately describing the initial condition (design values) of a structure from its current condition (actual values). Design restoration uses design values. On the other hand, if deflection is used as additional data, it reflects the present actual values. Also an indirect method for the estimation of yield strength of steel is needed. The required dimensions of the structure are determined through measurements [3.1]. Measurements shall be made at locations where maximum response is expected, i.e., the incremental instantaneous mid-span deflection of the bridge due to applied load needs to be measured. Additional measurements shall be made if required.

The deflection of the bridge computed using elastic beam deflection equation, based on the concept of the beam theory, may be used to compare with that of the actual deflection measured during load test. Two-dimensional FEM analyses are used for the prediction of deflection of the bridge. From the dimensions of the bridge, deflection and the corresponding load, the areas of reinforcing steel, effective depth, compressive strength of concrete and the actual yield strength will be estimated.

3.2.1 Method of Design Restoration

Direct and indirect methods can be used for the restoration process. Measurements and observations are one of the direct methods to be used. For computation of live load force effects on the structure, the Green's function for RC beams are applied. The effect of live loads on the bridge is computed based on AASHTO LRFD bridge design specification [3.2]. The assumptions used are as follows.

- Linear strain distribution, i.e., no severe bond deterioration between concrete and rebars
- Deflection of the beam obtained from load test

Based on the flow of design restoration for prestressed concrete bridges [3.3], the general flow chart for design restoration of RC slab bridges is shown in **Fig. 3.1** [3.1].

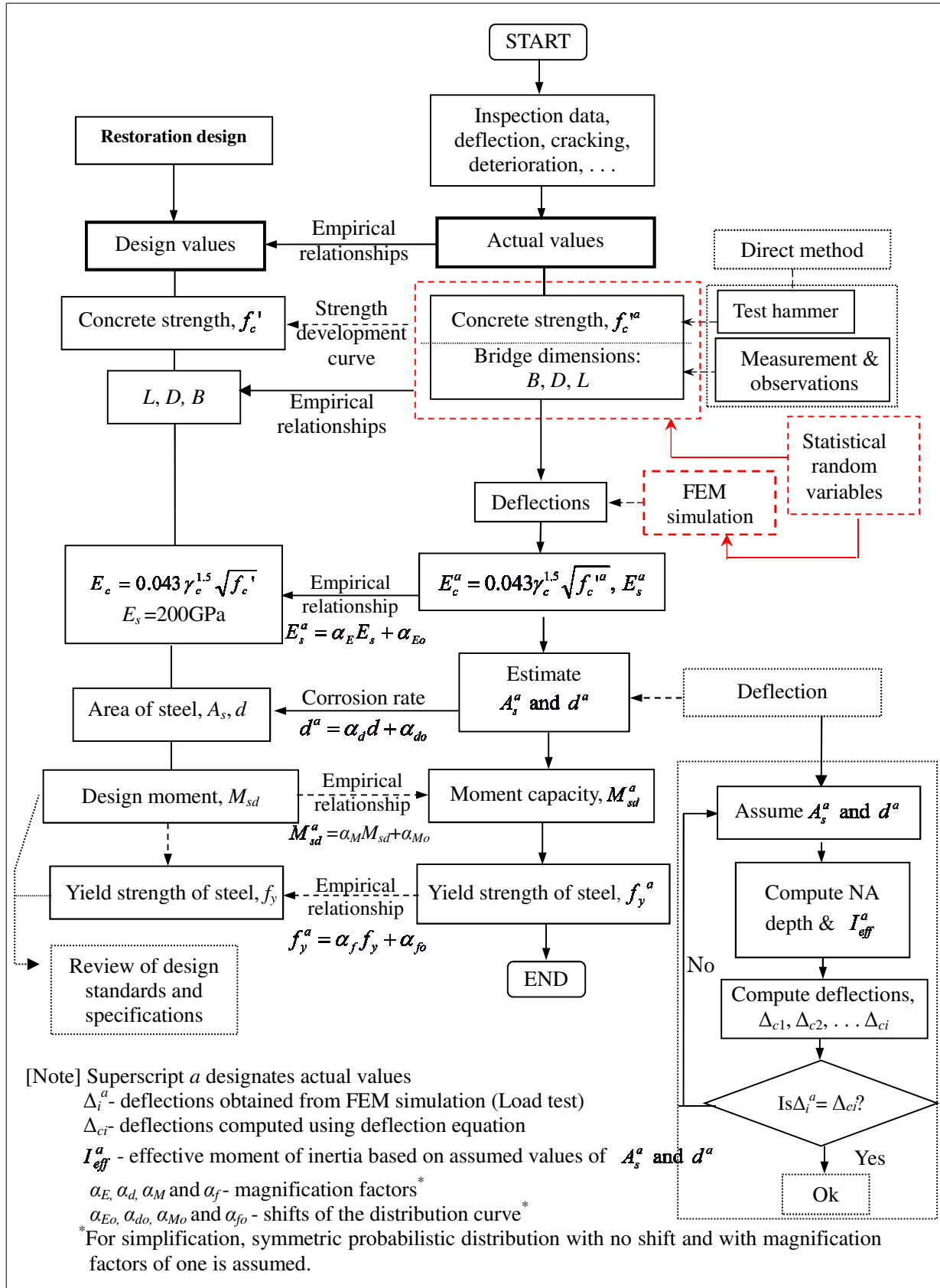


Fig. 3.1 Flow of design restoration of RC slab bridges [3.1]

In the design restoration process, the effect of random variables and the instantaneous incremental deflection of the structure are taken into account. The input and output in the design restoration are shown in **Fig. 3.2**.

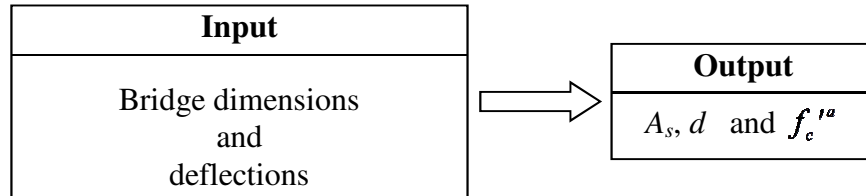


Fig. 3.2 Input and output in design restoration

For unknown effective depth, additional load tests should be done. For more accurate results, as many as measurements are needed.

3.2.2 Deterministic Design Restoration

Instead of using current concrete strength from the test hammer test and position of reinforcing bars by an electric magnetic device, main inputs for the design restoration in this study are the dimensional data and the deflections of the bridge. The flow to estimate effective depth, area of steel bars and compressive strength of concrete is shown in **Fig. 3.3** where superscript a designates actual values and subscript i designates the range of parameter (deflection), in this case, $i=1, 2, 3, \dots, n$.

Alternatively, initial design values can be restored graphically. In the method, distribution of objective function versus number of possible trials is of great importance. Mean values for random parameters can be set by considering engineering judgment and measurements. Moreover, realistic but arbitrary variations in random variables have to be used. Thus, from the graph, the optimal solution will be easily selected. To select an optimal solution, the schematic diagrams shown in **Fig. 3.4** should be considered.

3.2.3 Probabilistic Design Restoration

Many things actually are normally distributed, or very close to it. Measurement errors also often have a normal distribution [3.4]. Thus, in this study, to consider the effect of the probabilistic distribution of random variables on the result of the design

restoration and capacity performance analysis, the statistical variations of the design parameters are expressed by assuming normal distribution. The assumptions considered in the analysis is that random variables are independent each other and they follow normal distribution. Base on the probabilistic distributions of $f_c'^a$, A_s^a , d^a and f_y^a of a standard RC slab bridge, the design restoration is performed by using the LHS method.

The statistical data used in the probabilistic design restoration are shown in the dashed-line rectangles in **Fig. 3.1** and **Fig. 3.3**. In the LHS sampling method, the cumulative distribution function of each factor is divided into 32 intervals with equal probability, and then sampling is done by only once from each interval [3.5].

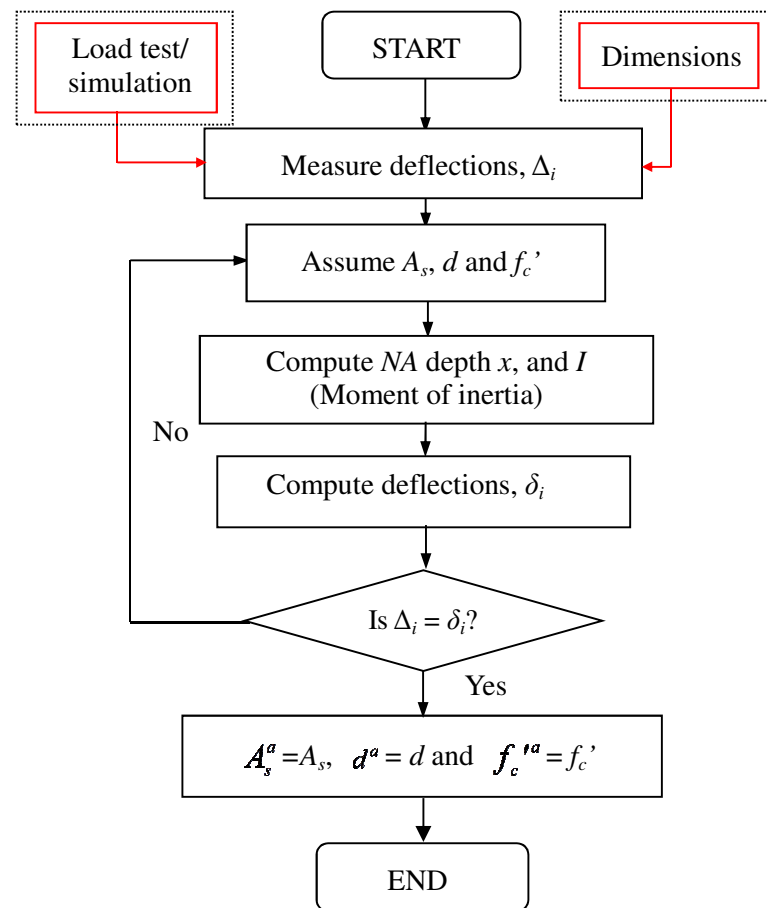


Fig. 3.3 Flow of estimating d^a , A_s^a and $f_c'^a$

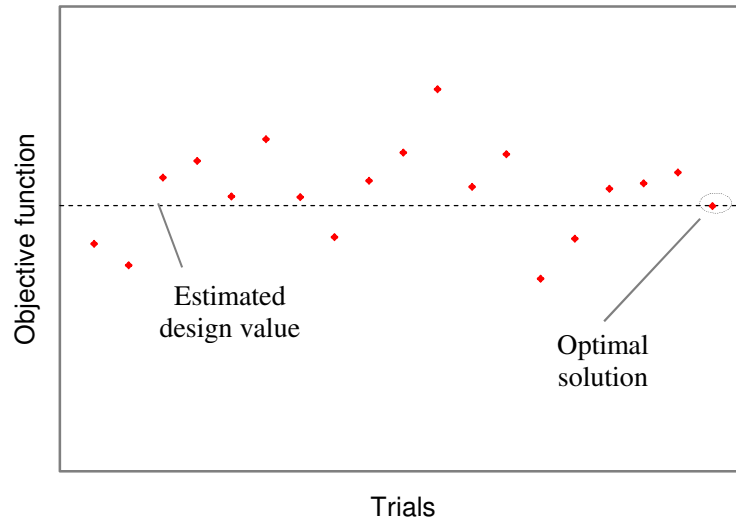


Fig. 3.4 Distribution of objective function

3.2.4 Computation of Moment of Inertia at a Section

For the computation of deflection, the variation in the neutral axis depth and moment of inertia along the bridge's span is taken into account. The neutral axis along the longitudinal line is not constant due to the tensile strength of concrete and effective reinforcement ratio at the section. For uniformly distributed loads, since the neutral axis depth is related to bending moment, a parabolic neutral axis profile and variable moment of inertia along the longitudinal direction are assumed [3.1].

For the derivations of neutral axis depth variation and to obtain expressions for the moment of inertia along the longitudinal line of a beam, consider the side view shown in **Fig. 3.5**. The basic assumptions considered are the neutral axis profile varies with the load, depends on its position and crack occurs when tensile stress exceeds the assumed tensile strength of concrete.

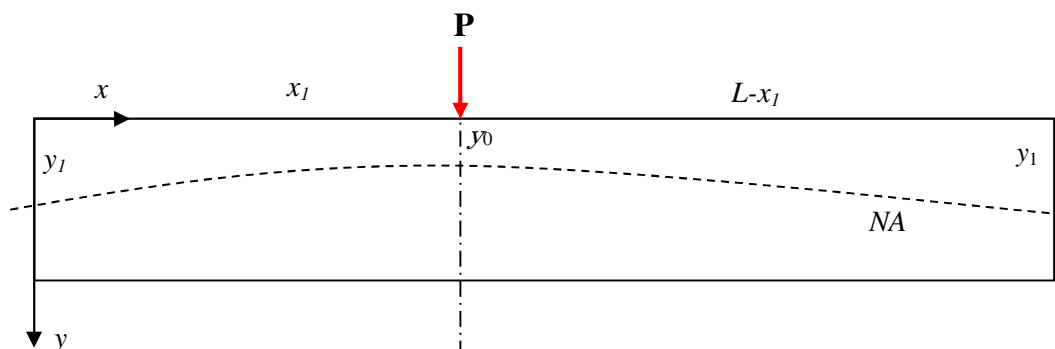


Fig. 3.5 Variation of neutral axis depth of new RC beam

Let the neutral axis depths for the fully cracked and uncracked sections, measured from the top fiber, be represented by y_0 and y_1 , and the corresponding moment of inertias by I_{cr} and I_{unc} , respectively. Let the neutral axis depth profile be expressed by a quadratic equation.

$$\bar{y} = ax^2 + bx + c \quad (3.1)$$

where, \bar{y} : neutral axis depth at section, measured from top fiber

x : distance measured from the left support of beam

In Eq. (3.1), the constants a , b and c are determined from boundary conditions. In reference to **Fig. 3.5**, the boundary conditions are: at $x=0$, $\bar{y} = c = y_1$, at $x = x_1$, $\bar{y} = y_0$ and at $x = L$, $\bar{y} = y_1$. Upon substitution, the following expression for the neutral axis depth, except at $x_1=0$ and $x_1=L$ is obtained.

$$\bar{y} = \frac{(y_0 - y_1)}{x_1(L - x_1)}(Lx - x^2) + y_1 \quad (3.2)$$

where, L : length of beam

x_1 : location of load position, measured from left support of beam

Due to the variation in applied load and cracking moment of concrete, the neutral axis depth, y_0 , is not constant and hence the effect of applied load has to be considered. The concept of variations in neutral axis profile due to a change in the applied load is shown in **Fig. 3.6**. Again, by considering the variation in y_0 as a quadratic equation, the modified neutral axis depth of the cracked section is expressed as follows.

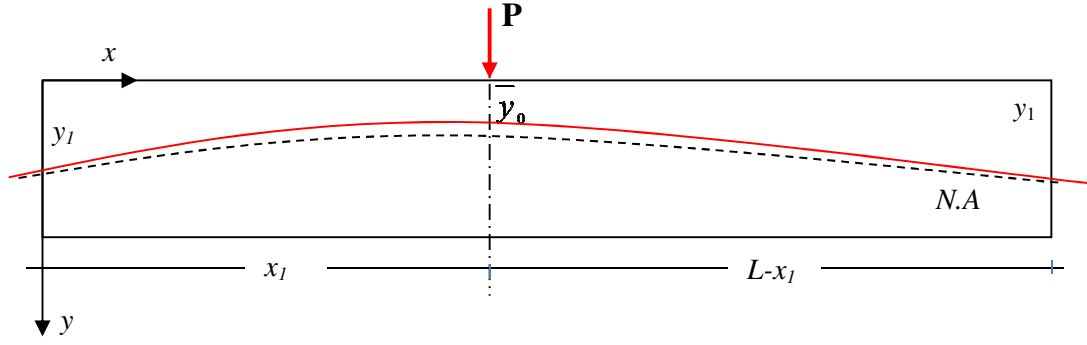


Fig. 3.6 Concept of variation in neutral axis profile at different loading conditions

$$\bar{y}_0 = a_1 \eta^2 + c_1 \quad (3.3)$$

where, a_1, c_1 : constants

\bar{y}_0 : modified neutral axis depth of cracked section, measured from top fiber

M_a : maximum moment in a beam or member at the stage for which deformation is computed

η : ratio of M_a to M_{cr}

The boundary conditions are: at $\eta=0$, $\bar{y}_0 = y_1$ and at $\eta \geq 1$, $\bar{y}_0 = y_0$. Upon substitution, \bar{y}_0 becomes:

$$\bar{y}_0 = \eta^2 y_0 + (1 - \eta^2) y_1 \geq y_0 \quad (3.4)$$

An expression for the modified neutral axis depth profile is given in Eq. (3.5) and a similar method is used to get an expression for the moment of inertia at a section.

$$\bar{y} = \frac{(\bar{y}_0 - y_1)}{x_1(L - x_1)} (Lx - x^2) + y_1 \quad (3.5)$$

$$\bar{I}_{cr} = \eta^2 I_{cr} + (1 - \eta^2) I_{unc} \geq I_{cr} \quad (3.6)$$

$$I(x) = \frac{(\bar{I}_{cr} - I_{ucr})}{x_1(L - x_1)} x(L - x) + I_{ucr} \quad (3.7)$$

where, \bar{I}_{cr} : modified moment of inertia of cracked section corresponding to \bar{y}_0 (mm⁴)

$I(x)$: moment of inertia at section (mm⁴)

For old structures, the distribution of the neutral axis is independent of load position, and it does not move with load and is assumed to be unchanged since the section is already cracked by the maximum possible load experienced in the past. For the derivation of neutral axis depth variation along its length, consider the longitudinal cross section shown in **Fig. 3.5** with $x_l=L/2$. The following equations for the neutral axis depth and moment of inertia are obtained [3.1]. The derivation of neutral axis depth profile and deflection equations is attached in **APPENDIX C**.

$$\bar{y} = \left(\frac{4x}{L^2} (L - x) \right) \bar{y}_0 + \left(1 - \left(\frac{4x}{L^2} (L - x) \right) \right) y_1 \quad (3.8)$$

$$I(x) = \left(\frac{4x}{L^2} (L - x) \right) \bar{I}_{cr} + \left(1 - \left(\frac{4x}{L^2} (L - x) \right) \right) I_{ucr} \quad (3.9)$$

where, \bar{y} : neutral axis depth at section, measured from top fiber

L : length of beam or span length

y_0, I_{cr} : neutral axis depth (mm) and moment of inertia of cracked section

y_1, I_{ucr} : neutral axis depth (mm) and moment of inertia of uncracked section

In most cases, the surface finish of a bridge is bituminous layer and hence for the computation of moment of inertia, the contribution of bituminous on the stiffness of the bridge using the modulus of elasticity of bituminous and the effect of temperature on it should be considered. Temperature versus elastic modulus relationship of asphalt concrete assumed in the Asphalt Institute Method is shown in **Fig. 3.7** [3.6].

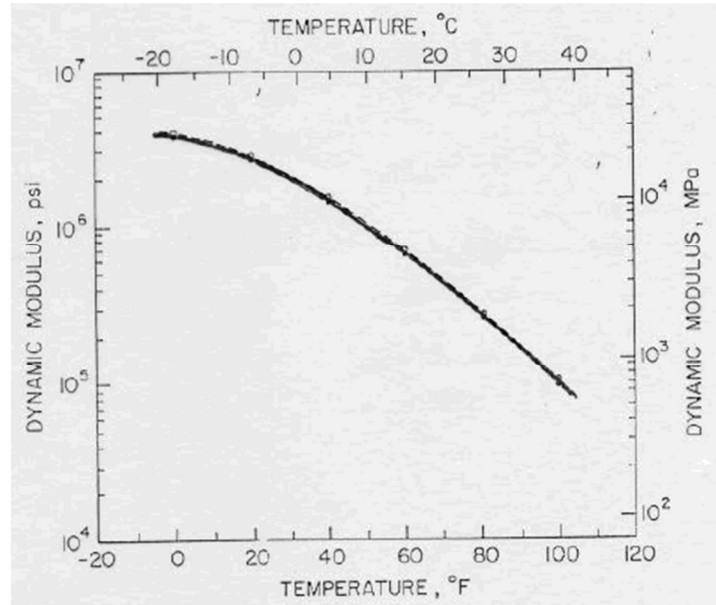


Fig. 3.7 Temperature - elastic modulus relationship of asphalt concrete [3.6]

In actual structures, bridges are subjected to temperature gradient. Thus, in computing the total deflection of bridges, deflection of beams due to temperature gradient should be considered.

System of nonlinear equations

In reference to **Fig. 3.5**, the deflection of a beam at section x from the left support, due to a concentrated load, is computed from the following equation [3.7].

$$\delta_{xi} = \frac{P_i(L-x_1)x}{6E_c^a I(x)L} (L^2 - (L-x_1)^2 - x^2) \text{ for } x \leq x_1 \quad (3.10)$$

where, P_i : applied load

δ_{xi} : deflection

E_c^a : Young's modulus of concrete

For n unknowns, there exist n system of nonlinear deflection equations ($i=1, 2, \dots, n$) and these nonlinear equations are solved simultaneously.

While computing the unknown parameters, for uniqueness of the solution, the followings should be considered to eliminate unnecessary results.

1. Only one neutral axis exists.
2. Any combination of negative results should be avoided,
i.e., all the results of the random variables should be positive and real numbers.
If not, the results should be neglected.
3. Reinforcement ratio does not exceed the maximum limit permitted in design codes and standards.
4. Effective depth exceeding the overall depth of the section should not be taken.

3.3 Estimation of Actual Yield Strength of Steel

The design value of yield strength of steel, f_y , is discrete whereas the actual value obtained from design restoration process is scattered. Thus, from the result, the range of f_y can be estimated. The basic assumption considered in the estimation of actual yield strength of steel is that the flexural capacity of the section is estimated by considering the effect of yield moment and the stress-strain relationship is linear.

For the derivation of empirical formula for the estimation of yield strength of steel, the effects of material constants and dimensional data are considered. The design moment is computed by considering the effects of dead and live loads as per AASHTO LRFD design specifications [3.2]. In this study, based on the working stress design of AASHTO LRFD design specifications, the actual allowable stress of steel, σ_{sa}^a , is considered as the actual yield strength of steel, f_y^a .

Since most of old bridges are designed using the working stress design method, in the derivation of actual allowable stress of steel, the same design principle is used here. A doubly reinforced RC section shown in **Fig. 3.8**, with linear stress-strain relationship, is considered. To compute capacity of the section, moment equilibrium at the neutral axis is taken.

3.3.1 Single-Layer Reinforcement Arrangement

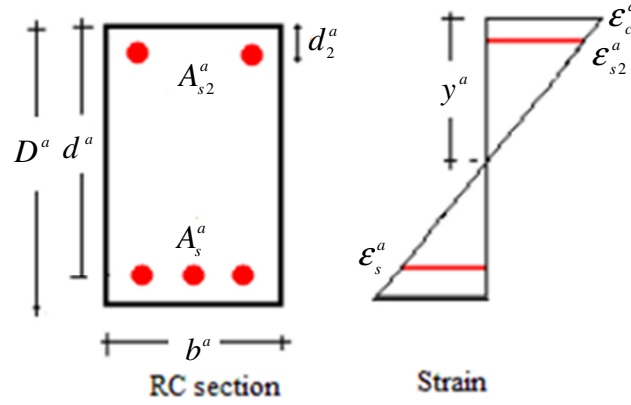


Fig. 3.8 RC section and strain diagram

$$M^a = M_c^a + M_{s2}^a + M_s^a \quad (3.11)$$

$$M_c^a = \sigma_c^a b^a (y^a)^2 / 3, \quad M_{s2}^a = A_{s2}^a \sigma_{s2}^a (y^a - d_2^a), \quad M_s^a = A_s^a \sigma_{sa}^a (d^a - y^a) \quad (3.12)$$

$$\sigma_{s2}^a = \begin{cases} E_s^a \epsilon_{s2}^a & \text{if } \epsilon_{s2}^a < \epsilon_s^a \\ \sigma_{sa}^a & \text{if } \epsilon_{s2}^a \geq \epsilon_s^a \end{cases} \quad (3.13)$$

$$\epsilon_c^a = \frac{\sigma_c^a}{E_c^a}, \quad \epsilon_s^a = \frac{f_y^a}{E_s^a}, \quad \epsilon_{s2}^a = \frac{y^a - d_2^a}{d^a - y^a} \epsilon_s^a \quad (3.14)$$

$$\sigma_c^a = E_c^a \frac{y^a}{d^a - y^a} \epsilon_s^a, \quad E_c^a = C_E \gamma_c^{1.5} \sqrt{f_c^{t^a}} \quad (3.15)$$

From force equilibrium, the neutral axis depth, y^a , can be obtained as follows:

$$\frac{b^a (y^a)^2}{2} + n(A_s^a + A_{s2}^a)y^a - n(A_s^a d^a + A_{s2}^a d_2^a) = 0 \quad (3.16)$$

where, M_c^a : actual bending moment carried by concrete per unit width

M_s^a : actual bending moment carried by tensile steel, A_s^a , per unit width

M^a : actual allowable flexural moment of section per unit width

M_{s2}^a : actual bending moment carried by compression steel, A_{s2}^a , per unit width

A_s^a : actual area of tensile steel per unit width

A_{s2}^a : actual area of compression steel per unit width

d^a : actual effective depth

b^a : actual width

d_2^a : actual position of A_{s2}^a , measured from top fiber

ϵ_s^a : actual tensile strain in steel

ϵ_c^a : actual compressive strain in concrete

ϵ_{s2}^a : actual tensile strain in steel

σ_{s2}^a : actual stress in compression steel

σ_c^a : actual compressive strain in concrete

σ_{sa}^a : actual allowable stress of steel

y^a : actual neutral axis depth, measured from top fiber

$f_c'^a$: actual concrete strength

C_E : coefficient used to compute E_c^a

E_s^a : actual Young's modulus of steel

E_c^a : actual Young's modulus of concrete

γ_c : unit weight of concrete

β : ratio of A_{s2}^a to A_s^a

n : ratio of E_s^a to E_c^a

Upon substitution and simplification, Eq. (3.11) is simplified to the following form.

$$\sigma_{sa}^a = \frac{3nM^a(d^a - y^a)}{b^a(y^a)^3 + 3nA_s^a[\beta(y^a - d_2^a)^2 + (d^a - y^a)^2]} \quad (3.17)$$

To obtain the value of A_{s2}^a , additional load tests at different load positions should be conducted. As per AASHTO LRFD Bridge Design Specification [3.2], the minimum amount of top reinforcements for shrinkage and temperature for RC slab bridges to be provided is given as follows.

$$A_{s2}^a \geq \frac{\phi A_g}{f_y^a}, \phi = 0.75 \text{MPa} \rightarrow \beta = \frac{\phi A_g}{A_s^a f_y^a}, \phi = 0.75 \text{MPa} \quad (3.18)$$

The actual total design moment, M^a , due to dead and live load force effects per unit width are given as follows [3.2].

$$M^a = M_{DL} + M_{LL} \quad (3.19)$$

$$M_{DL} = \gamma_{DL} \gamma_c DL^2 / 8,$$

$$M_{LL} = \frac{1}{E} \gamma_{LL} [1.33 \max(M_{tr}, M_{tm}) + M_{ln}] \quad (3.20)$$

where, M_{DL}, M_{LL} : dead and live load moments

γ_{DL}, γ_{LL} : factor of safety for dead and live loads

M_{tr}, M_{tm} : live load moments due to truck and tandem loads

M_{ln} : lane load

D : total depth

E : live load strip width

The effective interior strip width of the bridge is computed using Eq. (3.21). Thus the effective strip width becomes the lesser of E_1 and E_m .

$$E_1 = 250 + 0.42\sqrt{SR}, \quad (3.21)$$

$$E_m = 2100 + 0.12\sqrt{SR} \leq W / N_L$$

where, S : modified span length taken equal to the lesser of actual span length or 18m

E_l : interior strip width for one lane loaded

E_m : interior strip width for multiple lanes loaded

R : total roadway width $\leq 9000\text{mm}$

W : roadway width

N_L : Number of lanes loaded $= W/3.6$

For girder bridges, Eqs. (3.16) and (3.17) can be used with some modifications. In this case, for both interior and exterior girders, the followings should be considered.

- Distribution factors for moment and deflection per ASSHTO LRFD [3.2] should be applied.
- Effective width of flanges should be used to calculate the neutral axis depth and the moment carried by the section.

For the computation of neutral axis depth, y^a and M^a , consider the cross section of a T-beam shown in **Fig. 3.9**. The corresponding bending moment carried by concrete is given in Eq. (3.22).

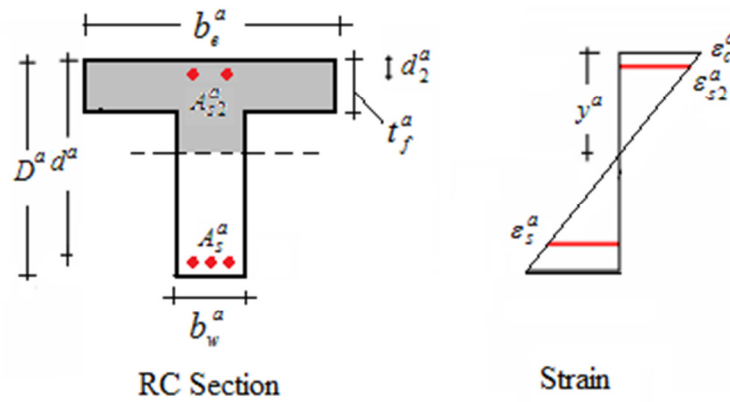


Fig. 3.9 RC T-section and strain diagram

$$M_c^a = \sigma_c^a [(b_e^a - b_w^a)t_f^a + (b_w^a y^a)] y^a / 3 \quad (3.22)$$

where, b_e^a : actual effective width of flange

b_w^a : actual web thickness

t_f^a : actual thickness of top slab

3.3.2 Multi-Layer Reinforcement Arrangement

Generally, in the case of multi-layer reinforcement arrangement, sufficiently accurate displacement transducers can be used to detect the deflection of the bridge with high accuracy. The unknown random parameters are increased by the increase of the number of layers and hence, additional and accurate measurement of deflections is required.

In the flow of estimating the unknown parameters, shown in **Fig. 3.3**, the subscript $i=1, 2, 3, \dots, n$ where n is the number of unknowns. For the derivation of an equation to estimate yield strength of steel for r layers of reinforcements, consider the RC section shown in **Fig. 3.10**.

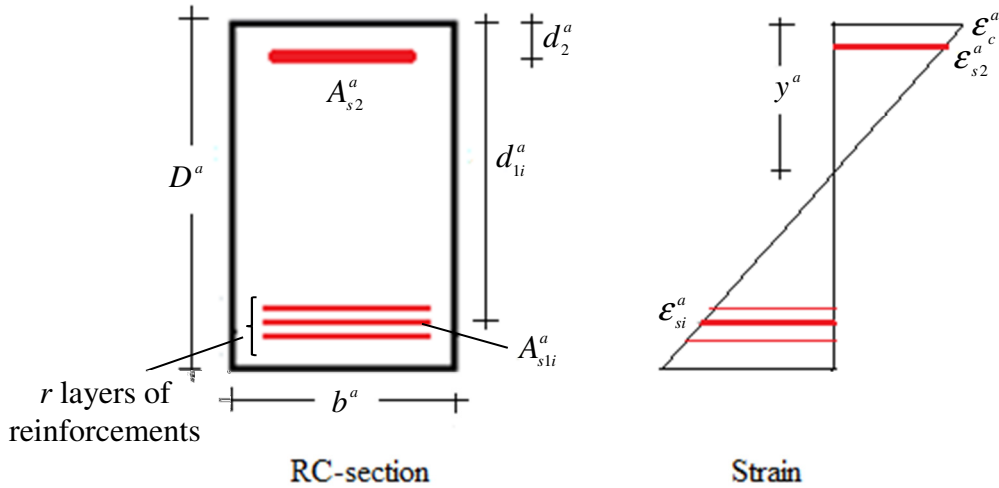


Fig. 3.10 Multi-layer reinforcement arrangement

$$M^a = M_c^a + M_{s2}^a + \sum_{i=1}^r M_{si}^a \quad (3.23)$$

$$M_{si}^a = A_{si}^a \sigma_{si}^a (d_{li}^a - y^a) \quad (3.24)$$

$$\epsilon_{s1}^a = \frac{f_y^a}{E_s^a}, \quad \epsilon_{s2}^a = \frac{y^a - d_2^a}{d_{11}^a - y^a} \epsilon_{s1}^a, \quad \epsilon_{si}^a = \frac{d_{li}^a - y^a}{d_{11}^a - y^a} \epsilon_{s1}^a, \quad \sigma_{si}^a = \epsilon_{si}^a E_s^a \quad (3.25)$$

In the analysis, the assumption considered is that the steel in the 1st layer yields. From force equilibrium, the neutral axis depth, y^a , is given in Eq. (3.26).

$$\frac{b^a (y^a)^2}{2} + n \left(\sum_{i=1}^r A_{s1i}^a + A_{s2}^a \right) y^a - n \left(\sum_{i=1}^r (A_{s1i}^a d_{1i}^a) + A_{s2}^a d_2^a \right) = 0 \quad (3.26)$$

where, M_{si}^a : actual bending moment carried by tensile steel of the i^{th} layer, A_{s1i}^a , per unit width

A_{s1i}^a : actual area of tensile steel of layer i per unit width

d_{1i}^a : actual effective depth corresponding to layer i

ϵ_{s1}^a : actual tensile strain in steel in the 1st layer, counted from the bottom

ϵ_{si}^a : actual tensile strain in steel of layer i

d_{11}^a : actual effective depth corresponding to layer 1, counted from the bottom

σ_{si}^a : actual tensile stress of steel of layer i

r : number of reinforcement layers

Upon substitution and simplification, Eq. (3.23) is simplified to the following form.

$$\sigma_{sa}^a = \frac{3nM^a (d_{11}^a - y^a)}{b^a (y^a)^3 + 3n[A_{s2}^a (y^a - d_2^a)^2 + \sum_{i=1}^r (A_{s1i}^a (d_{1i}^a - y^a)^2)]} \quad (3.27)$$

The moment of inertia of a section with multi-layer reinforcement arrangement can be computed using Eq. (3.28).

$$I_{cr} = \frac{b^a (y^a)^3}{3} + n \sum_{i=1}^r (A_{s1i}^a (d_{1i}^a - y^a)^2) + (n-1) A_{s2}^a (y^a - d_2^a)^2 \quad (3.28)$$

The system of nonlinear equations to compute the unknown random parameters is given in Eq. (3.29).

$$(\text{DE}_i)_n = (\Delta_i)_n \quad (3.29)$$

where, $(\Delta_i)_n$: n deflections obtained from load test

$(\text{DE}_i)_n$: n deflection equations containing n random variables $(d_{1i}^a, A_{s1i}^a, f_c'^a,$

$A_{s2}^a, d_2^a; i=1, 2, 3, \dots, r)$

To solve system of nonlinear simultaneous equations, Eq. (3.10) can be used. Moreover, to eliminate unnecessary results, similar criteria set for single layer reinforcement arrangement can also be established.

3.4 Sensitivity Analysis

Sensitivity analysis is the study of how the variation (uncertainty) in the output of a statistical model can be attributed to different variations in the inputs of the model. It is used to select the order of importance of random variables. The sensitivity of each random variable is represented by the squared value of the partial coefficient of correlation (r_p^2). For uncertainty analysis, the sensitivity factor α_i based on the first-order approximation second-moment method [3.8] is used. To determine effects of random variables, the sensitivity factor is obtained as follows.

$$\alpha_i = \frac{\partial F}{\partial x_i} \frac{\bar{x}_i}{\bar{F}} \quad (i = 1, 2, 3, \dots, n) \quad (3.30)$$

where, α_i : sensitivity factor of random variable i

F : function with statistical variations

\bar{F} : mean of F

x_i : random variable i

\bar{x}_i : mean of x_i

The sensitivity factor α_i is a kind of index to estimate the contribution of the uncertainty of x_i to the uncertainty of F . Using the central difference approximation equation, the uncertainty of each random variable can be obtained from Eq. (3.31).

$$\frac{\Delta F}{\Delta x} = \frac{F(\bar{x} + \Delta x) - F(\bar{x} - \Delta x)}{2\Delta x} \quad (3.31)$$

where, Δx : increment of each random variable

In this analysis, 1/1000 of the mean value is taken as Δx . The contributions of the uncertainty of each random variable are obtained by multiplying the sensitivity factor by

its coefficient of variation.

$$U_{x.Fi} = \alpha_i (COV_i) \quad (3.32)$$

where, $U_{x.Fi}$: contributions of the uncertainty of random variable i

COV_i : coefficient of variation for random variable i

α_i : sensitivity factor of random variable i

3.5 Probabilistic Analysis

As discussed earlier, design restoration is affected by current measurements of dimensions and material properties. Since measurements are inexact and contain errors of unknown magnitude, their effects on the design restoration have to be investigated. For such investigation, a probabilistic approach of design restoration is used. In this section, a probabilistic approach of design restoration of RC slab bridges, considering different combinations of the values of random variables, is investigated to make clear the influence and uncertainty of random variables selected by sensitivity analysis on the design restoration result.

There are different random variables which affect the design restoration process. To perform design restoration, different methods can be applied. In this study, a probabilistic approach of design restoration considering different combinations of random variables based on the Latin Hypercube Sampling (LHS) method is used. LHS is a sampling method designed to accurately recreate the input distribution through sampling in fewer trails when compared with the Monte Carlo method. LHS, a sampling technique used, forces the samples drawn to correspond more closely with the input distribution and thus converges faster on the true statistics of the input distribution [3.9]. Moderately deteriorated bond between concrete and steel bars with linear strain distribution is assumed. Due to the linear strain distribution of steel and concrete, moderate non-linearity in the problem and reduced number of FEM simulations, in this study, LHS method is used.

The probabilistic distribution and the influence of random variables on the statistical variation of the estimated yield strength of steel, cross-sectional area of steel and effective depth are investigated. To consider the probabilistic distribution of random variables on

the effect of the design restoration result, the concept of normal distribution is used. The assumptions considered in the analysis are that random variables are independent each other and that they follow normal distribution. The probability function, $f(x)$, using normal distribution [3.10] is given in Eq. (3.33).

$$f(x) = \frac{1}{\sigma\sqrt{2\pi}} e^{-(x-\mu)^2/2\sigma^2} \quad (3.33)$$

where, x : random variable

μ : mean value

σ : standard deviation

Based on the distribution of cover thickness of main reinforcing bars, bridge dimensions, compressive strength of concrete, a probabilistic analysis of random variables of a standard RC slab bridge, by using LHS method, is conducted.

In the LHS sampling method, the cumulative distribution function of each factor is divided into intervals with equal probability, and then sampling is done by only once from each interval [3.5]. The arrangement of sampling intervals and sampling of random variables is shown in **Fig. 3.11** [3.5]. The 32 combinations of random variables of LHS table are found to be sufficient in this simulation.

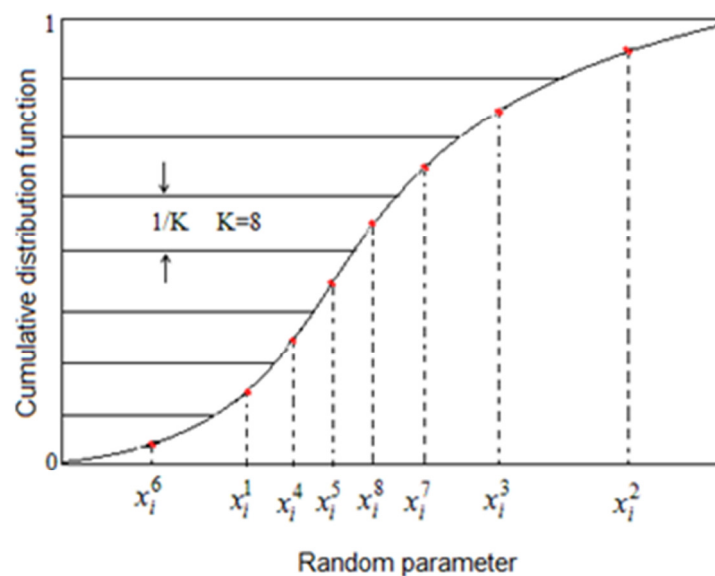


Fig. 3.11 Arrangement of sampling intervals and sampling of random variables [3.5]

Furthermore, the 95% confidence interval of the mean value is computed using the true standard error of the mean (variance). These confidence intervals are important to know how closely the estimated values to the actual ones and they tell us how good the estimated values are. As the confidence interval to the mean value gets smaller and smaller, the more precise the restored value be [3.11]. This gives the reliability of the design restoration results.

3.6 Summary

- Flow of design restoration and a probabilistic design restoration scheme for RC slab bridges are presented.
- Empirical formula for the estimation of yield strength of steel by considering the effects of material constants and dimensional data, for single and multi-layer reinforcement arrangement is obtained.

References

- [3.1] Tarekegn, A.G. and Tsubaki, T.: Restoration Design for RC Slab Bridges by AASHTO LRFD, The 21st PC Symposium on Developments in Prestressed Concrete, JPCA, pp. 29-34, Oct. 2012.
- [3.2] AASHTO: American Association of State Highway and Transportation Officials, LRFD Bridge Design Specifications, 4th edition, Washington, 2007.
- [3.3] Uomoto, T. et al.: Report of the Technical Committee on Design Restoration for Prestressed Concrete - Systematization of Structural Design Restoration and Utilization of Various Sensing Technologies, J. of Prestressed Concrete, Japan, Japan Prestressed Concrete Engineering Association (JPCEA), Vol.52, No.5, pp.74-81, 2010.
- [3.4] Normal Distribution: Retrieved from <http://www3.nd.edu/~rwilliam/stats1/x21.pdf>
- [3.5] Tsubaki, T.: Sensitivity Analysis, Trans. of the Japan Concrete Institute, Vol. 11, pp97-104, 1989.
- [3.6] Asphalt Institute Method for Design of Asphalt Pavement, Retrieved from <http://nersp.nerdc.ufl.edu/~tia/5837-13.pdf>
- [3.7] Popov, E.P.: Engineering Mechanics of Solids, Prentice-Hall Inc., New Jersey, 1990.
- [3.8] Tsubaki T., Ihara T. and Yoshida M.: Statistical Variation and Modeling of Drying

Shrinkage of Concrete, Trans. Of the Japan Concrete Institute, Vol. 14, 1992, pp. 123-130.

[3.9] Appendix A - Sampling Methods: Retrieved from

<http://www.uio.no/studier/emner/matnat/math/STK4400/v05/undervisningsmateriale/Sampling%20methods.pdf>

[3.10] Shirley D.: Statistics for Researchers, 3rd ed, John Wiley and Sons, Inc., 2004.

[3.11] Confidence Interval for a Population Mean, Retrieved from

<http://www.kean.edu/~fosborne/bstat/06amean.html>

4. NUMERICAL MODELING AND EXPERIMENTAL INVESTIGATIONS

4.1 Introduction

For statistical analysis, a standard RC bridge is designed following AASHTO LRFD Bridge Design Specification [4.1] and simulated using FEM. Since material model SBETA [4.2] includes biaxial strength failure criterion, reduction of compressive strength after cracking and fracture of concrete in tension is based on the nonlinear fracture mechanics [4.2], in the simulation, concrete is modeled as ‘SBETA Material’.

The mesh consists of rectangular elements of 0.05m in size with 4 nodes and SBETA material model of ATENA 2D v 4.2.2 [4.2] is used. The FEM simulation helps to predict deflection of bridges. The constitutive Model of SBETA [4.2] is discussed here below.

Experimental investigation under the achieved dimensions and concrete cover of RC beam specimens has been performed. Moreover load test on RC test specimens are conducted and from the result, the design values of the test specimens are estimated and the values are used for verifying the proposed design restoration method.

4.2 Constitutive Model

The formulation of constitutive relationships is considered in the plane stress state. A smeared approach is used to model the material properties, such as cracks or distributed reinforcement. This means that material properties defined for a material point are valid within a certain material volume, which is in this case associated with the entire finite element.

4.2.1 Material Model of Concrete

The material model SBETA includes the following features of concrete behavior:

- non-linear behavior in compression including hardening and softening
- fracture of concrete in tension based on the nonlinear fracture mechanics
- biaxial strength failure criterion
- reduction of compressive strength after cracking
- tension stiffening effect
- reduction of the shear stiffness after cracking (variable shear retention)
- two crack models: fixed crack direction and rotational crack direction

4.2.2 Stress-Strain Relationships for Concrete

The nonlinear behavior of concrete in the biaxial stress state is described by means of the so-called effective stress and the equivalent uniaxial strain. The effective stress is in most cases a principal stress. The equivalent uniaxial strain is introduced in order to eliminate the Poisson's effect in the plane stress state. A biaxial stress failure criterion is also used. The material model of concrete is shown in **Fig. 4.1**.

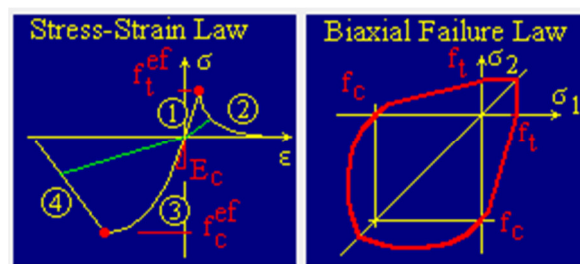


Fig. 4.1 Material model of concrete [4.2]

4.2.3 Material Stiffness Matrices

The material stiffness matrix for the uncracked concrete has the form of an elastic matrix of the isotropic material. For the cracked concrete the matrix has the form of the elastic matrix for the orthotropic material.

4.2.4 Material Model of Steel

The material model of steel is shown in **Fig. 4.2**. It is represented by a bilinear relationship to represent the elastic and plastic regions. The unloading path is parallel to the initial elastic path.

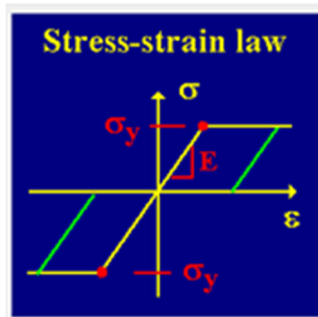


Fig. 4.2 Material model of steel [4.2]

4.2.5 Bond Model of Steel and Concrete

Perfect bond between concrete and reinforcement is assumed within the smeared concept. No bond slip can be directly modeled except for the one included inherently in the tension stiffening. The degradation of bond is expressed by the element characteristics of a composite element of concrete and steel.

4.2.6 Material Stiffness of Composite Material

The summation is over n smeared reinforcing components. In ATENA the smeared reinforcement is not added on the constitutive level, but it is modeled by separate layers of elements whose nodes are connected to those of the concrete elements. This corresponds to the assumption of perfect bond between the smeared reinforcement and concrete. This condition, however, is relaxed when the bond degradation must be considered.

Table 4.1 Parameters of constitutive model of concrete [4.2]

Parameter	Formula
Cylinder strength	$f'_c = -0.85f'_{cu}$
Tensile strength	$f'_t = 0.24f'_{cu}{}^{2/3}$
Initial elastic modulus	$f'_c = (6000 - 15.5f'_{cu})\sqrt{f'_{cu}}$
Poisson's ratio	$\nu = 0.2$
Softening compression	$w_d = -0.0005\text{mm}$
Type of tension softening	1-exponential, based on G_F
Compressive strength in cracked concrete	$c = 0.8$
Tension stiffening stress	$\sigma_{st} = 0$
Shear retention factor	variable
Tension-compression function type	linear
Fracture energy	$G_F = 0.000025f'_t{}^{ef}$ [MN/m]
Orientation factor for strain localization	$\gamma_{max} = 1.5$

4.3 FEM Simulation of RC Slab Bridges

The present design restoration method does not require FEM simulation. But, in this study, FEM simulation of RC slab bridge was carried out. This is to examine the appropriateness of the present method, to represent the typical RC slab bridge in size because preparation of such a large sample is difficult, to confirm the validity of the present method in case bond deterioration and other aging effect exists. That is, FEM simulation is used as an alternative method for load test.

A standard RC slab bridge with center to center length of 10.40m is designed as per AASHTO LRFD Bridge Design Specification [4.1] and simulated using FEM. Diameter 32mm reinforcing bars with c/c spacing of 180mm and cover thickness of 35mm are used. The material constants and the mesh data of the FEM model are shown in **Figs. 4.3 – 4.5**. The mesh consists of rectangular elements of 0.05m in size with 4 nodes and SBETA material model with compressive strength of 28MPa are used. Embedded type of reinforcing bar is used. For the reinforcing bar, yield strength of 400MPa with a bilinear stress-strain law and Young's modulus of 200GPa are used. For the analysis, load controlled method with a load increment of 1×10^{-3} MN and the standard Newton- Raphson method are used.

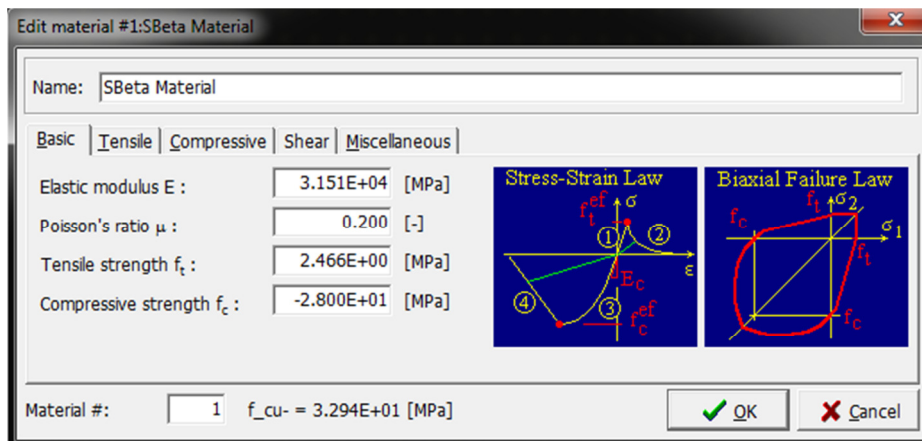


Fig. 4.3 Material data for concrete [4.2]

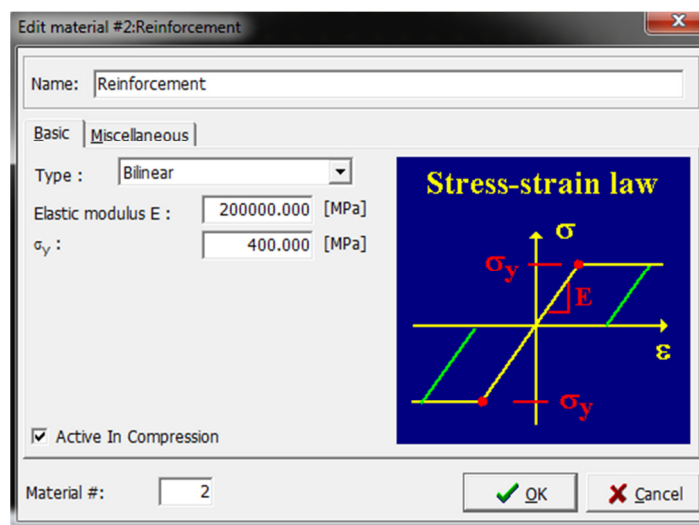


Fig. 4.4 Material data for reinforcement [4.2]

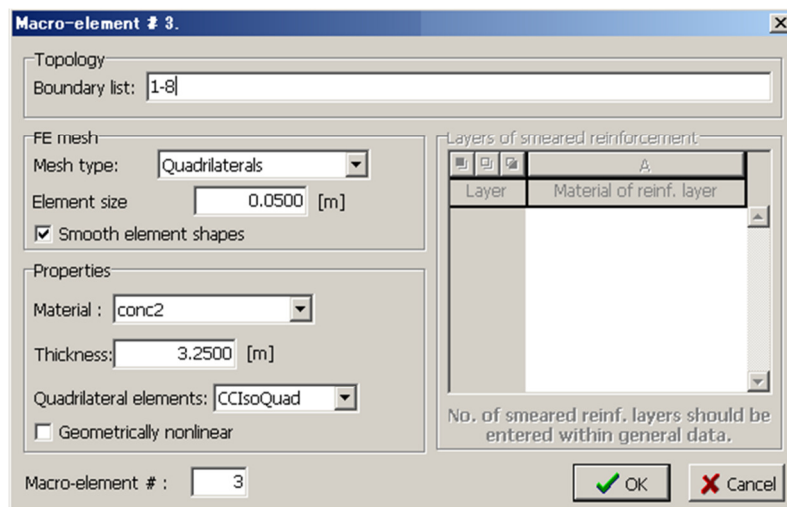


Fig. 4.5 Geometrical modeling of mesh [4.2]

In the simulation, half of the allowable limits permitted for measurement of dimensions are considered as a standard deviation. The statistical parameters of random variables used in FEM analysis are shown in **Table 4.2**. A two point load with a spacing of 2.0m is applied to the FEM model (**Fig. 4.6**). The meshing and position of reinforcing bar are shown in **Figs. 4.7- 4.8**. The locations of the rear load from the left support, x , are 2.2m, 3.2m and 4.2m to get the three deflection data. One load level with a magnitude of 100kN ($=2P$, P as a point load) is taken for the design restoration.

Table 4.2 Input variables

No.	Input variables	Mean values
1	Span length (mm)	10400
2	Effective width, b (mm)	3250
3	Total depth (mm)	540
4	Compressive strength of concrete (MPa)	28
5	Area of steel (mm^2/m)	4701.8
6	Cover thickness (mm)	35

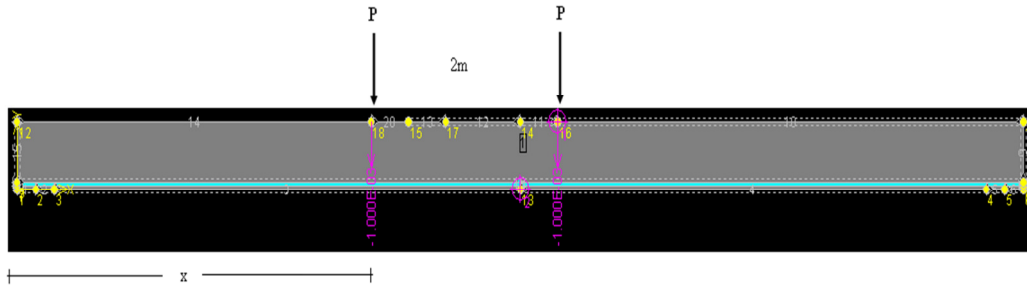


Fig. 4.6 FEM model of RC slab bridge

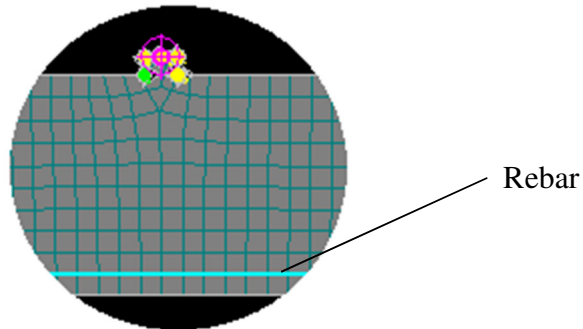


Fig. 4.7 Detail of FEM mesh and reinforcing bar

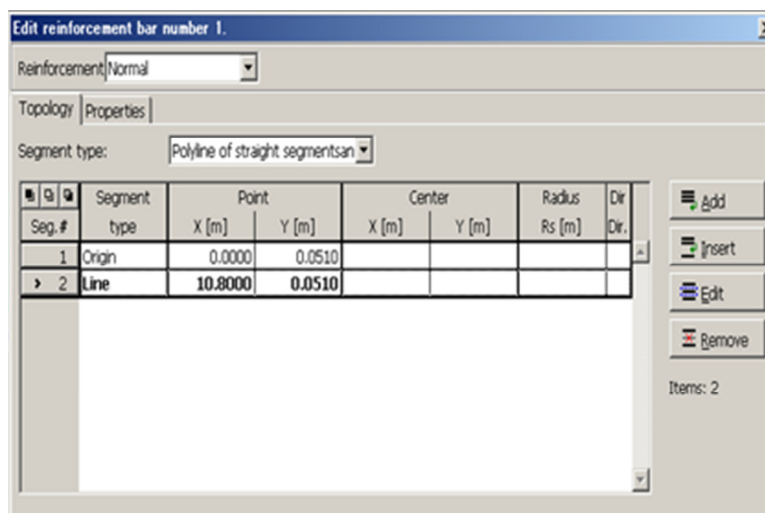


Fig. 4.8 Position of reinforcing bar [4.2]

The allowances for measurements of dimensions and tolerance, as per AASHTO Bridge Construction Specifications [4.3], for specified effective depth, d , and minimum clear concrete protection in flexural members, the tolerances on effective depth and cover thickness are given in **Table 4.3**. These allowable limits are used in FEM simulation.

Table 4.3 Tolerances on effective depth and cover thickness

Slab thickness	Tolerance on d	Tolerance on minimum cover
200 mm or less	± 9 mm	-9mm
More than 200 mm	± 12 mm	-12mm

But the tolerance on the clear distance to formed soffits shall be -6mm, and in no case shall the tolerance on cover exceed minimum 1/3 of the minimum cover stipulated on the structural drawings. For span length, the tolerance for the slab shall be 3mm/3000mm in the direction of traffic. Tolerance for bridge width is +5mm/m but +25mm is the maximum. A reasonable tolerance in spacing of reinforcing bars is +25mm [4.3].

For statistical analysis, six cases (each condition comprises of 32 combinations) are simulated using FEM. The input parameters used in the FEM simulation are bridge dimensions and material properties. These random variables are continuous and contains

small scatter. Effect of the random variables and their probabilistic distribution are analyzed and plotted. **Table 4.4** below shows the first two cases considered in FEM simulation.

Table 4.4 Two cases of FEM simulation

Case 1 (Normal condition)	Case 2 (Extreme condition)
Slip is disabled at bar beginning and end points (fully anchored bars)	Slip is allowed at bar beginning and end points

If severe damage (for instance cracking) is observed at the supports, this condition is expressed by bond deterioration. Such type of bridge is considered and modeled as Case 2. The load- mid span deflection curves for the mean values of Case 1, 2 and 3 are shown in **Fig. 4.9**. The location of the rear wheel from the left support is 4.2m.

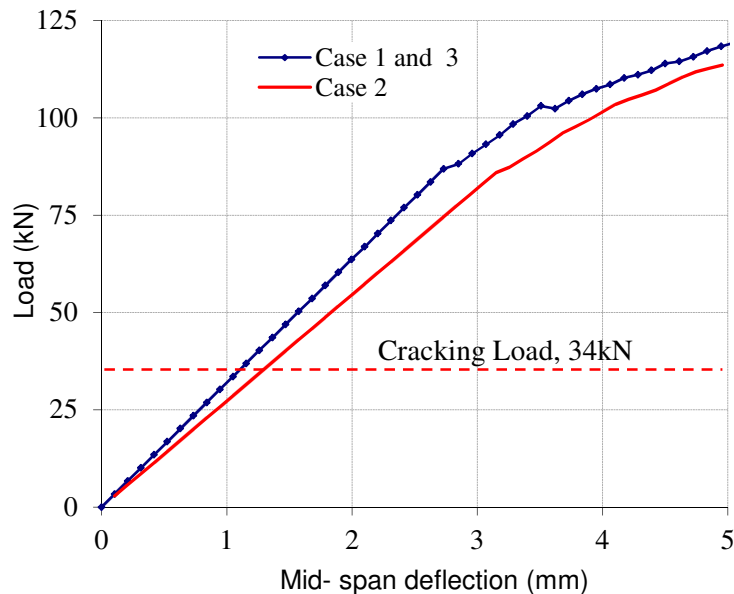


Fig. 4.9 Load- mid span deflection curves of mean values

Based on the results of FEM simulation, incremental instantaneous mid-span deflection due to applied load, the actual area of reinforcing bar, compressive strength of concrete and effective depth are computed using the elastic deflection equation. Three-dimensional influence function is attached in **APPENDIX D** to show the effect of three-dimensional deformation of a bridge on the design restoration result.

4.4 Experimental Investigations

4.4.1 Distribution of Dimensions and Cover Thickness

Although the specified concrete cover is normally carefully checked and controlled before placing the concrete, experience shows that significant deviations from the design value may still occur during concrete construction. The loads during placing the concrete may occasionally be too high compared to the stiffness of the rebar system, or the spacers may occasionally have been insufficiently or wrongly placed [4.4].

Experimental investigations on a control of achieved concrete cover thickness and dimensions of nine test beams at 180 locations were carried out. This helps to know the variations in measurements of dimensions and their distributions. The dimension of the test beams are 3.30x0.5m with a depth of 0.5m. The design cover thickness of the main bars is 52.5mm. Four bottom and three top reinforcing bars of diameter 35mm were provided [4.5]. The cross section of the beam is shown in **Fig. 4.10**. Measurement of dimensions is taken at 5 locations with equal intervals. For the stirrups, the cover thickness is measured at its mid-height. The achieved measurements in dimensions of the test beams are summarized in **Table 4.5** and their distributions are shown in **Figs. 4.11-13**. These distributions imply the appropriateness of the assumption of normal distribution for these parameters.

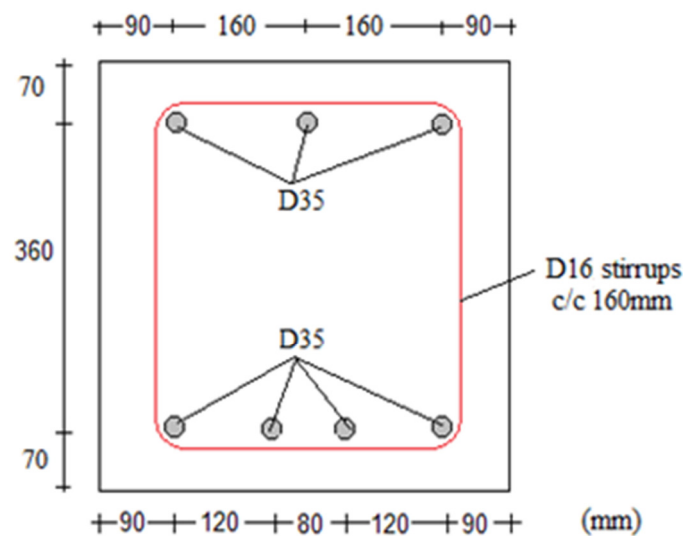
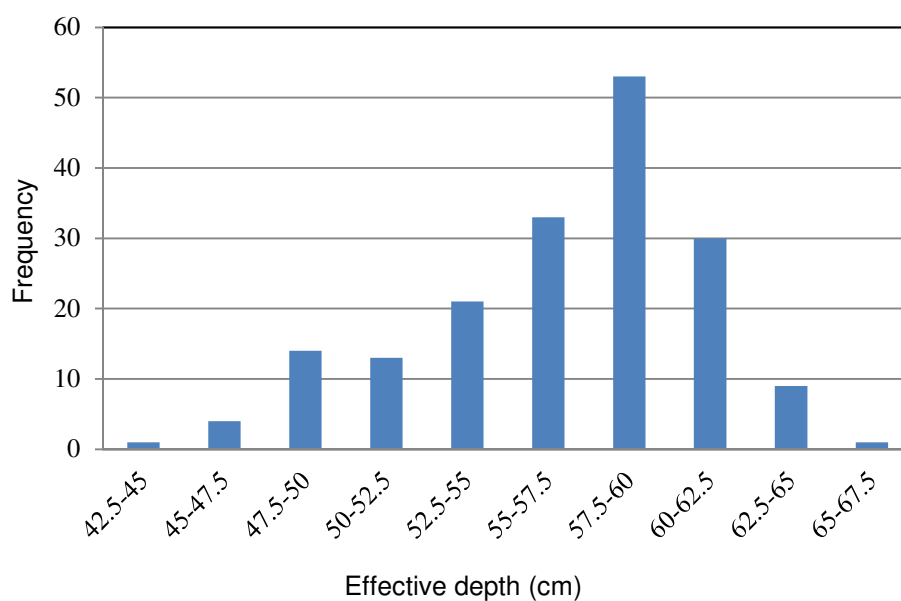
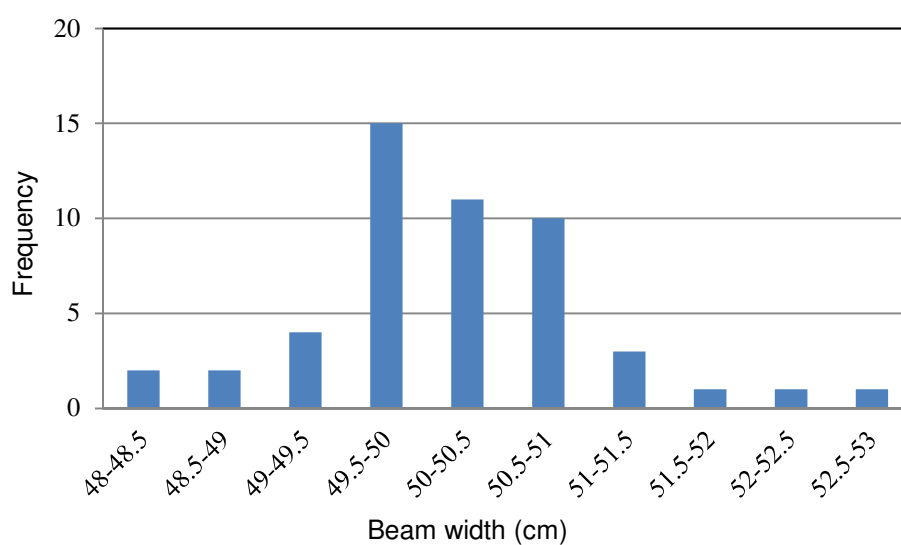


Fig. 4.10 Cross section of RC beam

Table 4.5 Achieved measurements of dimensions

	Cover thickness (mm)	Dimensions (mm)		
		Width	Depth	Length
Design values	52.5	500	500	3300
Mean	56.75	503.23	500.38	3301.3
Std. dev.	4.40	10.31	4.88	0.82
COV (%)	7.75	2.05	0.98	0.03

**Fig. 4.11** Effective depth distribution**Fig. 4.12** Top width distribution

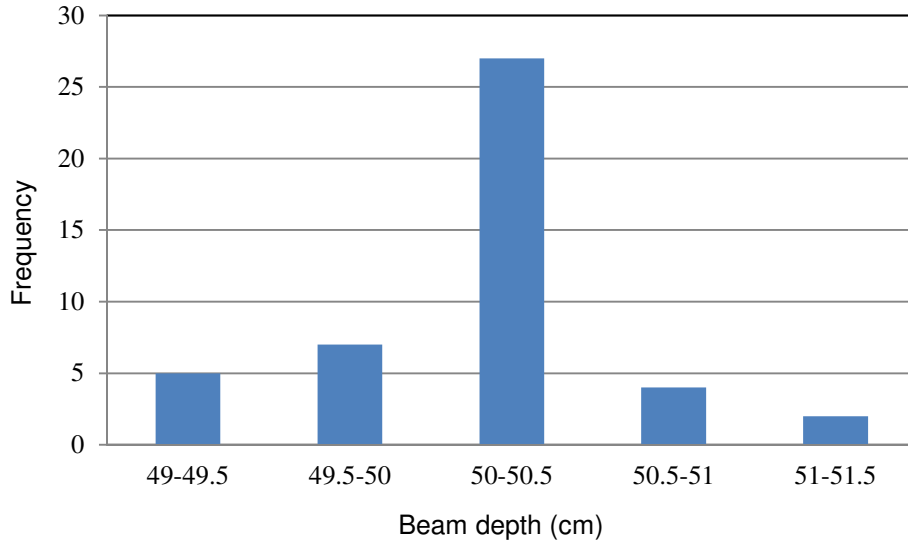


Fig. 4.13 Distribution of beam depth

The probability density function (or hereafter, probability density) and cumulative distribution function (or hereafter, cumulative percent) of achieved beam dimensions and cover thickness in RC test specimens, assuming normal distribution, are shown in **Figs. 4.14-4.16**.

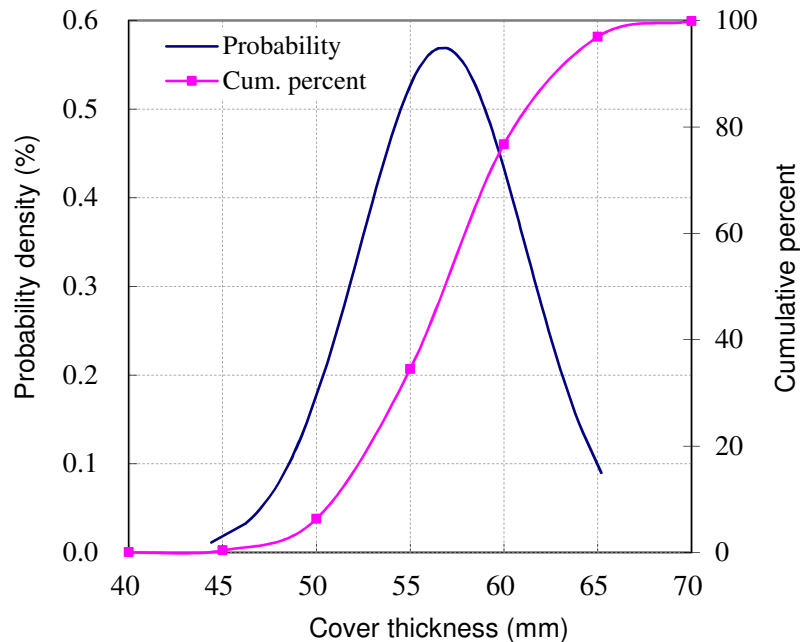


Fig. 4.14 Probability distribution of achieved cover thicknesses of main bars

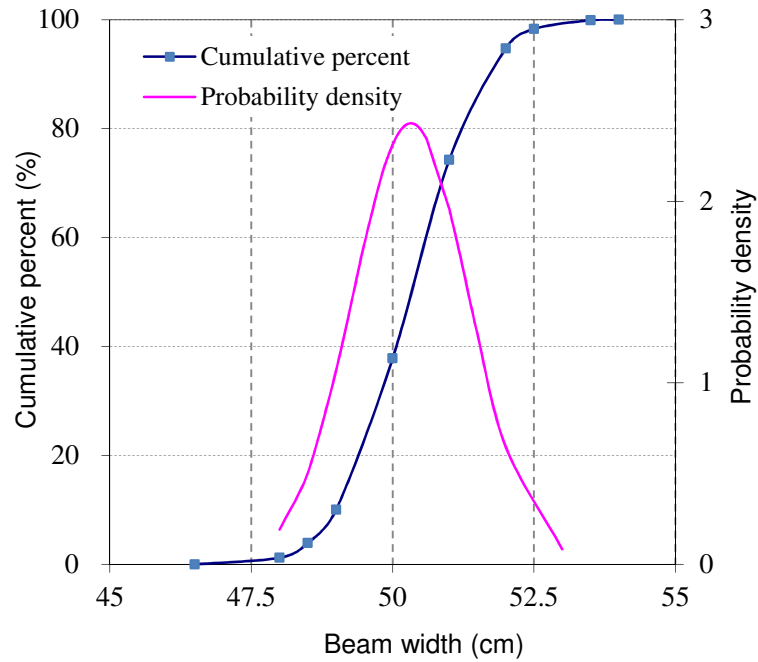


Fig. 4.15 Probability distribution of achieved beam widths (top width)

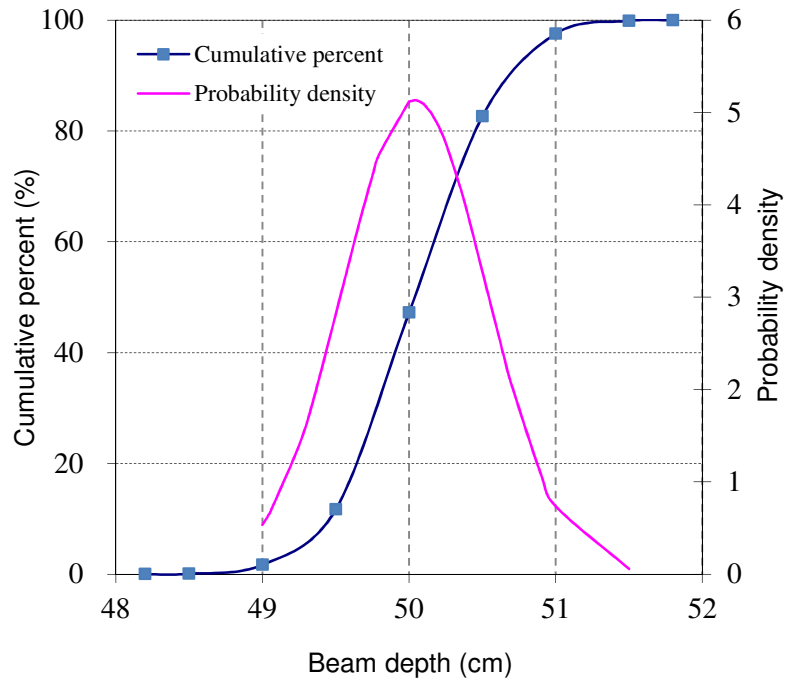


Fig. 4.16 Probability distribution of achieved beam depth

4.4.2 Load Test of RC Slab Specimen

The slab is rectangular in cross section of $b \times h = 600 \times 200$ mm, with overall length of 2700 mm and 2300 mm distance between supports [4.6]. Longitudinally, 8 mm diameter deformed bars on both top and bottom surfaces with a spacing of 40 mm were provided

(Fig. 4.17). Concrete with 28-day compressive strength, f'_c , of 19.37MPa and steel bar with yield strength of 344MPa were used. The experimental data is shown in Table 4.6. Load-mid span deflection relationship of the specimen is shown in Fig 4.18.

Table 4.6 Experimental data of RC slab specimen

No.	Input variables	Mean values
1	Span length (mm)	2300
2	Width (mm)	600
3	Total depth (mm)	200
4	Tension and compression bars	D8 c/c 40mm
5	Transverse bars	D6 c/c 40mm
6	Cover thickness (mm)	52.5
7	Compressive strength of concrete (MPa)	19.37
8	Yield strength of steel (MPa)	344

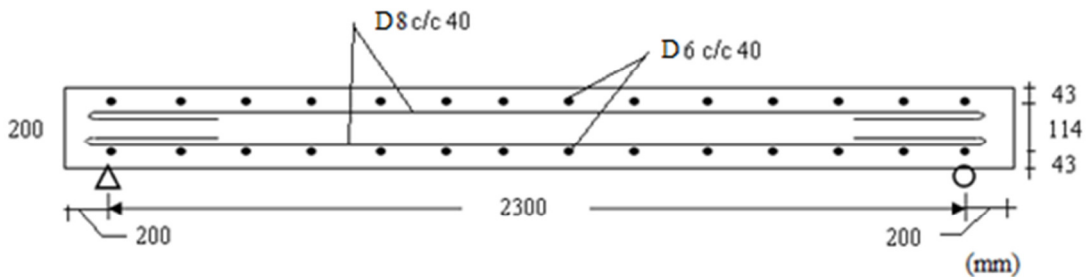


Fig. 4.17 Longitudinal section of specimen

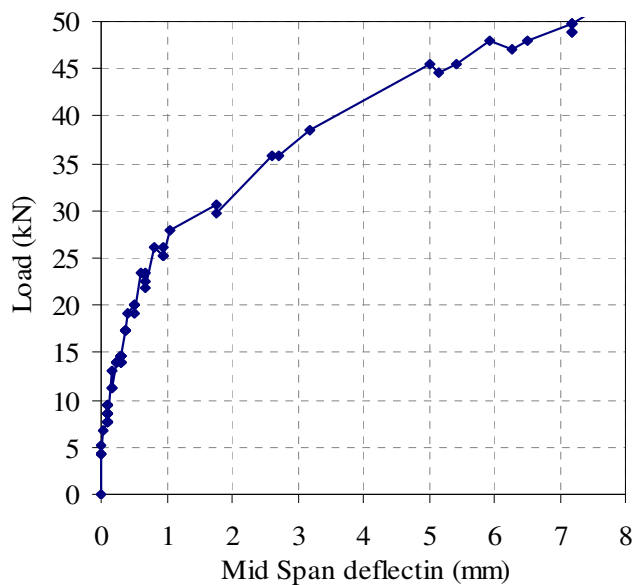


Fig. 4.18 Load-mid span deflection diagram [4.6]

4.4.3 Load Test of RC Beam Specimen-1

A beam with rectangular cross section of $b \times h = 500 \times 500\text{mm}$ (shown in **Fig. 4.10**), with overall length of 3200mm and 2800mm distance between supports was prepared [4.5]. Four deformed bars on the bottom and three deformed bars on the top with 35mm in diameter were provided. For the stirrups, 16mm diameter deformed bars with a spacing of 160mm were used.

Concrete with 28-day compressive strength, f'_c , of 31.82MPa and steel bar with yield strength of 528MPa were used. The experiment data is shown in **Table 4.7**. The specimen is simply supported at both ends and tested for two-point loading with loading points spaced at 400mm apart. Load-mid span deflection diagram is shown in **Fig. 4.19**.

Table 4.7 Experimental data of RC beam specimen

No.	Input variables	Mean values
1	Span length (mm)	2800
2	Width (mm)	500
3	Total depth (mm)	500
4	Area of steel, compression bars	3D35
5	Area of steel, tension bars	4D35
6	Cover thickness (mm)	52.5
7	Compressive strength of concrete (MPa)	31.82
8	Yield strength of steel (MPa)	528

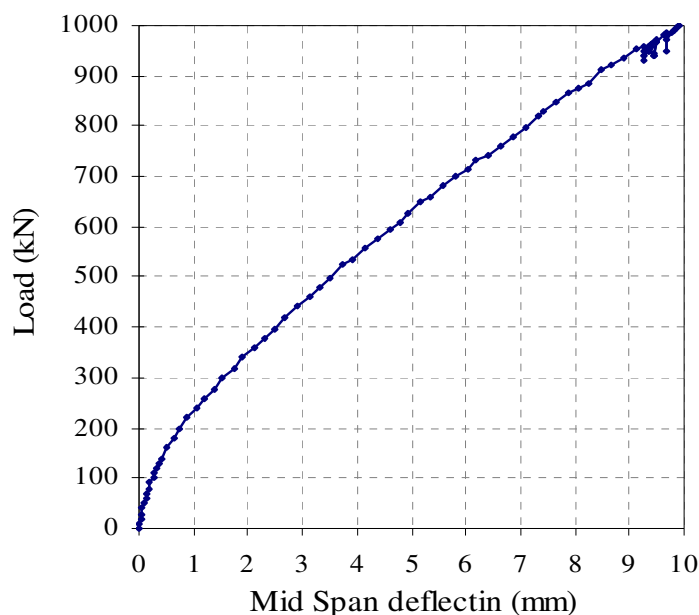


Fig. 4.19 Load-mid span deflection diagram [4.5]

4.4.4 Load Test of RC Beam Specimen-2

For verification of the design restoration method, a specimen similar to that of RC Beam Specimen-1 with an overall depth of 485mm and different cover thicknesses was prepared. **Fig. 4.20** and **Fig. 4.21** show the longitudinal profile and cross section of the beam, respectively. Loads are applied at different positions and it is shown in **Table 4.8**. Strain gauges for steel bars and concrete are attached at 0.4m intervals. The specimen was simply supported at both ends and tested for two-point loading with loading points symmetrically spaced at 400mm, 1200mm and 2000mm apart.

Initially, at the specified load positions, the beam was loaded with 70kN load (below cracking load). This test was repeated twice and subsequently a load beyond cracking load was applied at the same load positions. The maximum load applied was 300kN. The load deflection diagram and the cracking pattern are shown in **Fig. 4.22** and **Fig. 4.23**. Test results of RC beam specimen 2 are attached in **APPENDIX E**.

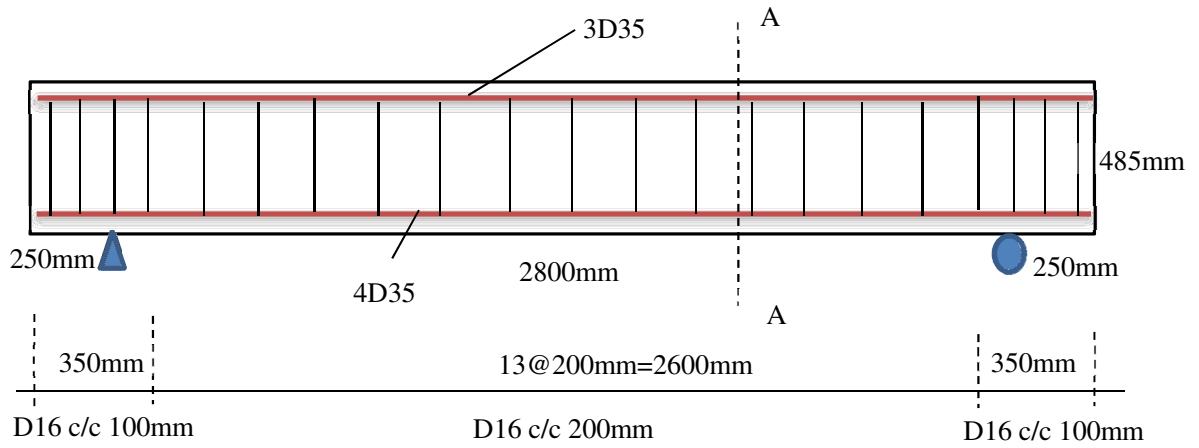


Fig. 4.20 Longitudinal section of RC test beam 2

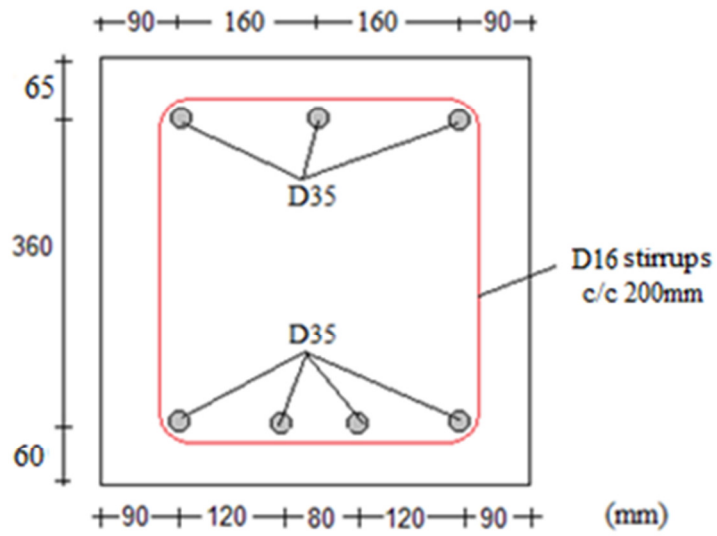


Fig. 4.21 Cross section of RC test beam 2

Table 4.8 Loading positions of RC beam test specimen

Load position	1 st load from left support (x)	Load spacing (y)
Pos_1	1.2m	0.4m
Pos_2	0.8m	1.2m
Pos_3	0.4m	2.0m

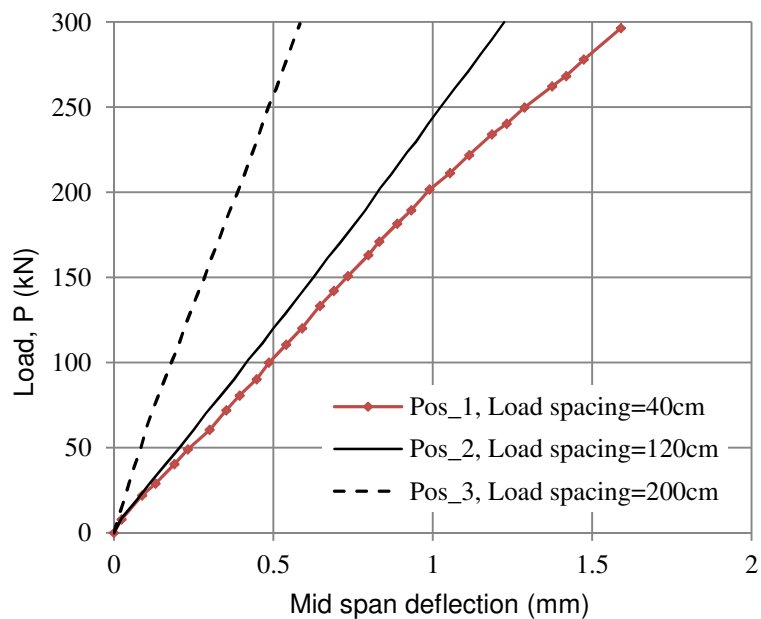


Fig. 4.22 Load- mid span deflection diagram (top surface)

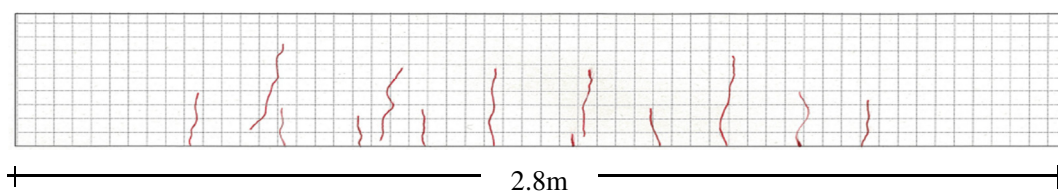


Fig. 4.23 Crack pattern at the end of loading of 300kN

4.5 Summary

- FEM simulation of bridges for different cases is shown.
- Experimental investigation under the achieved dimensions and concrete cover of RC beam specimens has been performed.

References

- [4.1] AASHTO: American Association of State Highway and Transportation Officials, LRFD Bridge Design Specifications, 4th edition, Washington, 2007.
- [4.2] Červenka, V., et al.: ATENA Program Documentation, Part 1-Theory, Prague, March 22, 2010.
- [4.3] AASHTO: American Association of State Highway and Transportation Officials, LRFD Bridge Construction Specifications, Washington, 2002.

- [4.4] Odd E. Gjørv: Durability Design of Concrete Structures in Severe Environments, Taylor & Francis Group, 2009.
- [4.5] Kurata, S.: Experimental Study for Mechanical Performance of Post-installed Shear Reinforcement, Master's Thesis, Graduate School, Yokohama National University, 2013.
- [4.6] Naganuma, H.: RC Jacketing Type Seismic Strengthening Method Using Perfobond Rib Shear Connectors, Master's Thesis, Graduate School, Yokohama National University, 2012.

5. ESTIMATION OF CURRENT VALUES, RESTORING INITIAL VALUES AND VERIFICATION OF PROPOSED METHOD

5.1 Introduction

As discussed in chapter 4, for the prediction of deflections, six different cases are simulated using FEM. These are:

Case 1: Bridges with two unknowns (A_s and d) and no bond deterioration at bar end points. This case comprises of 4 random variables (span length, effective width, total depth and compressive strength of concrete)

Case 2: Bridges with two unknowns (A_s and d) and bond deterioration at bar end points. This case comprises of 4 random variables (span length, effective width, total depth and compressive strength of concrete)

Case 3: Bridges with three unknowns (f_c^a , A_s and d). This case comprises of 6 random variables (span length, effective width, total depth, cover thickness, cross-sectional area of steel and compressive strength of concrete)

Case 4-6: Bridges with three unknowns (f_c^a , A_s and d) and different COVs.

Based on the results, incremental instantaneous mid-span deflection due to applied load, the current values of the bridges are estimated using the elastic deflection equation. Finally, the actual yield strength of steel is estimated using Eq. (3.17). In the equation, $E_s^a = 200\text{GPa}$, $C_E = 0.043$ and $\gamma_c = 24\text{kN/m}^3$ are used. For the estimation of actual yield strength of steel, the ultimate design moment, M_{sd} , of 705kN-m/m is used. The design restoration scheme is shown in **Fig. 5.1**.

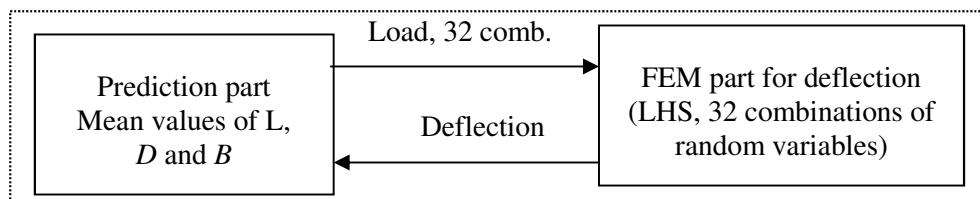


Fig. 5.1 Design restoration scheme

5.2 Estimation of Current Values

5.2.1 Bridges with Two Unknowns (Case 1 and 2)

The statistical parameters of random variables of Case 1 and 2 are shown in **Table 5.1**. The 32×4 LHS sampling of random variables is shown in **Table 5.2**.

Table 5.1 Statistical parameters of random variables (Case 1 and 2)

No.	Random variables	Mean values	COV (%)
1	Span length (mm)	10400	0.05
2	Effective width (mm)	3250	0.05
3	Total depth (mm)	540	1.10
4	Compressive strength of concrete (MPa)	28	5

Table 5.2 Sampling of random variables (Case 1 and 2)

Sampling no.	Random variables			
	1	2	3	4
1	26	8	5	4
2	7	24	3	19
3	6	27	2	30
4	19	29	27	7
5	5	6	13	8
6	24	16	8	18
7	18	5	23	27
8	4	14	21	24
9	9	19	17	25
10	25	32	15	11
11	12	7	1	3
12	15	13	14	9
13	16	31	31	29
14	32	15	30	2
15	1	28	11	15
16	21	10	18	5
17	28	20	4	16
18	8	17	10	17
19	2	3	7	22
20	11	25	22	32
21	20	21	25	1
22	22	9	6	23
23	13	18	26	21
24	17	22	19	10
25	3	2	29	12
26	14	12	28	6
27	27	23	12	28
28	29	26	24	20
29	30	4	16	26
30	31	30	32	13
31	23	11	9	31
32	10	1	20	14

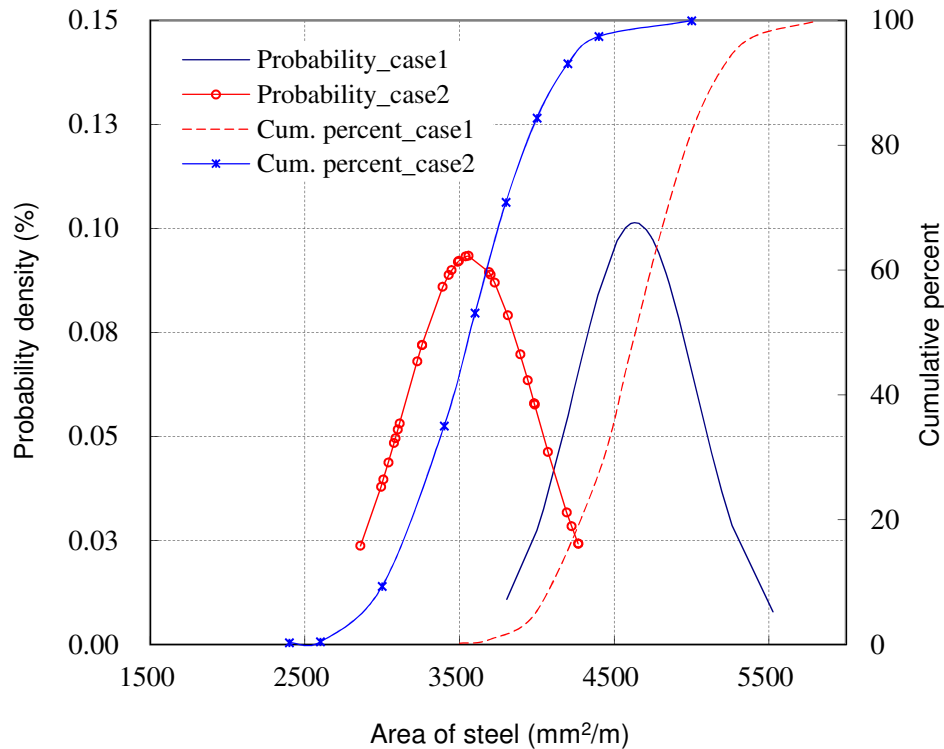
Results of statistical analysis showing mean value, standard deviation and coefficient of variation of the set of random variables are shown in **Table 5.3**.

Table 5.3 Results of statistical analysis (Case 1 and 2)

	Estimated values (Case 1)			Estimated values (Case 2)		
	d^a (mm)	A_s^a (mm ² /m)	f_y^a (MPa)	d^a (mm)	A_s^a (mm ² /m)	f_y^a (MPa)
Mean	489.47	4636.45	377.51	490.50	3566.03	482.31
Std. dev.	5.73	393.64	30.09	3.39	426.99	50.59
COV (%)	1.17	8.49	7.97	0.69	11.97	10.49

For Case 2, the reinforcement area is reduced. This loss in cross-sectional area is considered as bond deterioration and aging. As a result of this, the yield strength of steel is greater than that of Case 1. Practically, to account the effect of bond deterioration, the reduction in moment capacity should be investigated.

The probabilistic distributions of the estimated actual area of steel and yield strength of steel, for both conditions, following normal distribution function are shown in **Fig. 5.2** and **Fig. 5.3**, respectively. Moreover the cumulative percent distributions are plotted.

**Fig. 5.2** Probabilistic distribution of A_s^a (Case 1 and 2)

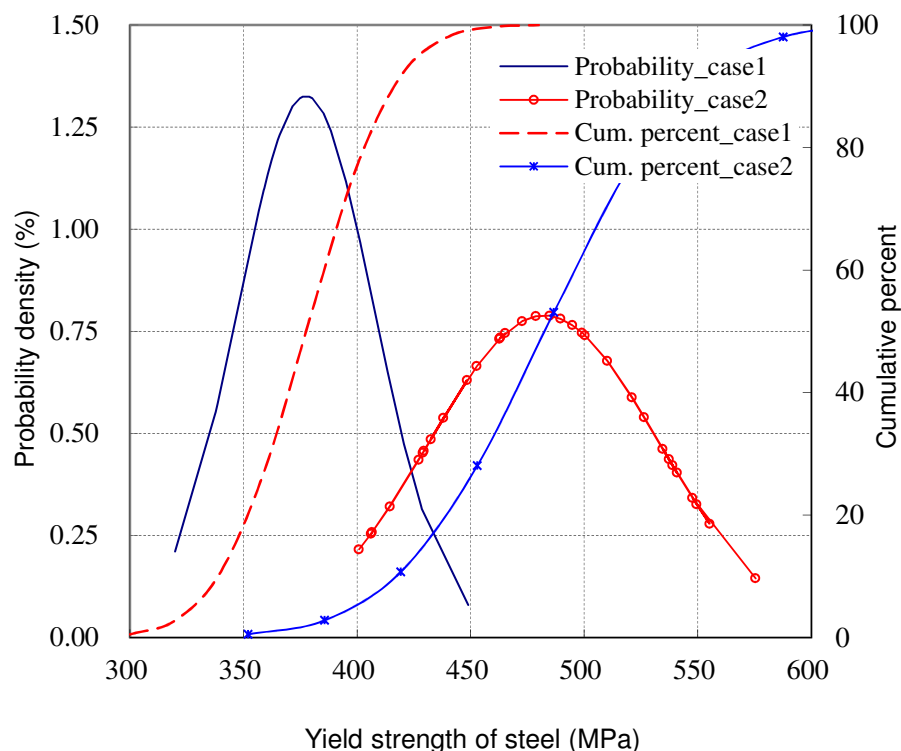


Fig. 5.3 Probabilistic distribution of f_y^a (Case 1 and 2)

Based on the results, confidence limits for the mean values with 95 % confidence levels are estimated. Thus, the confidence intervals for the mean value of f_y^a and A_s^a are shown in **Table 5.4**.

Table 5.4 Confidence intervals for f_y^a and A_s^a (Case 1 and 2)

Cases	f_y^a (MPa)		A_s^a (mm ² /m)	
	Lower limit	Upper limit	Lower limit	Upper limit
Case 1	367.08	387.93	4499.94	4772.96
Case 2	464.783	499.837	3418.05	3713.95

For the typical RC slab bridge case, with 95 % confidence levels, confidence intervals of $\pm 2.76\%$ and $\pm 3.66\%$ of the mean values of f_y^a for Case 1 and 2 are obtained respectively.

Using the estimated effective depth, the cover thickness of the simulated bridge for both cases are computed and their cumulative percent distributions are plotted in **Fig. 5.4**.

For Case 1, an average concrete cover of 33.75mm with a standard deviation of 3.12mm and COV of 9.28% is obtained, which has a variation of -3.57% from the actual cover thickness. Almost the same result is obtained for Case 2.

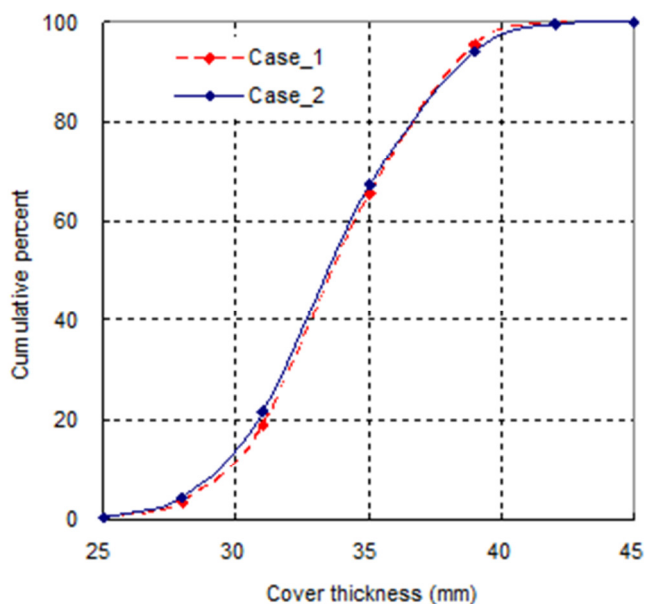


Fig. 5.4 Distribution of cover thickness (Case 1 and 2)

5.2.2 Bridges with Three Unknowns (Case 3)

The statistical parameter of random variables of Case 3 and the 32x 6 LHS sampling of random variables are shown in **Table 5.5** and **Table 5.6** respectively.

Table 5.5 Statistical parameter of random variables (Case 3)

No.	Random variables	Mean values	COV (%)
1	Span length (mm)	10400	0.05
2	Effective width, b (mm)	3250	0.05
3	Total depth (mm)	540	1.10
4	Compressive strength of concrete (MPa)	28	10.0
5	Area of steel (mm^2/m)	4701.80	5.0
6	Cover thickness (mm)	35	7.75

Table 5.6 Sampling of random variables (Case 3)

Sampling no.	Random variables					
	1	2	3	4	5	6
1	26	8	5	4	14	18
2	7	24	3	19	29	10
3	6	27	2	30	26	22
4	19	29	27	7	22	9
5	5	6	13	8	5	3
6	24	16	8	18	4	2
7	18	5	23	27	11	6
8	4	14	21	24	12	14
9	9	19	17	25	13	8
10	25	32	15	11	2	11
11	12	7	1	3	15	26
12	15	13	14	9	8	29
13	16	31	31	29	32	5
14	32	15	30	2	30	1
15	1	28	11	5	18	21
16	21	10	18	5	18	21
17	28	20	4	16	21	28
18	8	17	10	17	9	27
19	2	3	7	22	23	25
20	11	25	22	32	24	12
21	20	21	25	1	6	23
22	22	9	6	23	19	16
23	13	18	26	21	20	13
24	17	22	19	10	7	17
25	3	2	29	12	28	20
26	14	12	28	6	17	19
27	27	23	12	28	10	24
28	29	26	24	20	3	7
29	30	4	16	26	1	31
30	31	30	32	13	27	15
31	23	11	9	31	6	4
32	10	1	20	14	25	32

The probabilistic distributions of the estimated values of f_c^a , A_s^a , d^a and f_y^a are shown in **Figs. 5.5-5.8**, respectively. The mean and standard deviations of the estimated values are shown in parentheses. Based on the results, confidence limits for the mean

values with 95 % confidence levels are estimated and the confidence intervals are shown in **Table 5.7**.

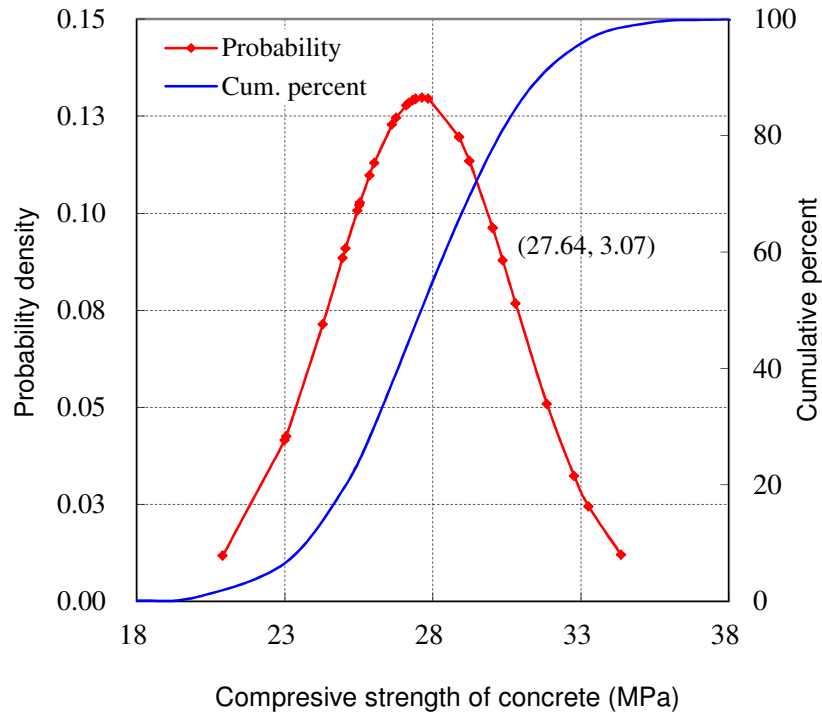


Fig. 5.5 Probabilistic distribution of f_c^a (Case 3)

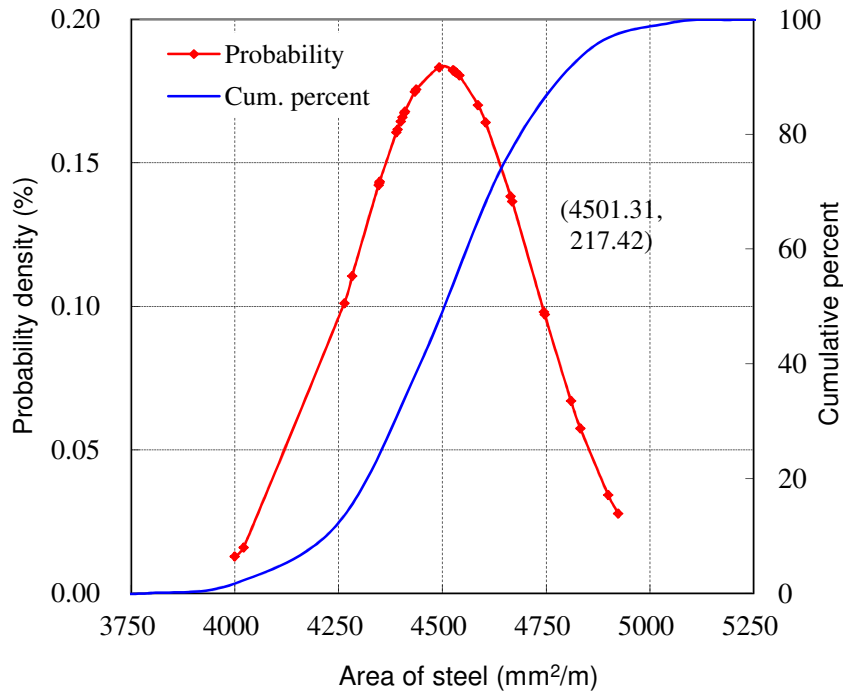


Fig. 5.6 Probabilistic distribution of A_s^a (Case 3)

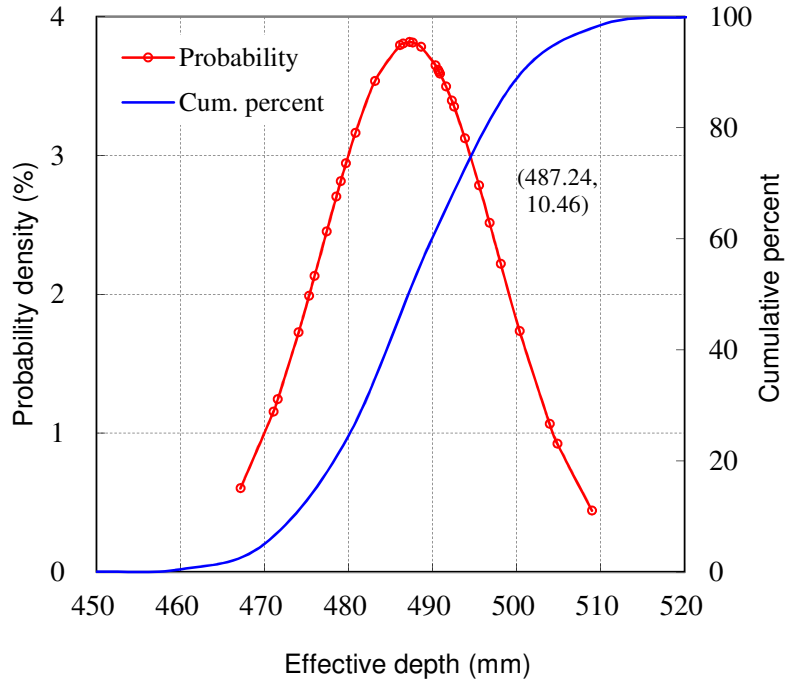


Fig. 5.7 Probabilistic distribution of d^a (Case 3)

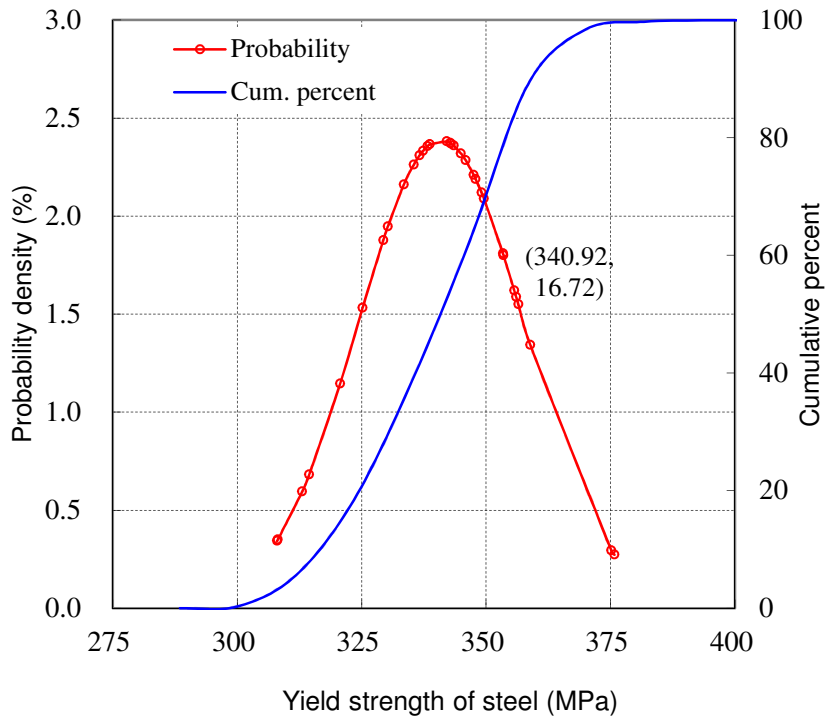


Fig. 5.8 Probabilistic distribution of f_y^a (Case 3)

Table 5.7 Confidence intervals of variables (Case 3)

Parameters	Mean values	COV (%)	Lower limit	Upper limit
f_c^a (MPa)	27.64	11.11	26.58	28.71
A_s^a (mm ² /m)	4501.31	4.83	4425.98	4576.64
d^a (mm)	487.24	2.14	483.61	490.86
f_y^a (MPa)	340.92	4.90	335.13	346.72

Comparison of design restoration results obtained using the present and the conventional method is shown in **Table 5.8**. The lower and upper limits are computed based on the accuracies given in the conventional method [APPENDIX A]. The accuracy of the present method is calculated using the confidence limits shown in **Table 5.7**. As shown in **Table 5.8**, the accuracy of the present method is better than the conventional method.

Table 5.8 Comparison of results (Case 3)

Parameters	Present method		Conventional method		
	Mean values	Accuracy	Lower limit	Upper limit	Accuracy
f_c^a (MPa)	27.64	±3.85%	25.2	30.8	±10%
A_s^a (mm ² /m)	4501.31	±0.6mm*	3870.64	4861.32	±1-2mm*
d^a (mm)	487.24	±3.62mm**	485	495	±5mm**
f_y^a (MPa)	340.92	±1.70%	396.06	344.66	±6.94%

* The accuracy is for bar diameter.

** The accuracy is for concrete cover.

Actually, the scatter or tolerance in measurements of dimensions, cover thickness and compressive strength of concrete of structures is much larger than expected. For instance, the achieved scatter in reinforcement cover of Gimsoystraumen bridge is 30.0% [5.1]. Dimensional tolerances for concrete structures [5.2, 5.3 and 5.4] are shown in **Table 5.9**.

Table 5.9 Summary of tolerances

No.	Random variables	Tolerances [5.2]	Tolerances [5.3]	Tolerances [5.4]
1	Span length	½ inch in 20ft	+13mm or -5mm	¾ inch
2	Effective width	½ inch in 20ft	+13mm or -5mm	¾ inch
3	Total depth	½ inch	± 6mm	Bridge slabs vertical dimension +¼ inch, - 1/8 inch
4	Effective depth/cover thickness	d of 8 inches or less: ± ¼ inch d between 8 and 24 inches: ± 3/8 inch d of 24 inches or more: ± ½ inch	+25mm or -0mm	When member size is over 12 inch, tolerance in cover thickness is -½ inch. Reduction in cover shall not exceed one-third of the specified concrete cover.

FEM simulation of RC slab bridge with large scattering in cover thickness and measurements of dimensions, including data from actual field investigations, is conducted. The final design restoration results are summarized in **Table 5.10**. As shown in **Table 5.10**, the result shows that the input and output COVs of random variables are of the same order.

Table 5.10 Summary of design restoration results

Cases	Input value			Output value			
	Random variable	Mean	COV (%)	Mean	COV (%)	Lower limit	Upper limit
Case 4	f'_c (MPa)	28	10	24.75	8.91	23.98	25.52
	f_y (MPa)	400	-	320.65	5.41	320.05	321.25
	A_s (mm ² /m)	4701.8	10	4803.5	7.90	4672.02	4934.98
	d' (mm)	51	10	54.87	8.97	53.17	56.58
Case 5	f'_c (MPa)	Same	15	24.52	13.58	23.37	25.67
	f_y (MPa)		-	314.49	9.15	304.52	324.45
	A_s (mm ² /m)		15	5025.98	10.69	4839.75	5212.22
	d' (mm)		20	61.89	18.78	55.38	63.40

Cases	Input value			Output value			
	Random variable	Mean	COV (%)	Mean	COV (%)	Lower limit	Upper limit
Case 6	f_c^a (MPa)	28	20	25.36	20.41	23.30	27.42
	f_y^a (MPa)	400	-	334.18	15.61	316.10	352.26
	A_s^a (mm ² /m)	4701.8	20	4751.21	14.97	4504.79	4997.63
	d^a (mm)	51	30	58.32	22.98	53.68	62.96

Quantitatively, sensitivity analysis and contributions of the uncertainty of random variables on the function M_y^a , in terms of rank coefficient (r_p), are computed and the results are shown in **Table 5.11**. and **Table 5.12**, respectively. Based on **Fig. 3.10**, the yield moment equation given in Eq. (5.1) is considered as an objective function.

$$M^a = \frac{b^a (y^a)^3 + 3n[A_{s2}^a (y^a - d_2^a)^2 + \sum_{i=1}^r (A_{si}^a (d_{li}^a - y^a)^2)]}{3n(d_{l1}^a - y^a)} f_y^a \quad (5.1)$$

Table 5.11 Uncertainty analysis of random variables

Variables	Case 1 and 2		Case 3		Case 4		Case 5		Case 6	
	COV _i (%)	$U_{x.F}$								
A_s^a	5	4.85	5	4.85	10	9.70	15	14.55	20	19.40
d^a *	5	-0.40	7.75	-0.62	10	-0.80	20	-1.60	30	-2.4
f_c^a	5	0.009	10	0.018	10	0.018	15	0.027	20	0.036

* The COVs are for concrete cover.

Table 5.12 Rank correlation coefficient r_p

Random variables	Case 1 and 2	Case 3	Case 4	Case 5	Case 6
A_s^a	0.96	0.96	0.95	0.96	0.98
d^a	-0.02	-0.02	-0.09	-0.34	-0.35
f_c^a	0.23	0.24	0.22	0.25	0.20

As shown in the **Table 5.11** and **Table 5.12**, the largest contributions to M_y^a are cross-sectional area of steel bar and cover thickness. From these tables, it is also observed that the uncertainty of the random variables is linearly related to the input COV and the nonlinearity of the system is moderate. Thus, under the constraining condition of constant yield strength of steel and no severe bond damage between concrete and steel bars with linear strain relationship, LHS method is considered suitable.

5.3 Restoring Initial Design Values

Design restoration, which is important to estimate the initial condition of bridges, is a basic tool for capacity performance assessment [5.5]. In the following subsections, initial conditions of bridges such as material strengths, dimensions, cross-sectional area of steel bar and position of reinforcing bars are estimated based on the current values.

5.3.1 Material Strengths

The design values of compressive strength of concrete and yield strength of steel are selected from the nearest small discrete nominal design value given in design standards. Initial design value of compressive strength of concrete can also be obtained from the compressive strength development curve of concrete. The rate of gain of compressive strength of concrete, strength development of concrete, with a water/ cement ratio of 0.49 made with cements of different types is shown in **Fig. 5.9** [5.6].

For yield strength of steel, based on the estimated value, the design value of f_y is selected from the nearest small discrete nominal value. The different discrete nominal yield strengths of steel [5.7] are shown in **Table 5.13**. Moreover, the values by the standard specification as per JSCE [5.8] are given in **Table 5.14**.

Table 5.13 Discrete nominal yield strength, f_y

AASHTO M31 M Grade	Grade 300	Grade 420	Grade 520
Tensile strength, min. MPa	500	620	690
Yield strength, min. MPa	300	420	520

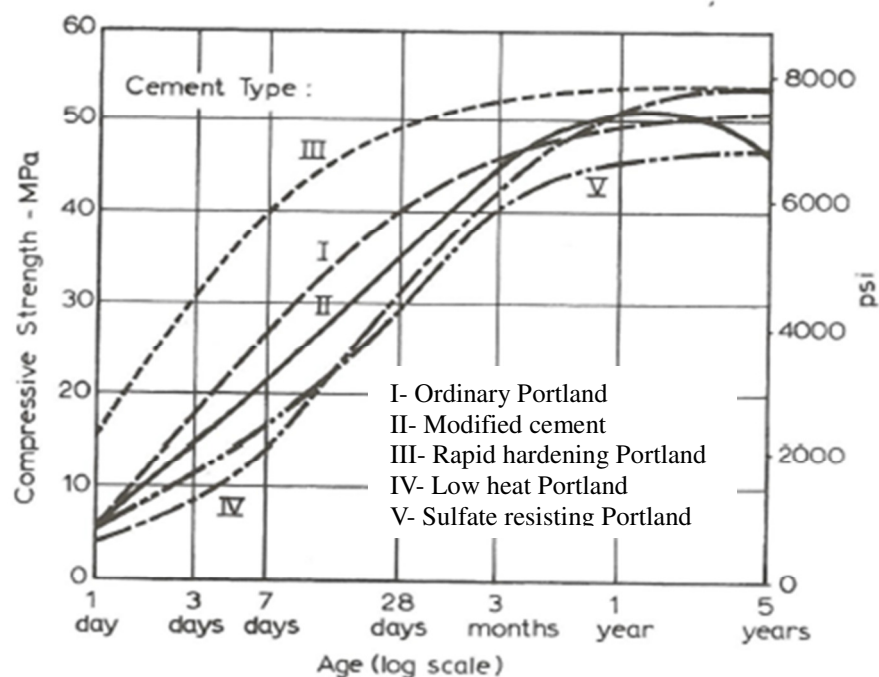


Fig. 5.9 Compressive strength development curve of concrete [5.6]

Table 5.14 Steel properties in JSCE Standard Specifications

Published in 1956 Type of bar	Tensile strength (kgf/mm ²)	Yield point (kgf/mm ²)
JIS G 3101 Steel Bar,		
Type 2, SS41	41	≥ 23
Type 3, SS50	50	≥ 28
Type 4, SS39	39	≥ 24
Type 5, SS49	49	≥ 30
JIS G 3110 Deformed Round Bar,		
Type 1, SSD39	39	≥ 24
Type 2, SSD49	49	≥ 30

5.3.2 Bridge Dimensions

The initial dimension of the bridges can be estimated using permitted allowances given in ASSHTO LRFD specification [5.9].

5.3.3 Cross-sectional Area of Steel

The original cross-sectional area of steel, A_s , is computed based on deterioration factors. The residual cross-sectional loss of the embedded bar can be estimated through the following expression for the diameter [5.10]:

$$\phi_t = \phi_0 - \alpha P_x \quad (5.2)$$

where, ϕ_t : residual diameter at time t (mm)

ϕ_0 : nominal diameter (mm)

α : is equal to 2 (for carbonated concrete) and it is up to 10 at the pits (chloride contaminated concrete)

P_x : average value of the attack penetration (mm)

Alternatively, Eq. (5.2) can be simplified and written as follows:

$$A_s^a = A_s (1 - \delta)^2 \quad (5.3)$$

where, A_s : nominal steel area (mm²)

δ : decrease in steel bar diameter (%)

It was found that the accelerated corrosion setup provided a steel mass content loss of 12 % in the corroded region, corresponding to an average decrease in steel bar diameter by 6 % [5.11]. In this study, two δ values (3% and 6%) are considered and the corresponding probabilistic distribution of A_s is shown in **Fig. 5.10**.

5.3.4 Effective Depth

To estimate the initial effective depth, d , the COV of cover thickness obtained from the test beam specimens (**Table 4.5**) is used. The initial cover thickness can be estimated from Eq. (5.4). The probabilistic distribution of initial effective depth is shown in **Fig. 5.11**.

$$d = D^a - [(D^a - d^a)(1 - \text{COV})] \quad (5.4)$$

where, D^a : actual total depth (mm)

d : initial effective depth (mm)

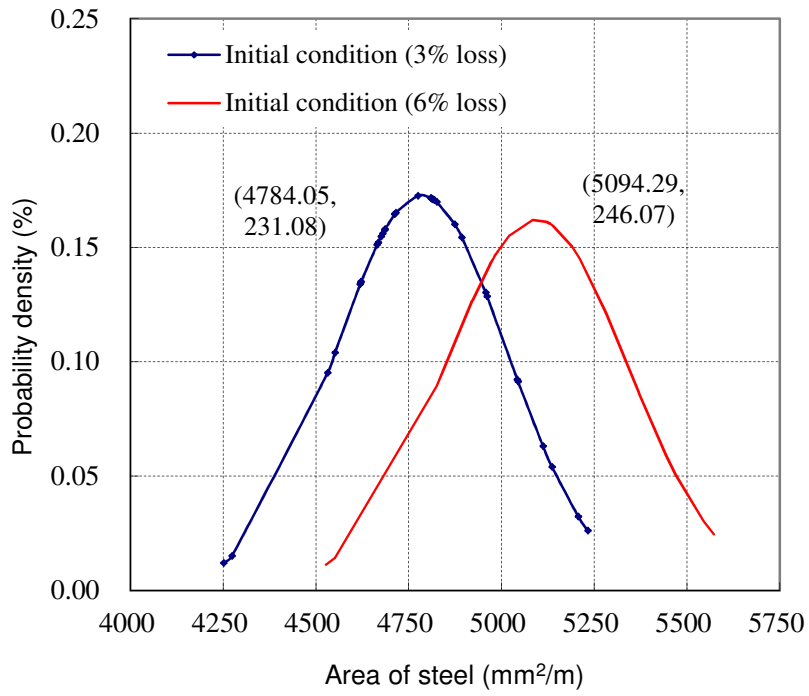


Fig. 5.10 Probabilistic distribution of A_s (Case 3)

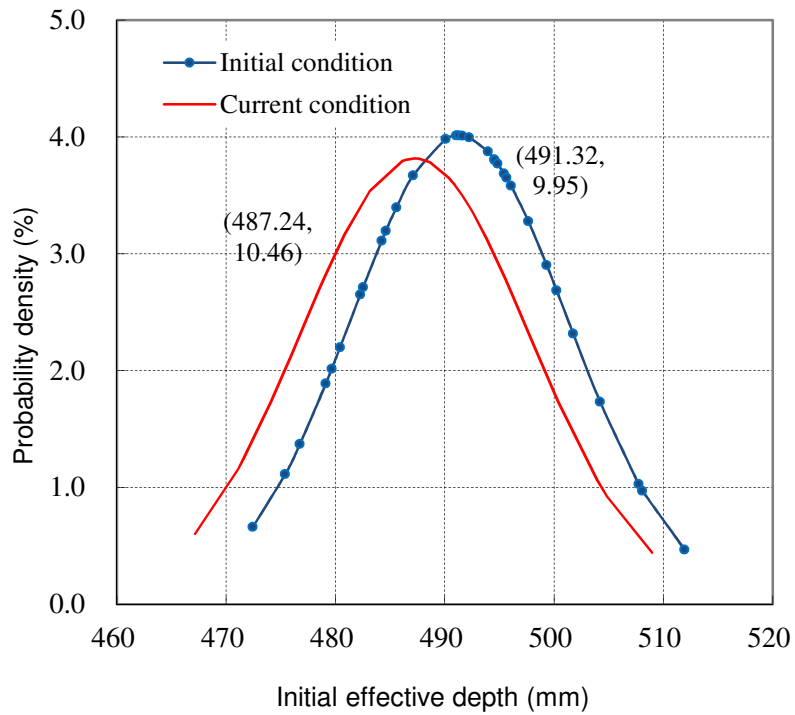


Fig. 5.11 Distribution of initial effective depth, d (Case 3)

Alternatively, the initial design values are restored using a graphical method. The design moment is taken as 705kN-m/m. The corresponding initial design values are restored from **Fig. 5.12**; $A_s = 4541.46\text{mm}^2/\text{m}$, $d = 489.34\text{mm}$ and $f'_c = 26.69\text{MPa}$.

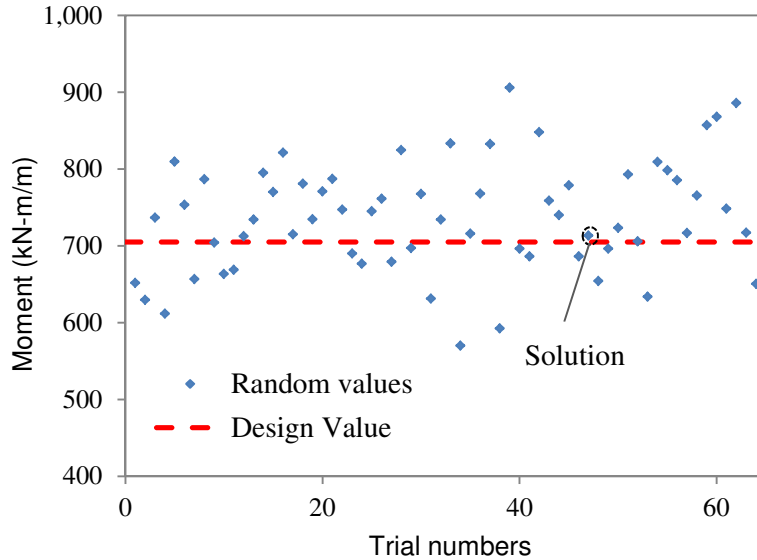


Fig. 5.12 Distribution of moment

5.4 Verification of Proposed Method

Test specimens of RC slab and RC beams are used to verify analytical results. For the probabilistic design restoration of these test specimens, the coefficients of variation for dimensions (**Table 4.5**) are used and 0.1% COV is considered for the deflection. The same 32x 6 LHS table shown in **Table 5.6** with random variables, in the order of length, width, depth and three deflections (δ_1 , δ_2 and δ_3), is used. In addition the result which is obtained from the FEM simulation is verified by using the proposed method.

5.4.1 Design Restoration for Test Specimens

5.4.1.1 RC Slab Specimen

The slab is rectangular in cross section of $b \times h = 600 \times 200\text{mm}$, with overall length of 2700mm and 2300mm distance between supports [5.12]. Longitudinally, 8mm diameter deformed bars on both top and bottom surfaces with a spacing of 40mm were provided (**Fig. 5.13**). Concrete with 28-day compressive strength, f'_c , of 19.37MPa and steel bar with yield strength of 344MPa were used.

The specimen is simply supported at both ends and tested for two-point loading with loading points symmetrically spaced at 400mm apart. The load-mid span deflection diagram is shown in **Fig. 5.14**. Three load levels with 10kN intervals are used for the design restoration.

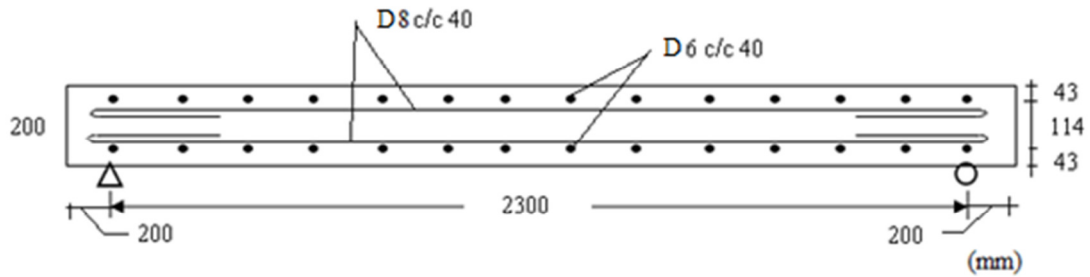


Fig. 5.13 Longitudinal section of specimen

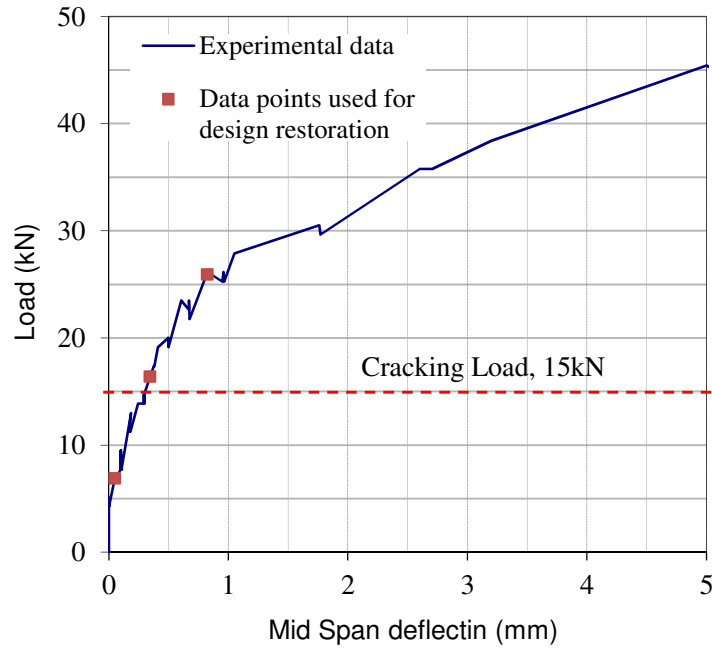


Fig. 5.14 Load- mid span deflection diagram [5.12]

For a particular load and mid-span deflection, within the elastic range, the area of steel reinforcement embedded in concrete and the effective depth are obtained using elastic deflection equation. The probabilistic distributions of the estimated values are shown in **Figs. 5.15-5.18**. $M^d = 46.18$ kN-m/m. The confidence limits for the mean values with 95 % confidence levels are estimated and the confidence intervals are shown in **Table 5.15**. The comparison of results is given in **Table 5.16**.

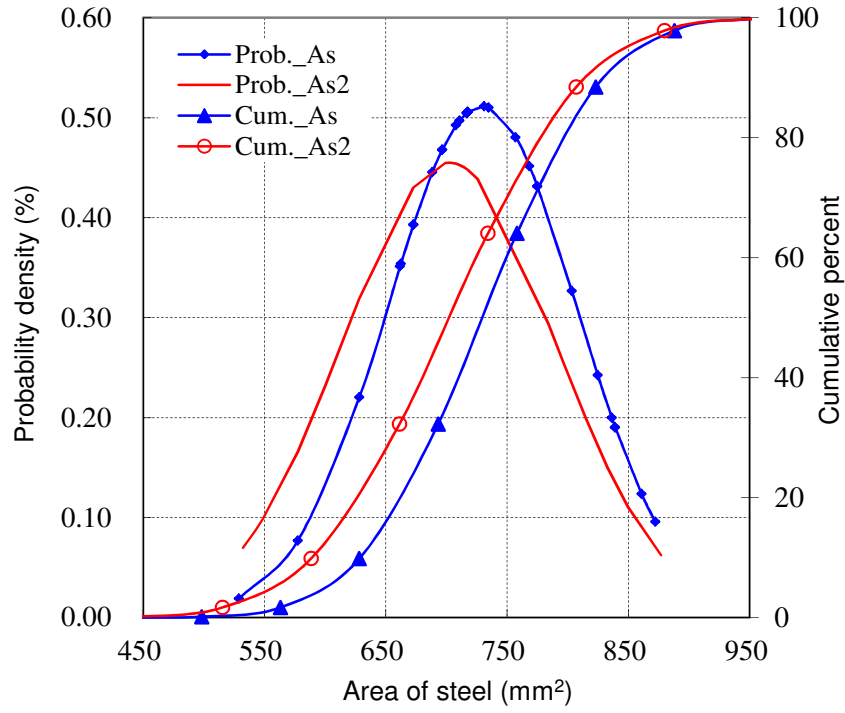


Fig. 5.15 Probabilistic distribution of A_s^a and A_{s2}^a

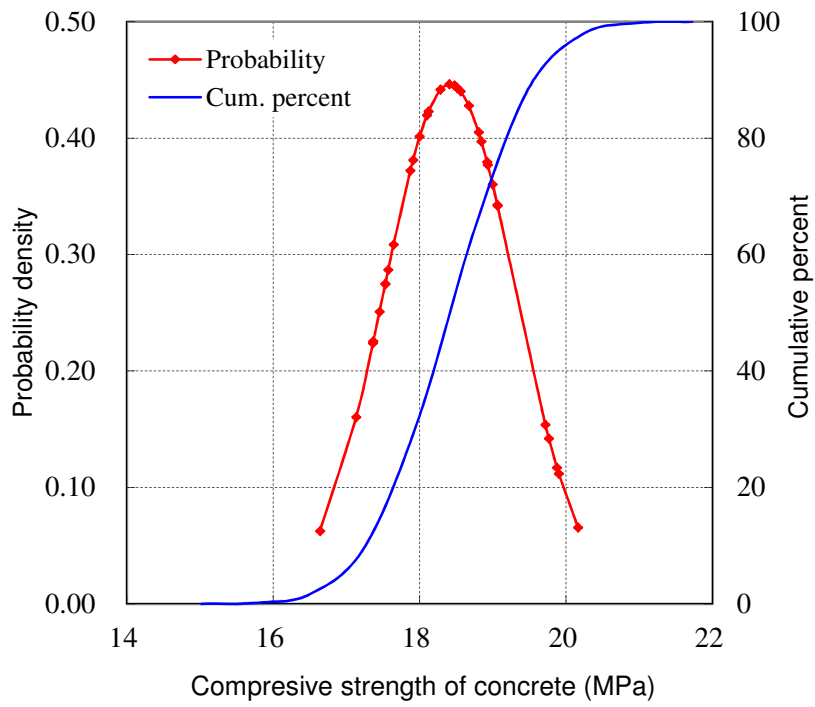


Fig. 5.16 Probabilistic distribution of f_c^a

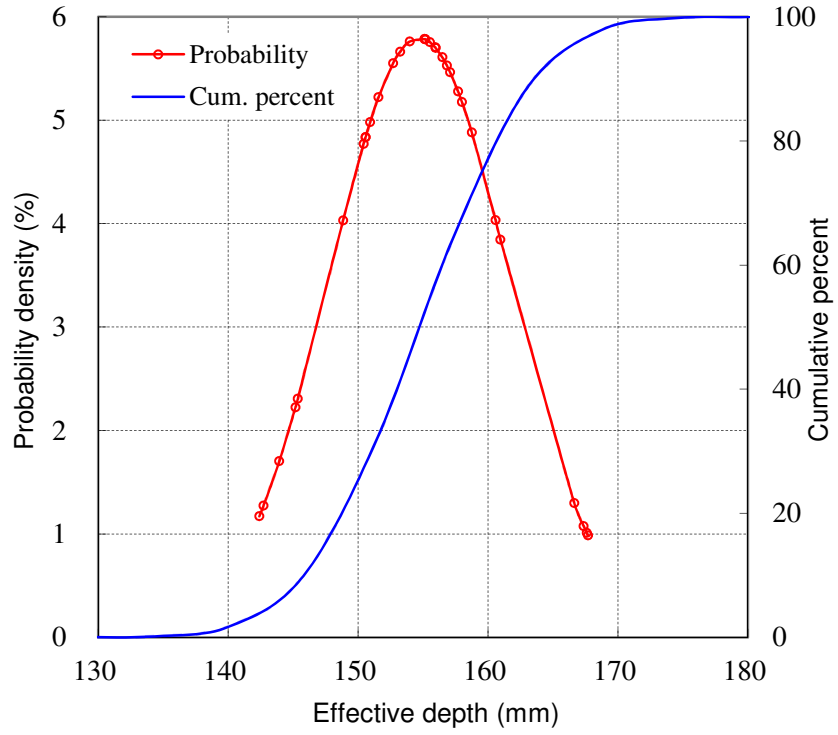


Fig. 5.17 Probabilistic distribution of d^a

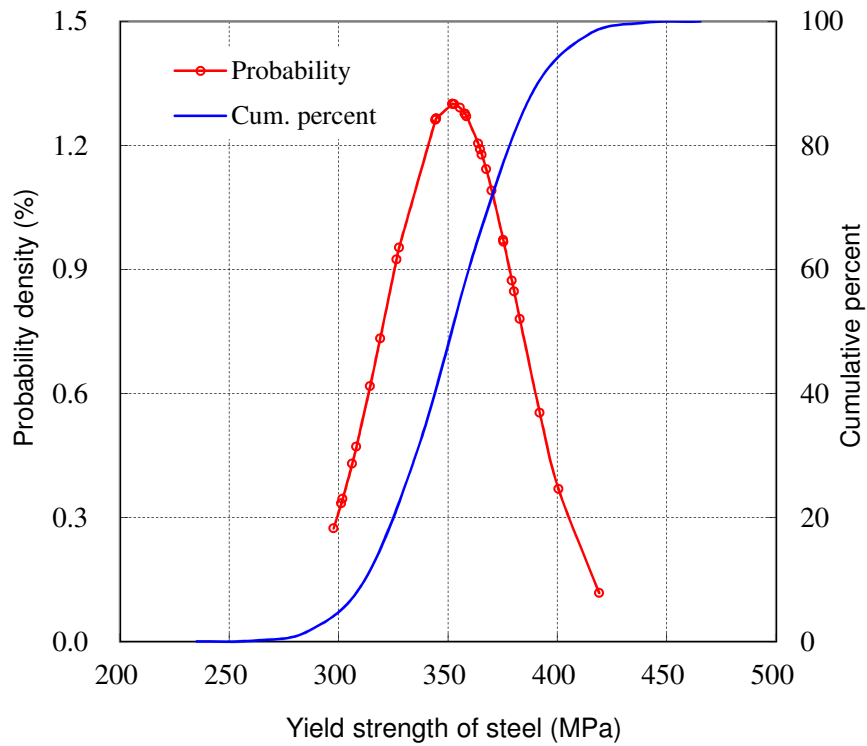


Fig. 5.18 Probabilistic distribution of f_y^a

Table 5.15 Confidence intervals of variables of RC slab test specimen

Parameters	Mean values	COV (%)	Lower limit	Upper limit
A_s^a (mm ²)	725.74	10.69	725.74	733.14
A_{s2}^a (mm ²)	702.09	12.49	697.76	706.42
f_c^a (MPa)	18.41	4.86	18.10	18.72
d^a (mm)	154.72	4.45	152.40	157.04
f_y^a (MPa)	351.86	8.72	341.23	362.49

Table 5.16 Estimation of design data of RC slab specimen

(1) Restored mean values		(2) Initial values	(1)/(2)
A_s^a (mm ²)	725.74	753.6	0.96
A_{s2}^a (mm ²)	702.09	753.6	0.93
f_c^a (MPa)	18.41	19.37	0.95
d^a (mm)	154.72	157	0.98
f_y^a (MPa)	351.86	344	1.02

The output of COV of compressive strength of concrete, as shown in **Table 5.15**, is of the same magnitude to that of the input COV. This shows that the assumed COV is large enough to cover all the variations in f_y^a . The output COVs for A_s^a and A_{s2}^a are larger than the input COVs. This may be resulted from the data points used in the design restoration process.

5.4.1.2 RC Beam Specimen-1

For verification of the analysis result, a beam with rectangular cross section of $b \times h = 500 \times 500$ mm, with overall length of 3200mm and 2800mm distance between supports is used [5.13]. Four deformed bars on the bottom and three deformed bars on top surfaces with 35mm in diameter were provided. For the stirrups, 16mm diameter deformed bars with a spacing of 160mm were used. The cross section of the test beam is shown in **Fig. 5.19**. Concrete with 28-day compressive strength, f'_c , of 31.82MPa and steel bar with yield strength of 528MPa were used. The specimen is simply supported at both ends and

tested for two-point loading with loading points symmetrically spaced at 400mm apart. Load-mid span deflection diagram is shown in **Fig. 5.20**. Three load levels with 70kN interval are used for the design restoration.

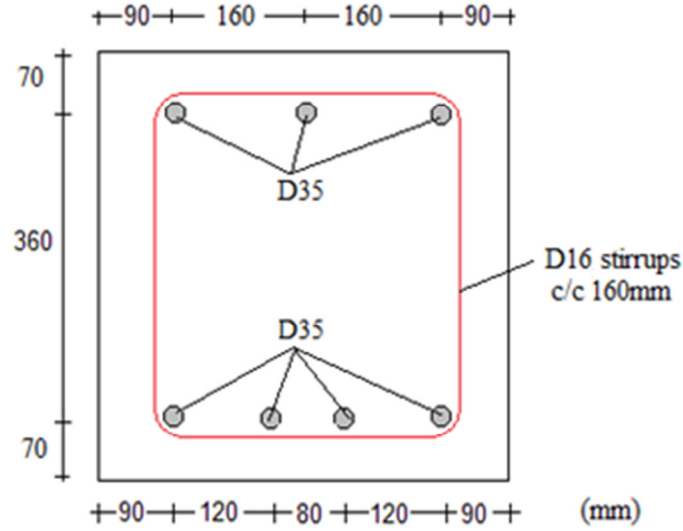


Fig. 5.19 Cross section of RC test beam

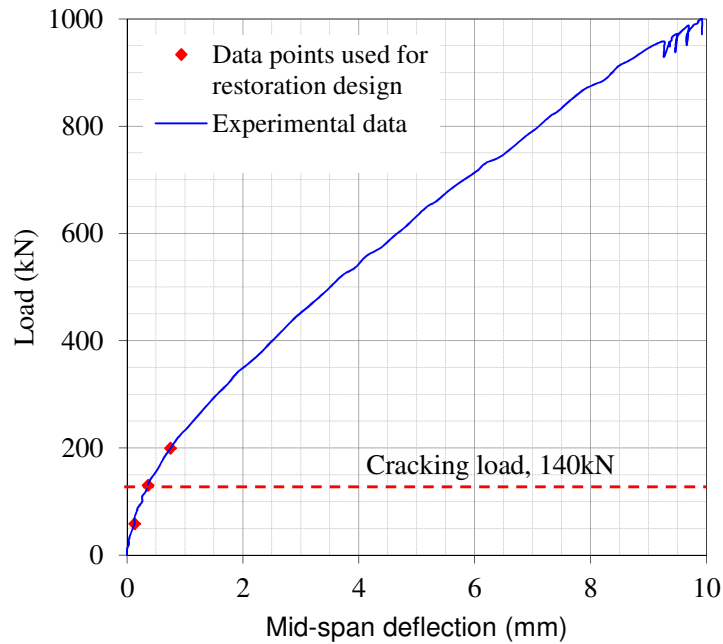


Fig. 5.20 Load- mid span deflection diagram [5.13]

The probabilistic distributions of the estimated values of A_s^a , A_{s2}^a , f_c^a , d^a and f_y^a are shown in **Figs. 5.21-5.24**, respectively. To estimate f_y^a , M_{sd} of 824.5kN-m is used.

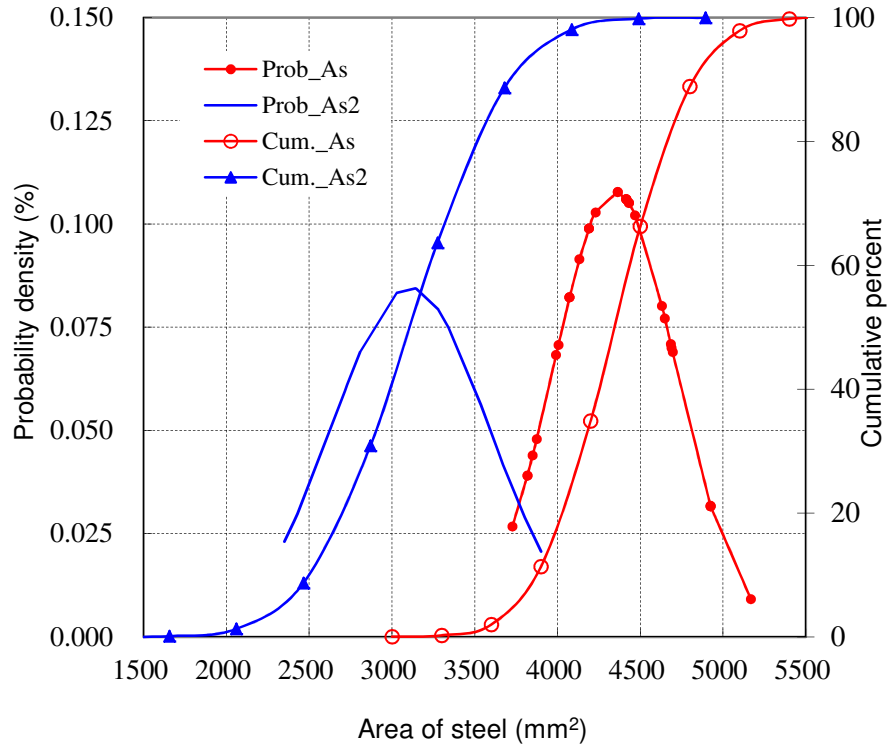


Fig. 5.21 Probabilistic distribution of A_s^a and A_{s2}^a

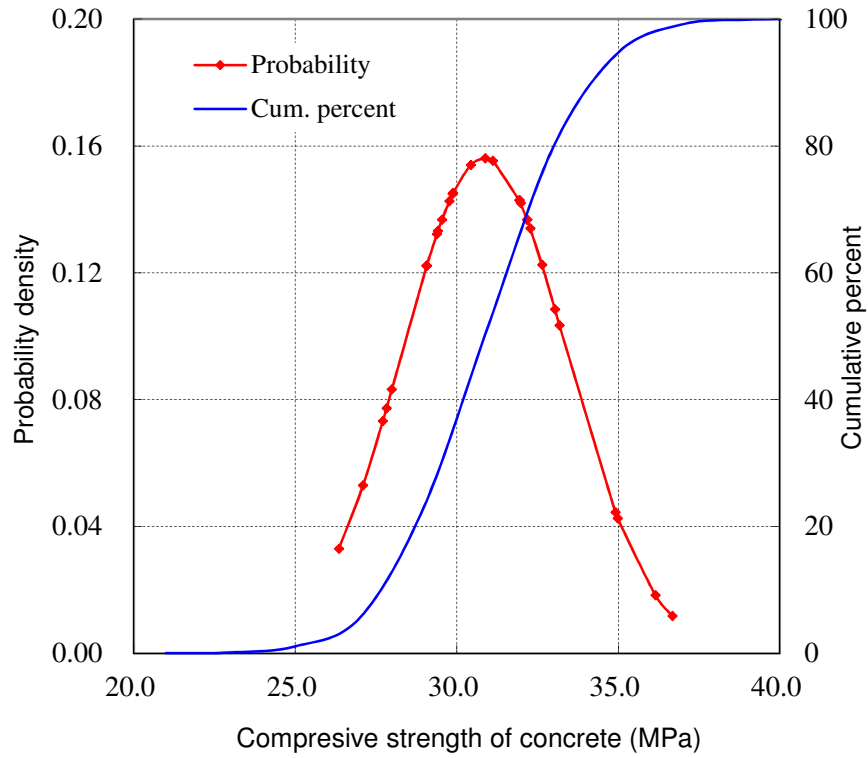


Fig. 5.22 Probabilistic distribution of f_c^a

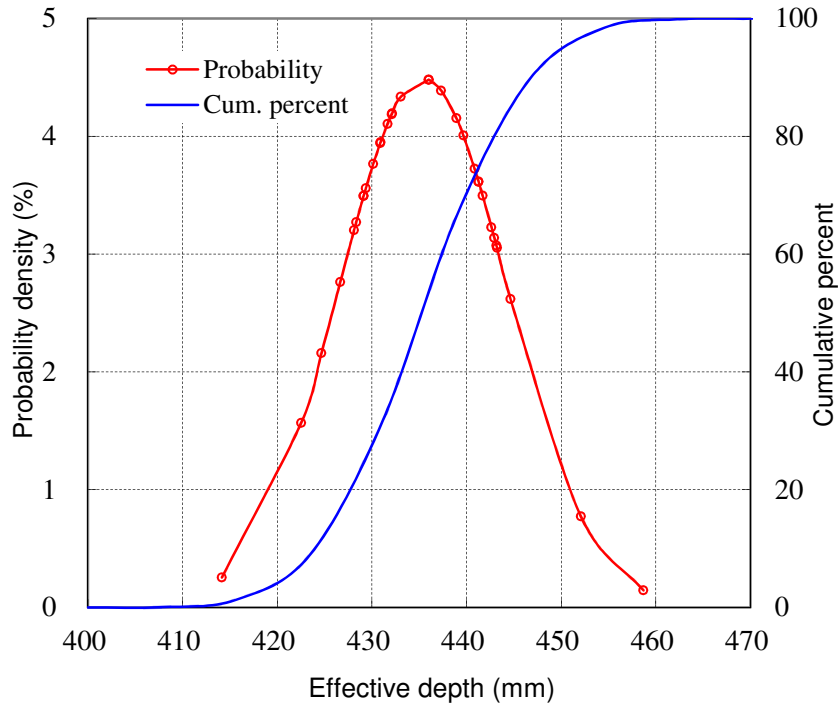


Fig. 5.23 Probabilistic distribution of d^a

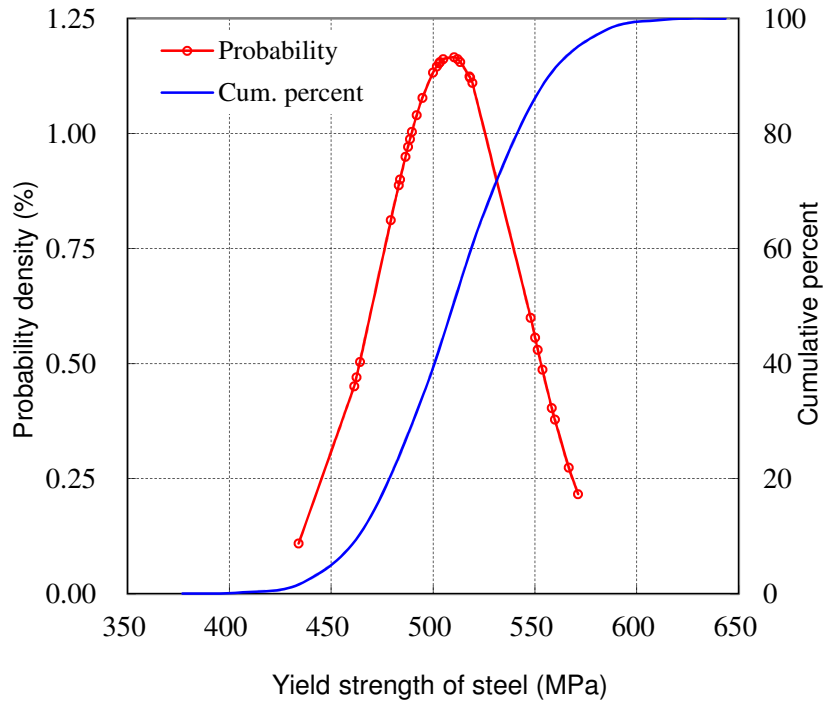


Fig. 5.24 Probabilistic distribution of f_y^a

The confidence limits for the mean values with 95 % confidence levels are estimated and the confidence intervals are shown in **Table 5.17**. The comparison of results of the design and restored values is shown in **Table 5.18**.

Table 5.17 Confidence intervals of variables of RC beam test specimen

Parameters	Mean values	COV (%)	Lower limit	Upper limit
A_s^a (mm ²)	4345.8	8.51	4217.68	4473.96
A_{s2}^a (mm ²)	3110.3	15.2	2946.48	3274.09
d^a (mm)	435.4	2.05	432.33	438.52
f_c^a (MPa)	30.86	8.28	29.97	31.75
f_y^a (MPa)	508.43	6.72	496.59	520.28

Table 5.18 Estimation of design data of RC beam test specimen

	(1) Restored mean values	(2) Initial values	(1)/(2)
A_s^a (mm ²)	4345.82	3846.50	1.13
A_{s2}^a (mm ²)	3110.29	2884.88	1.08
d^a (mm)	435.42	430.00	1.01
f_c^a (MPa)	30.86	31.82	0.97
f_y^a (MPa)	508.43	528	0.96

5.4.1.3 RC Beam Specimen-2

For verification of the design restoration method, a specimen similar to that of RC Beam Specimen-1 with an overall depth of 485mm and different cover thicknesses (as shown in **Fig. 4.20** and **Fig. 4.21** of chapter 4), is prepared. The specimen is simply supported at both ends and tested for two-point loading with loading points symmetrically spaced at 400mm, 1200mm and 2000mm apart. The load deflection diagram is shown in **Fig. 5.25**.

In actual load test of RC bridges, the deflections of the top surface are to be measured and used for restoring design values. To account this, based on deflection of the test beam of the top surface, the restored mean values and confidence limits for the mean values with 95 % confidence levels are estimated and the confidence intervals are shown in **Table 5.19**.

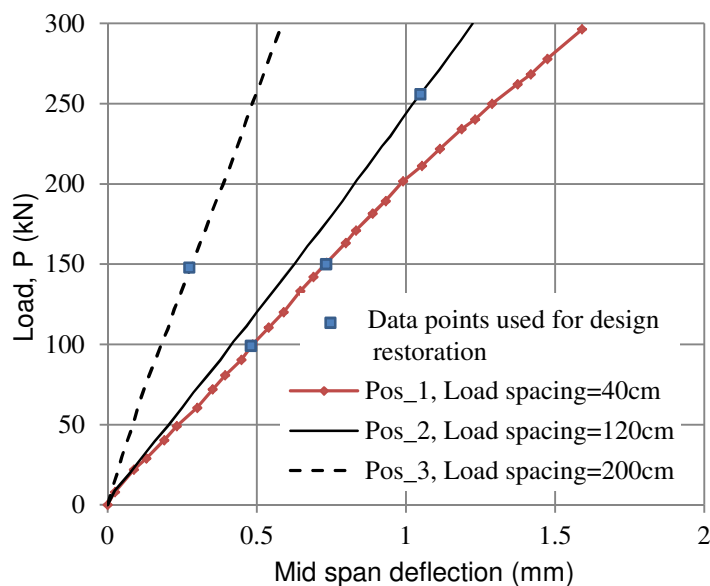


Fig. 5.25 Load- mid span deflection diagram (top surface)

Table 5.19 Output of results and confidence intervals of RC beam specimen-2

Parameters	Initial values (1)	Restored mean values (2)	COV (%)	(2)/(1)	Lower limit	Upper limit
A_s^a (mm^2)	3846.50	3941.06	4.06	1.02	3885.58	3996.54
A_{s2}^a (mm^2)	2884.88	2598.56	13.01	0.90	2467.66	2729.46
d^a (mm)	430.00	424.73	1.52	0.98	422.50	426.96
f_c^a (MPa)	29.67	30.778	11.62	1.04	29.54	32.01
f_y^a (MPa)	528	565.52	4.62	1.07	556.46	574.58

Actually, due to many reasons, the variation in compressive strength of concrete along the beam is large. The output of COV of compressive strength of concrete, as shown in **Table 5.19**, is of the same magnitude to that of the assumed COV (10%). This result shows that the assumed COV is large enough to cover all the variations in compressive strength of concrete. The COV for A_{s2}^a is larger. This may be resulted from the data points used for design restoration.

5.4.2 Design Restoration for Numerical Model

The comparisons of results of the three cases (the values restored in sections 5.2.1 and 5.2.2) are given in **Table 5.20** and **Table 5.21**, respectively.

Table 5.20 Estimation of design data of RC slab specimen (Case 1 and 2)

	Restored mean values		(3) Initial values	(1)/(3)	(2)/(3)
	Case 1 (1)	Case 2 (2)			
A_s^a (mm ²)	4636.45	3566.03	4701.80	0.98	0.76
d^a (mm)	489.47	490.50	489.0	1.00	1.01
f_y^a (MPa)	377.51	482.31	400	0.94	1.21

Table 5.21 Estimation of design data of RC beam specimen (Case 3)

(1) Restored mean values		(2) Initial values	(1)/(2)
A_s^a (mm ²)	4501.31	4701.80	0.96
f_c^a (MPa)	27.64	28	0.99
d^a (mm)	487.24	489	0.99
f_y^a (MPa)	340.92	400	0.85

5.5 Summary

- Estimation of current values for six FEM simulation cases and for three test specimens are performed. From the result, mean values and confidence limits for the mean are obtained. The present method gives better accuracy than the conventional method.
- Sampling of random variables is made by LHS method which is used to improve the computational efficiency in the estimation of values.
- Sensitivity and uncertainty analysis for the simulated bridges are performed.
- Initial condition of bridges based on the current values is estimated.
- RC test specimens are used to verify the present design restoration method.

References

- [5.1] R. Kompen: What Can Be Done to Improve the Quality of New Concrete Structures?, Road Research Laboratory, pp. 1519-1529, Oslo, Norway, 1998.
- [5.2] Reasonable Tolerances for Cast-In-Place Concrete: Publication No. C740210, The Aberdeen Group, 1974.
- [5.3] ACI Committee 117M-10: Specifications for Tolerances for Concrete Construction and Materials (ACI 117), ACI Materials Journal, USA, July 2010.
- [5.4] ACI Committee 117: Standard Specifications for Tolerances for Concrete Construction and Materials (ACI 117), ACI Materials Journal I, November-December 1988.
- [5.5] Tarekegn, A.G. and Tsubaki, T.: Restoration Design for RC Slab Bridges by AASHTO LRFD, The 21st PC Symposium on Developments in Prestressed Concrete, JPCA, pp. 29-34, Oct. 2012.
- [5.6] A.M. Neville, Properties of Concrete, Pearson Prentice Hall, England, 2002.
- [5.7] AASHTO: American Association of State Highway and Transportation Officials, LRFD Bridge Design Specifications, 4th edition, Washington, 2007.
- [5.8] JSCE: Standard Specifications for Reinforced Concrete Structures, 2007.
- [5.9] AASHTO: American Association of State Highway and Transportation Officials, LRFD Bridge Construction Specifications, Washington, 2002.
- [5.10] CONTECVET, A Validated User Manual of Assessing the Residual Service Life of Concrete Structures, Retrieved from http://www.ietcc.csic.es/files/manual_ingles.pdf
- [5.11] Bergström, M: Life Cycle Behaviour of Concrete Bridges, Luleå University of Technology, 2006.
- [5.12] Naganuma, H.: RC Jacketing Type Seismic Strengthening Method Using Perfobond Rib Shear Connectors, Master's Thesis, Graduate School, Yokohama National University, 2012.
- [5.13] Kurata, S.: Experimental Study for Mechanical Performance of Post-installed Shear Reinforcement, Master's Thesis, Graduate School, Yokohama National University, 2013.

6. PERFORMANCE ASSESSMENT OF BRIDGES

6.1 Introduction

Constructed bridges nowadays are subjected to increasingly heavy traffic loads than expected. This together with the effect of wear and tear due to external and environmental factors has made it necessary to devote particular attention to the evaluation of load capacity of bridges. The problem of aging and rapid deterioration of bridges also leads to decrease in the capacity of the structural member.

The condition of bridges is normally assessed through a condition rating or condition index, as a ranking of a bridge condition in comparison to others of a bridge stock [6.1]. The condition index should be an indicator for:

- A ranking of bridges in a bridge stock from the most deteriorated to the best.
- Assessment of the capacity of a bridge to determine eventual capacity reduction factors.
- Identification of trends in the deterioration process that can lead to an estimation of the expected serving life using the condition rating extrapolated to successive time intervals.

The steps required for the detailed structural evaluation of bridges include the followings [6.2]:

1. Frequent inspection
2. Material testing to assess strength of structural components and condition of materials
3. Load rating
4. Nondestructive load testing
5. Remaining fatigue life evaluation.

6.2 Bridge Load Rating

The bridge load rating determines the safe load carrying capacity. Ratings are calculated for a new bridge and are recalculated throughout the bridge's life as changes occur. Unlike design where only one benchmark or level of safety is used, two different levels have historically been used for load rating. These rating levels are referred to as the "inventory rating" and "operating rating" [6.3]. Calculations for overload permit evaluations and for bridge weight postings are made at the operating level.

The evaluation or rating of existing bridges is a continuous activity of the agency to ensure the safety of the public. The evaluation provides necessary information to repair, rehabilitate, post, close, or replace the existing bridge [6.4].

The condition of a bridge is evaluated by structural assessment of its components and during an inspection; an attempt is made to determine the condition of an element based on the subjective opinion of qualified experts.

6.2.1 Live Load Rating

This is used to determine the usable live load capacity by inspection and by rating. Each component is evaluated and the lowest component rating is the most critical [6.2]. Live load rating is for two load levels,

- i) Inventory rating:** A load level which can safely utilize a bridge for an indefinite period of time. Inventory level reflects the existing bridge and material conditions with regard to corrosion, loss of section and

other deficiencies. It does not exceed the design stresses.

- ii) Operating rating:** The absolute maximum permissible load to which the bridge can be subjected. The use of bridge by unlimited number of heavier vehicles would exceed the capacity and is not permitted.

6.2.2 Sufficiency Rating

It is defined as a calculated rating indicating the bridge's sufficiency or capability.

6.2.3 Rating Aspects for Existing Bridges

Load rating is expressed as a rating factor for a particular live load and it is important to [6.2]:

- monitor safety of bridges over time
- help determining when rehabilitation or replacement is needed

Rating is dependent upon: magnitude of live load (legal rating load), intensity and frequency of traffic, number of lanes, existing conditions of structure, bridge age and material properties. Live load capacity is based on bridge inspections:

- Identifying condition changes
- Measurement of any losses
- Field measurements

6.2.4 Legal Rating Loads

The loads used by various countries for rating purposes, are of three types: (i) design live loads at the time of construction; (ii) presently allowed legal loads; and (iii) specific loads for rating purposes only. Some of the loads in category (iii) are military loads and not much information is available on them [6.5].

6.3 Rating Method

The portion of the rating vehicle will be given by the ratio between the available capacity for live load effect and the effect of the rating vehicle. This ratio is called the rating factor (RF) as given in Eq. (6.1) [6.4].

$$RF = \frac{\phi R_n - \sum_{i=1}^m \gamma_{Di} D_i - \sum_{i=1}^k \gamma_{Li} L_i (1 + I)}{\gamma_L L (1 + I)} \quad (6.1)$$

- where, RF : rating factor
- ϕR_n : nominal resistance = $A_s f_y (d - a/2)$
- a = $A_s f_y / (0.85 f_c' b)$
- d : effective depth
- b : width
- f_y : yield strength of steel
- f_c' : compressive strength of concrete
- A_s : cross-sectional area of steel
- D_i : effect of dead loads
- L_i : live-load effect for load i other than the rating vehicle
- L : nominal live-load effect of the rating vehicle
- I : impact factor for the live-load effect
- γ_{Di} : dead load factor
- γ_{Li}, γ_L : live load factors
- m : number of dead-load components
- k : number of live-loads

The area of tension steel to be used in computing the ultimate flexural strength of reinforced concrete members shall not exceed that available in the section or 75 percent of the steel reinforcement required for a balanced condition. The steel yield stresses to be used for various types of reinforcing steel are given in **Table 6.1** [6.6, 6.7].

Table 6.1 Reinforcing steel yield stresses

Reinforcing steel	Yield stress (MPa)
Unknown steel (prior to 1954)	228
Structural grade	248
Intermediate Grade 300 and unknown after 1954 (former Grade 40)	276
Hard grade (former Grade 50)	314
Grade 420 (former Grade 60)	614
Grade 520 (former Grade 75)	517

6.4 Posting Analysis

Once the current performance assessment of bridges is done, the next step is the recommended actions to be made by the respective bridge authorities. This is expressed in terms of load posting analysis.

When the Rating Factor (R.F.) is less than 1.0, the loads are to be restricted. In such instances, consideration should be given to truck weight surveys and vigorous enforcement programs. If there is a reason to believe that truck posting signs are being ignored then consideration should be given to further raising the live load factor. The procedure for rating existing bridges requires knowledge of the physical conditions of the bridge and the applied loadings [6.7]. As described in AASHTO rating manual [6.8], the following rating results are used for posting analysis:

1. When $RF > 1.0$, posting is not required.
2. When $RF > 0.3$ but < 1.0 , the safe posting load = $W (RF - 0.3)/0.7$
3. When lane load governs, $W = 40$ tons.
4. For any vehicle when $RF < 0.3$, the vehicle type should not be allowed on the span.
5. When RF for all three legal loads (Type 3; Type 3-S2 and Type 3-3 units) < 0.3 , the bridge shall be closed for vehicular traffic.
6. Speed limit may be lowered to reduce impact live load.

6.5 Probabilistic Performance Analysis of RC Bridges

The reliability of a reinforced concrete bridge is a time variant which is dependent on both the applied loads and remaining strength of the structural elements [6.9]. Based on the probabilistic design restoration process, the performance capacity of the bridge can be done by using the same procedure.

The live load to be used to rate bridges should be the HS20 truck or lane loadings as defined in [6.6, 6.8]. For posting considerations, other loadings specified in AASHTO's manual for condition evaluation of bridges [6.8] are used.

Factors of $\gamma_{Di}=1.25$, $\gamma_{Li}=1.25$, and $\gamma_{LI}=1.75$ for inventory rating are used [6.6, 6.8]. Impact factor is added to the live load rating in accordance with the current AASHTO Design Specification.

Performance rating of RC slab bridge analyzed in subsection 5.2.2 (Case 3) is performed and probabilistic distributions of rating factors for inventory loadings and posting analysis based on the current values are shown in **Fig. 6.1** and **Fig. 6.2**, respectively. The general rating equation given in Eq. (6.1) and the legal rating loads for the assessment of bridges [6.6, 6.7] are used.

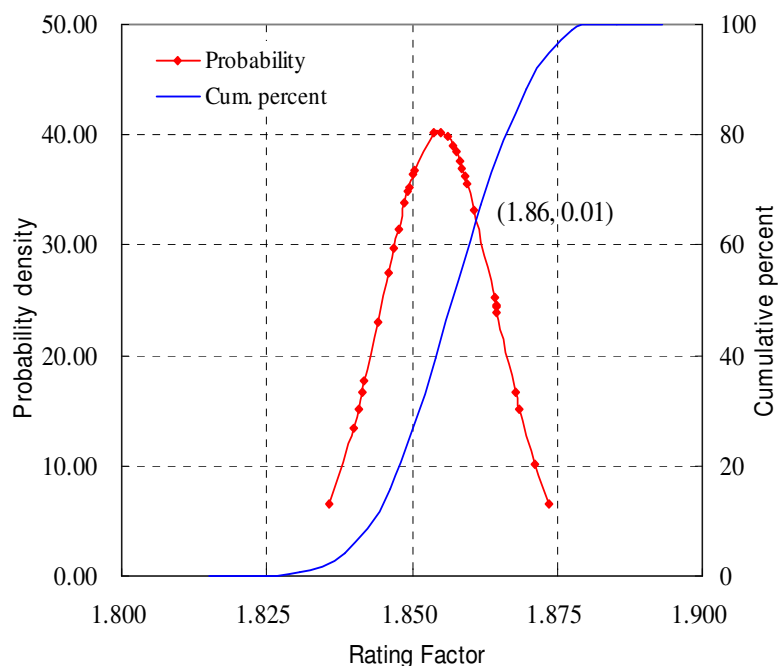


Fig. 6.1 Distribution of inventory rating factor

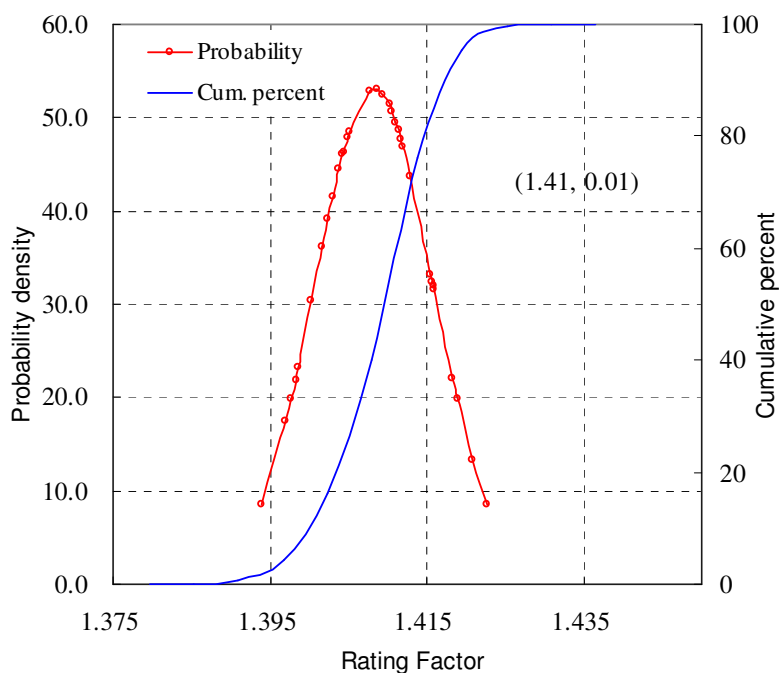


Fig. 6.2 Distribution of rating factor for load posting

From the analysis, as shown in **Fig. 6.1** and **Fig. 6.2**, mean values of rating factors of 1.855 and 1.405 with a standard deviation of 0.010 and 0.008 for inventory rating and posting load analysis are obtained, respectively. Using conventional method, the rating factors for inventory and posting load analysis are obtained as 2.01 and 1.54, respectively.

6.6 Summary

- Performance evaluation of bridges which is one of the most important process in bridge management cycle has been discussed and summarized.
- Live load rating determines the safe load carrying capacity of bridges.
- Using the design restoration scheme, load rating can be done and hence the lifetime of the bridge can easily be predicted from the current and initial conditions.

References

- [6.1] Wenzel, H.: Health Monitoring of Bridges, John Wiley & Sons, Ltd, VCE Holding GmbH, Vienna, Austria, 2009.
- [6.2] Mohiuddin A. Khan: Bridge and Highway Structure Rehabilitation and Repair, The McGraw-Hill Companies, Inc., New York, 2010.
- [6.3] Minnesota Department of Transportation, LRFD Bridge Design Manual, Manual 5-392, March 2010.
- [6.4] Chen, W. F.: Bridge Engineering Handbook, CRC Press LLC, Washington, D. C., 2000.
- [6.5] Umarani Gunasekaran,U. et al.: Load Rating of Bridges- Current Practices and Issues, Prague Development Center, 2010.
- [6.6] AASHTO: American Association of State Highway and Transportation Officials, LRFD Bridge Design Specifications, 4th edition, Washington, 2007.
- [6.7] ERA: Ethiopian Roads Authority, Bridge Design Manual, Addis Ababa, 2002.
- [6.8] AASHTO: American Association of State Highway and Transportation Officials, Manual for Condition Evaluation of Bridges, Washington D.C, 20001, 1994.
- [6.9] Michael P. Enright, Dan M. Frangopol: Probabilistic Analysis of Resistance Degradation of Reinforced Concrete Bridge Beams under Corrosion, Engineering Structures, Vol. 20, No. 11, pp. 960–971, 1998.

7. CONCLUSIONS AND RECOMMENDATIONS

7.1 Conclusions

From the present study, the following conclusions are drawn.

- 1) A design restoration scheme, flow and an alternative method for restoring initial conditions for RC slab bridges has been presented. It is used to establish a methodology for the capacity performance assessment of existing RC slab bridges. The steps and design restoration flow used for practical application are shown in **APPENDIX F**.
- 2) A probabilistic design restoration method for RC slab bridges has been presented to take into account the statistical variations in the design parameters and to obtain the mean values and the confidence limits for the mean of the restored design data. The confidence limits give a certain range of information to search an optimal result. A Latin Hypercube Sampling (LHS) method is used to improve the computational efficiency.
 - For the typical RC slab bridge case, with 95 % confidence levels, confidence intervals of $\pm 2.76\%$ and $\pm 3.66\%$ of the mean values of f_y^a

for Case 1 and Case 2 are obtained, respectively. Deterioration rate of Case 2 is taken into account by considering the loss or reduction in the cross-sectional area of steel bar.

- For Case 3, with 95 % confidence levels, confidence interval of $\pm 1.70\%$ of the mean value of f_y^a is obtained. These intervals are small and hence the obtained results are considered reasonable. Similarly, for other cases (Cases 4-6), small confidence intervals of the mean value of f_y^a are obtained.
 - For Case 3, as shown in **Table 5.8**, better accuracy is obtained as compared to the conventional one.
- 3) From the verification results, it has been noticed that the design values can be restored using the proposed design restoration scheme.
 - 4) As shown in **Table 5.10** and **Table 5.11**, the largest contributions to the uncertainty of M_y , yielding moment, are the cross-sectional area of steel and cover thickness.
 - 5) A probabilistic performance rating for inventory loadings and posting analysis of RC bridges based on the current values has been performed.

7.2 Recommendations

- 1) By using sufficiently accurate displacement transducers, the method can be applicable for RC sections with multi-layer reinforcement arrangement.
- 2) The design restoration scheme can also be extended for RC T-girder bridges, arch bridges and composite structures.

APPENDIX A – CONVENTIONAL NON-DESTRUCTIVE MEASUREMENT TECHNIQUES

A.1 Introduction

Concrete testing with a test hammer is the most frequently used method worldwide for non-destructive testing of concrete and structural components [A.1]. Moreover, determination of compressive strength of concrete from core test is commonly used. Position of reinforcing bars can be detected by using a magnetic device [A.2]. The devices are shown in **Fig. A.1** and **Fig. A.2**.



Fig. A.1 Concrete test hammer [A.1]



Fig. A.2 Rebar detection device [A.2]

Image of reinforcing bars in concrete by electromagnetic induction method is shown in **Fig. A.3** [A.3].

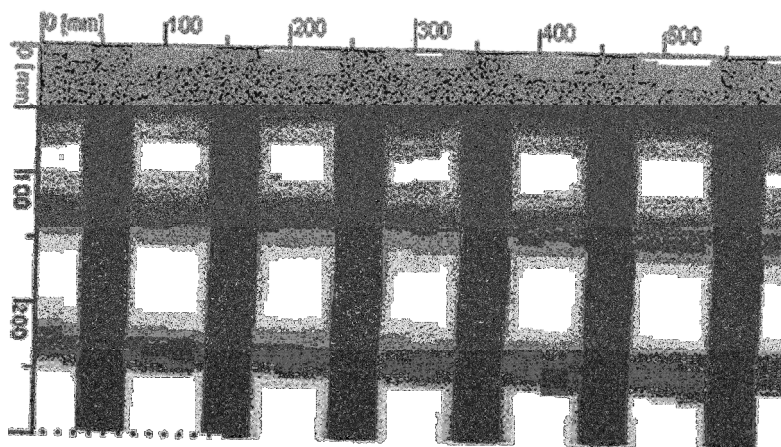


Fig. A.3 Image of rebars in concrete by electromagnetic induction method [A.3]

A.2 Summary of Non-Destructive Tests' Accuracy

Summary of conventional non-destructive tests' accuracy for cross-sectional shape of main girders and investigation of PC tendons and shear reinforcement [A.3] are shown in **Table A.1** and **Table A.2**.

Table A.1 Non-destructive tests’ accuracy for cross-sectional shape of main girder [A.3]

Contents	Inspection part	Inspection level	Inspection direction	Inspection method	Accuracy	Remark	
Inspection of main beam cross-sectional shape	Upper flange thickness	Bottom part	Top end surface	Radar method	○	If correction by dielectric constant is possible, accuracy is ± 5 mm.	
					△	If correction by dielectric constant is not possible, accuracy is ± 30 mm.	
				Ultrasonic wave method	○	If correction by ultrasonic velocity is possible, accuracy is $\pm 2-3\%$.	
					△	If correction by ultrasonic velocity is not possible, accuracy is $\pm 10\%$.	
				Impact elastic wave method	○	If correction by ultrasonic velocity is possible, accuracy is $\pm 2-3\%$. It is desirable to measure at wide surfaces. In complex parts multiple reflections are caused.	
					△	If correction by ultrasonic velocity is not possible, accuracy is $\pm 10\%$.	
				Side surface	Core sampling method	◎	Core has to be properly collected from upper and lower surfaces of the upper flange.
				1-Top of member	Upper surface of upper flange	Radar method	○
		△	If correction by dielectric constant is not possible, accuracy is ± 30 mm.				
		Ultrasonic wave method	○			If correction by ultrasonic velocity is possible, accuracy is $\pm 2-3\%$..	
			△			If correction by ultrasonic velocity is not possible, accuracy is $\pm 10\%$.	

Contents	Inspection part	Inspection level	Inspection direction	Inspection method	Accuracy	Remark		
				Impact elastic wave method	○	If correction by ultrasonic velocity is possible, accuracy is ± 2-3%. It is desirable to measure at wide surfaces. In complex parts multiple reflections are caused.		
					△	If correction by ultrasonic velocity is not possible, accuracy is ± 10%.		
				Core sampling method	◎	It is difficult to collect cores from lower surfaces of the upper flange.		
		2-Pavement part	Peel of the pavement		Radar method	○	If correction by dielectric constant is possible, accuracy is ± 5mm.	
						△	If correction by dielectric constant is not possible, accuracy is ± 30mm.	
					Ultrasonic wave method	○	If correction by ultrasonic velocity is possible, accuracy is ± 2-3%.	
						△	If correction by ultrasonic velocity is not possible, accuracy is ± 10%.	
					Impact elastic wave method	○	If correction by ultrasonic velocity is possible, accuracy is ± 2-3%. It is desirable to measure at wide surfaces. In complex parts multiple reflections are caused.	
						△	If correction by ultrasonic velocity is not possible, accuracy is ± 10%.	
				Core sampling method	◎	To avoid cutting of bars, searching location of bars inside the concrete is required .		
					Peel of the pavement	Radar method	○	It is necessary to correct the dielectric constant.
						Thickness of filling deck slab	Top	Same as 1
					Pavement surface	Same as 2		

◎-Excellent ○- Good △- Fair (relative comparisons)

Table A.2 Non-destructive tests’ accuracy for investigation of PC tendons and shear reinforcement [A.3]

Contents	Inspection part	Inspection level	Inspection direction	Inspection method	Accuracy	Remark
Investigation of main PC tendons	Arrangement of bottom flange (including cover thickness)	Top	Side surface	Radar method	○	If correction by dielectric constant is possible, -accuracy for bar position is $\pm 10\text{mm}$ (with the travel distance of 600mm). - accuracy for concrete cover is $\pm 5\text{mm}$ (within 50-200mm). It is known that inspection accuracy of prestressing steel is affected by precaution reinforcement the travel distance of 600mm).
					△	If correction by dielectric constant is not possible, accuracy is about $\pm 30\text{mm}$.
				Core sampling method	◎	Core should be collected as the same number as prestressing steel.
				Electro-magnetic induction method	△	If PC tendons are surrounded by rebars, it might not be possible to detect their positions.
				X-ray method	◎	Measurement accuracy is high, but different performance is caused due to the performance of the film and the strength of the output of the x-ray.
	Bar diameter of bottom flange	Top	Side surface	Core sampling method	◎	Core should be collected as the same number as prestressing steel.
				Electro-magnetic induction method	○	If PC tendons are surrounded by rebars, it might not be possible to detect their positions.
				X-ray method	◎	Measurement accuracy is high, but different performance is caused due to the performance of the film and the strength of the output of the x-ray.

Contents	Inspection part	Inspection level	Inspection direction	Inspection method	Accuracy	Remark
Investigation of shear reinforcement	Arrangement of web	Top	Side surface	Radar method	○	-accuracy for bar position is about ± 10 mm (with the travel distance of 600mm). - accuracy for concrete cover is ± 5 mm (within 50-200mm).
					△	If correction by dielectric constant is not possible, accuracy is about ± 30 mm.
				Core sampling method	◎	It needs some core samples.
				Electro-magnetic induction method	○	-accuracy for bar position is about ± 10 mm. - when concrete cover is 20mm and less than 100mm, the accuracy is $\pm 1-2$ mm.
				X-ray method	◎	Measurement accuracy is high, but different performance is caused due to the performance of the film and the strength of the output of the x-ray.
	Bar diameter of web	Top	Side surface	Core sampling method	◎	Core should be collected as the same number as prestressing steel.
				Electro-magnetic induction method	○	If the range is less than 60mm, the accuracy is less than ± 4 mm.
				X-ray method	◎	Measurement accuracy is high, but different performance is caused due to the performance of the film and the strength of the output of the x-ray.

References

- [A.1] Compressive Strength Measurement and Damage Assessment: Retrieved from <http://www.concretex-ray.com.au/strength-measurement?format=pdf>
- [A.2] Profometer: Rebar Detection System, Retrieved from http://www.proceq.com/fileadmin/documents/proceq/products/Concrete/Profometer_5_/English/Proceq_Brochure_Profometer_5__E.pdf
- [A.3] JPCEA, Report of the Technical Committee on Design Restoration of Prestressed Concrete, Japan Prestressed Concrete Engineering Association, March 2010.

APPENDIX B - ITALIAN BRIDGE DESIGN STANDARDS

B.1 Introduction

According to Italian Bridge Design Standards [B.1], different loads are considered for different type of roads. Subdivisions of roads in relation to traffic are: busy roads (Type-1), medium traffic (Type-2) and roads of small traffic (Type-3). The following loads are considered for each type of roads. Among each case the one which gives the maximum force effect is considered for design of bridges.

Type I

- a) A train of trucks weight of 12 tons with a crowd load of 400kgf/m^2 on the sidewalks.
- b) A truck weight of 12 tons and a train type vehicle of weight up to 40 ton with a crowd load of 400kgf/m^2 on the sidewalks.
- c) Uniform load of 400kgf/m^2 over the entire width of the bridge

Type II

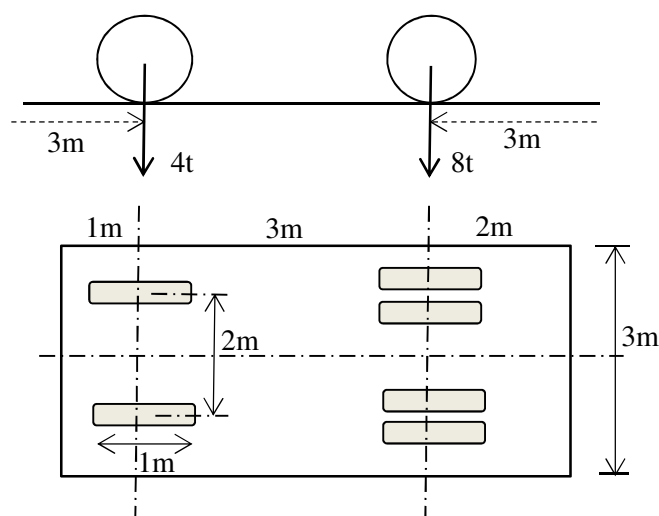
- A train of trucks weight of 12 tons with a crowd load of 400kgf/m^2 on the sidewalks.
- Undefined type of trucks weighing 12 tons and a column of two 18ton rollers with a crowd load of 400kgf/m^2 on the sidewalks.
- A two rollers weight of 18 tons with a crowd load of 400kgf/m^2 on the sidewalks.
- Uniform load of 400kgf/m^2 over the entire width of the bridge.

Type III

- A train of trucks of weight 12tons and at the same time compact crowd load of 400kg/m^2 on the area not occupied by the vehicles.
- A steam roller weighing 18 ton with a crowd load of 400kgf/m^2 on the sidewalks.
- Uniform load of 400kgf/m^2 over the entire width of the bridge.

B.2 Live Loads

The live loads to be taken in the calculation are shown in **Figs. B.1 - B.4** [B.1]. To account the effect of dynamic actions of loads, whatever the type of the road, will have to be increased by 25%. All figures in this section are taken from Italian Bridge Design Standards [B.1].

**Fig. B.1** Truck weighing 12tons

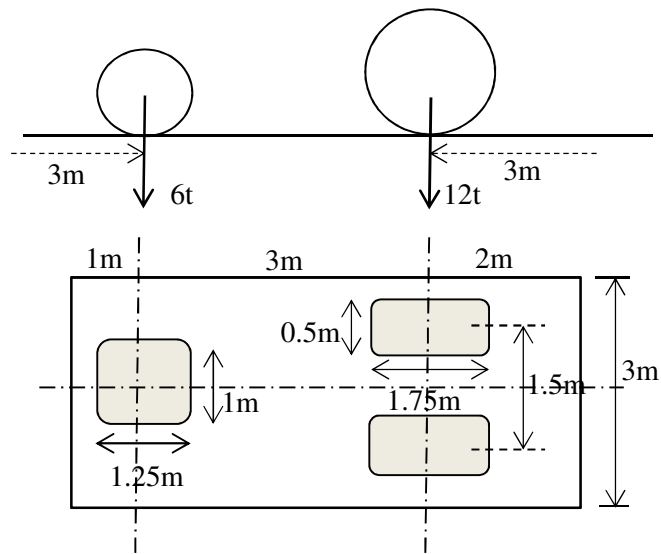


Fig. B.2 18tons steam roller

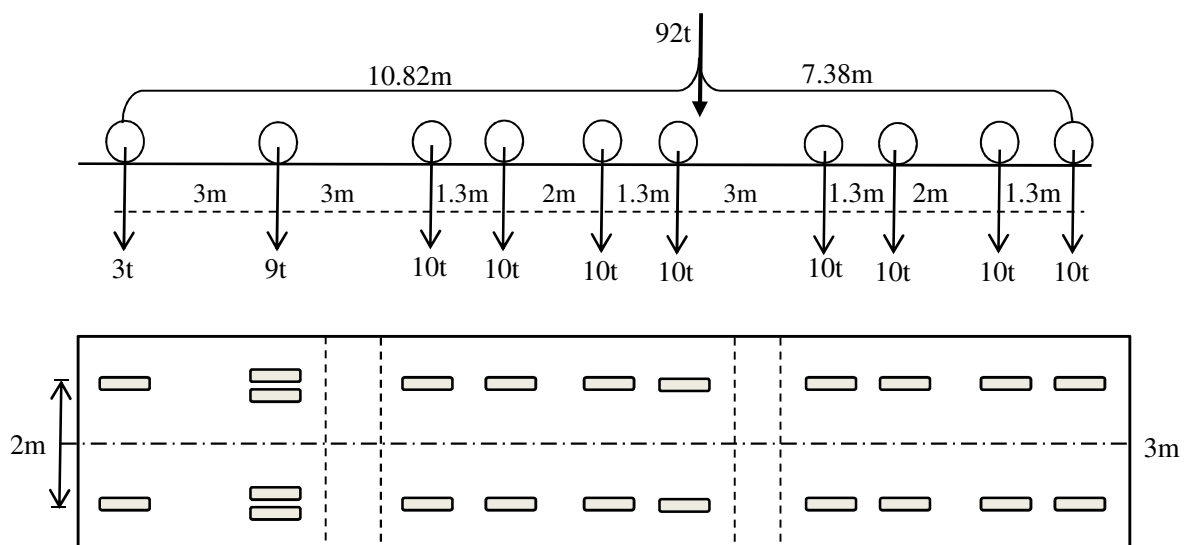


Fig. B.3 Vehicles weighing up to 40tons

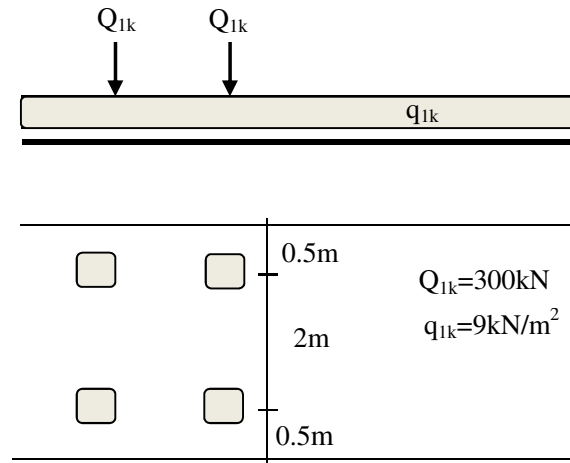


Fig. B.4 Design tandem load

The five load combinations for the computation of maximum force effects, shear forces and bending moments, at various points in the beam are shown in **Figs B.5-B.9** [B.1].

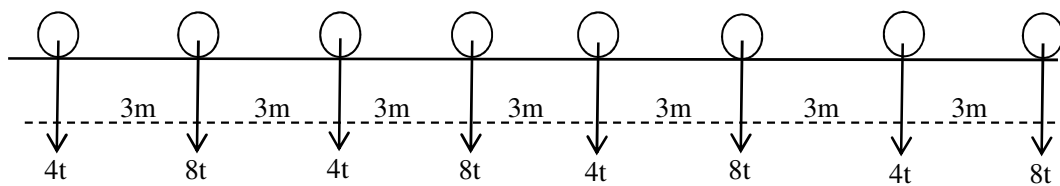


Fig. B.5 Undefined column of trucks weighing 12tons

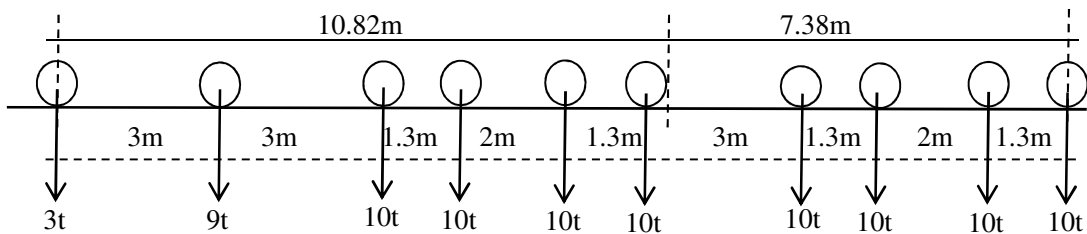


Fig. B.6 Towing tractor and two trailers

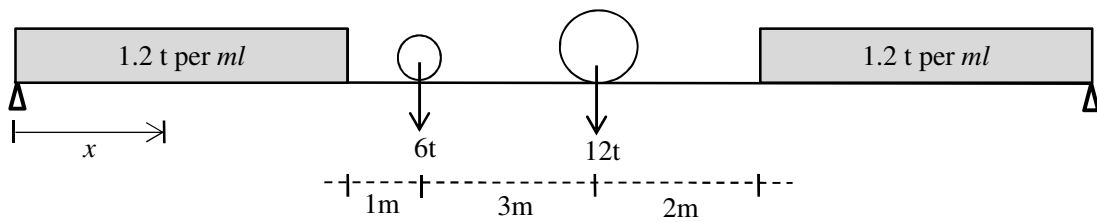


Fig. B.7 Towing consists of a roller of 18 tons and UDL

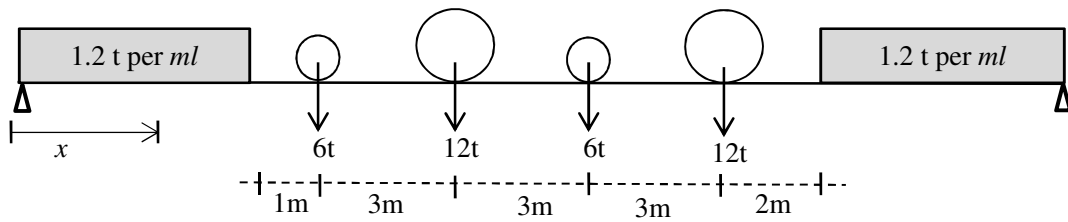


Fig. B.8 Towing consists of two rollers and UDL

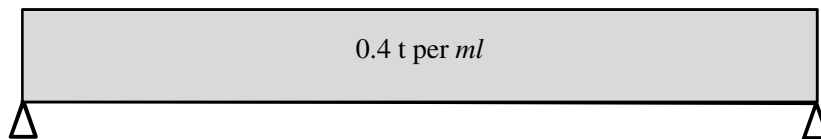


Fig. B.9 Uniformly distributed load of 400kgf/m

Moreover, for highway bridges, the distribution of loads to a corresponding index of the total weight of 17.5tons is considered.

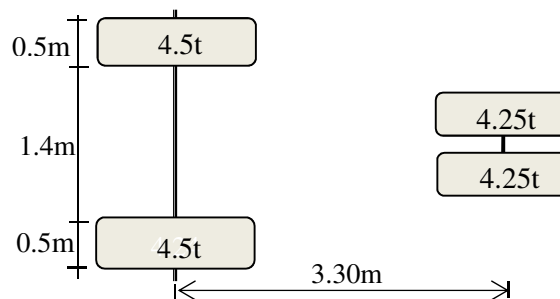


Fig. B.10 Roller weighting 17.5tons

For flows greater than 20m, overloading condition can observe. The following formula is used to deduce the load, q , per m^2 equivalent to the weight of a row of wagons (6 tons).

$$q = 360 + \frac{1200}{L} \quad (\text{B.1})$$

For loads from 10-12tons,

$$q = 440 + \frac{1400}{L} \quad (\text{B.2})$$

where, q : weight of a row of wagons

L : the length of the bridge in meters

B.3 Positive Permanent Loads

Positive permanent loads of bridges due to vehicular loads are highly dependent on the type, scope and purpose of the bridge. The assumption to be considered for calculating a load is that the only reinforcement of the bridge excluding the weight of the floor and road. The weight per square meter in kilograms is Eq. (B.3).

$$\begin{aligned} g_1 &= 8.25L + 230 \\ g_2 &= 25L + 540 \end{aligned} \quad (\text{B.3})$$

where, g_1 : bridges with wooden floor

g_2 : bridges with roadbed

B.4 Horizontal External Forces

The intensity of these horizontal forces can be calculated with the formula

$$F_h = \frac{V}{240} \sqrt{P} \quad (\text{B.4})$$

where, F_h : horizontal force (tons)

V : maximum allowable speed (km/hr)

P : maximum pressure (tons)

The different load type and the maximum bending moments for simply supported girders, 3.00 m. to 50.00 m, for movable loads are shown in **Fig. B.11**.

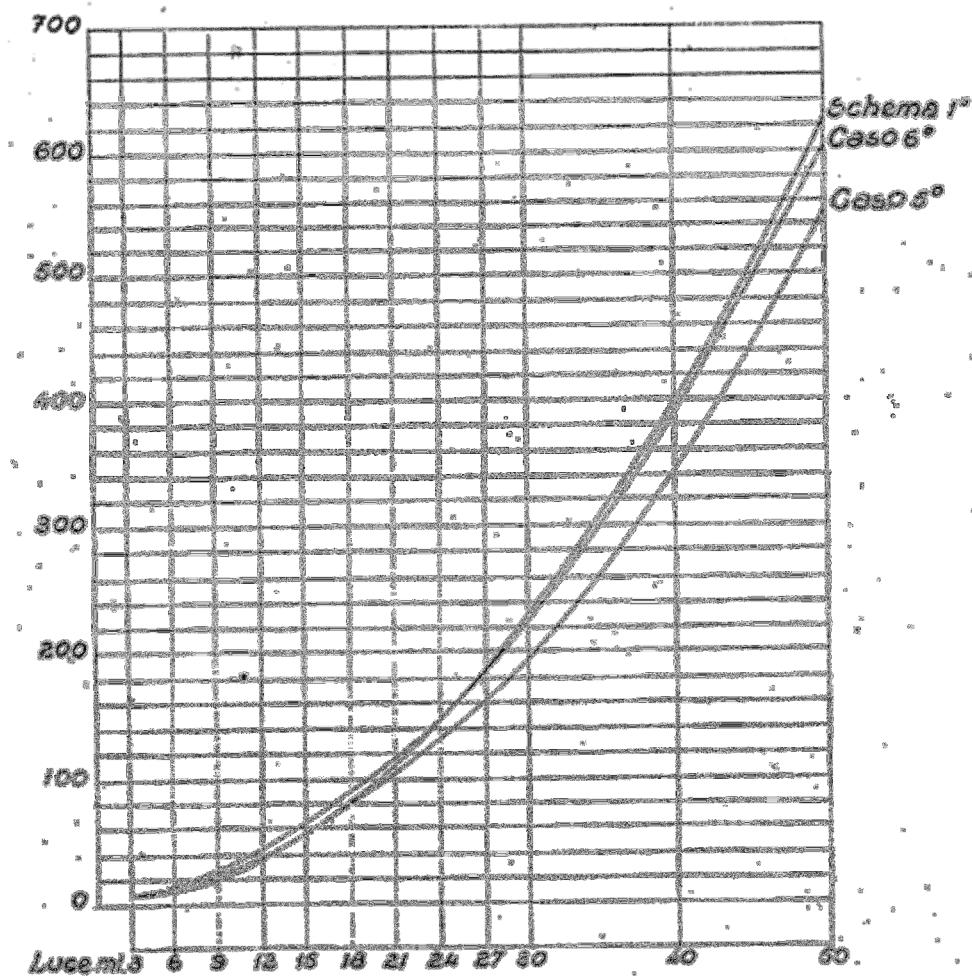


Fig. B.11 Maximum bending moments [B.1]

B.5 Summary

- The old Italian bridge design specifications of Italy has been reviewed.
- Performance assessment of bridges constructed by the Italian authority can be made by using the given live loads.

References

[B.1] Ministero Dei Lavori Pubblici: Direzione General Dei Servizi Tecnici, Roma, 1945.

APPENDIX C - INFLUENCE FUNCTION FOR DEFLECTION OF RC BEAMS CONSIDERING VARIATION IN NEUTRAL AXIS DEPTH PROFILE

C.1 Introduction

Many studies have been conducted for the estimation of effective moment of inertia expressions for RC beams. To compute deflection of beams, the study results show that the expressions for effective moment of inertia, in each case, are different. In this study, using a concept of influence lines, new closed-form explicit equations for the computation of slope and deflection of RC beams by considering variation in neutral axis depth profile are obtained. Moreover; a neutral axis depth profile and moment of inertia expression with parabolic functions for different types of beams with different end conditions are proposed.

The variation in the modulus of elasticity with the increasing load is caused by the inelastic stress-strain behavior of concrete beyond the elastic limits, while the variation in the moment of inertia is associated with the cracking of concrete due to the tensile strains greater than the cracking strain of concrete. The cracked zones in a concrete beam are ineffective in resisting stresses originating from applied loads and moments [C.1].

The overall moment of inertia of a concrete beam decreases gradually from the uncracked moment of inertia (I_{ucr}) to the fully-cracked moment of inertia (I_{cr}), as flexural cracks form at discrete locations along the span [C.1].

Deflections may be computed using the modulus of elasticity for concrete as specified in AASHTO [C.2] by taking the effective moment of inertia expression proposed by Branson and it is given in Eq. (C.1).

$$I_{eff} = \left(\frac{M_{cr}}{M_a} \right)^3 I_g + \left[1 - \left(\frac{M_{cr}}{M_a} \right)^3 \right] I_{cr} \leq I_g \quad (C.1)$$

where, I_{eff} : effective moment of inertia (mm^4)

M_{cr} : cracking moment (kN-m)

$$M_{cr} = f_r I_g / y_t$$

f_r : modulus of rupture of concrete (MPa) = $0.63\sqrt{f_c'}$

I_g : gross moment of inertia (mm^4)

y_t : distance from the neutral axis to the extreme tension fiber (mm)

f_c' : compressive strength of concrete (MPa)

I_{cr} : moment of inertia of the cracked section (mm^4)

M_a : maximum moment in a component at the stage for which deformation is computed (kN-m)

In cases when the effective flexural stiffness is assumed to be a function of flexural moment, the same expression as that of Eq. (C.1) with different exponent (power 4) is given in JSCE Standard Specifications for Concrete Structures [C.3].

An influence function of RC beams considering the variations of neutral axis profile is presented in the following. Moreover, expressions for neutral axis depth and moment of inertia are proposed.

C.2 Computation of Neutral Axis Depth and Effective Moment of Inertia

To compute the effective moment of inertia, the variation in the neutral axis depth and moment of inertia along the span is taken into account. The neutral axis along the longitudinal line is not constant due to the tensile strength of concrete and the variation in effective reinforcement ratio in the section. For uniformly distributed loads, since the neutral axis depth is related to bending moment, a parabolic neutral axis profile and variable moment of inertia along the longitudinal direction are assumed [C.4].

For old structures, the distribution of the neutral axis profile is independent of load position, and it does not vary with load and is assumed to be unchanged since the section is already cracked by the maximum possible load experienced in the past [C.4].

C.2.1 Neutral Axis Profile for New Structures

For the derivations of neutral axis depth variation and to obtain expressions for the moment of inertia along the longitudinal line of a beam, consider the side view shown in **Fig. C.1**. The basic assumption considered is that the neutral axis profile varies with the load, depends on its position and crack occurs at points where the bending moment is sufficiently large.

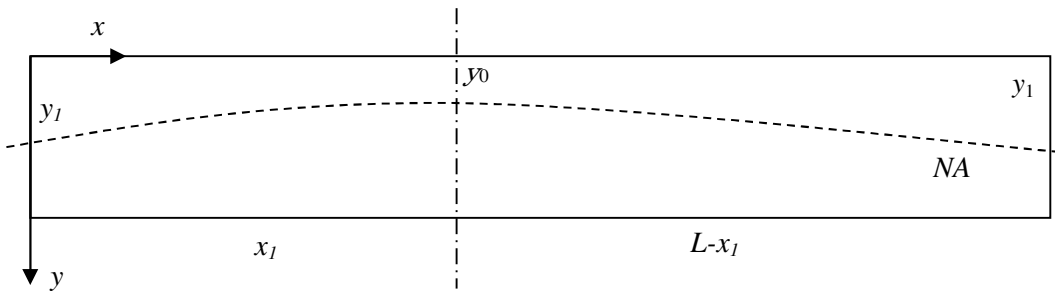


Fig. C.1 Variation of neutral axis depth of new RC beam

Based on AASHTO LRFD [C.2] and Chen et al. [C.5], for cracked section, the neutral axis depth and moment of inertia are given in Eqs. (C.2a) and (C.2b), respectively.

$$0.5by_0^2 = nA_s(d - y_0) + (n - 1)A'_s(d' - y_0) \quad (C.2a)$$

$$I_{cr} = \frac{by_0^3}{3} + nA_s(d - y_0)^2 + (n-1)A'_s(y_0 - d')^2 \quad (C.2b)$$

where, d : effective depth (mm)

h : total depth (mm)

b : width (mm)

d' : position of compression steel, measured from top fiber (mm)

A_s : area of steel in tension (mm²)

A'_s : area of steel in compression (mm²)

E_s : Young's modulus of steel (GPa)

E_c : Young's modulus of concrete (GPa)

n : modular ratio, E_s/E_c

y_0 : neutral axis depth of cracked section, measured from top fiber (mm)

I_{cr} : moment of inertia of cracked section (mm⁴)

For uncracked section, the neutral axis depth and moment of inertia [C.2, C.5] are given in Eqs. (C.3a) and (C.3b), respectively.

$$y_1 = \frac{0.5bh^2 + (n-1)(A_s d) + (n-1)(A'_s d')}{bh + (n-1)A_s + (n-1)A'_s} \quad (C.3a)$$

$$I_{unc} = \frac{bh^3}{12} + bh\left(\frac{h}{2} - y_1\right)^2 + (n-1)A_s(d - y_1)^2 + (n-1)A'_s(y_1 - d')^2 \quad (C.3b)$$

where, y_1 : neutral axis depth of uncracked section, measured from top fiber (mm)

I_{unc} : moment of inertia of uncracked section (mm⁴)

Let the neutral axis depth profile be expressed by a quadratic equation.

$$\bar{y} = ax^2 + bx + c \quad (C.4)$$

where, \bar{y} : neutral axis depth at section, measured from top fiber

x : distance measured from the left support of beam

In Eq. (C.4), the constants a , b and c are determined from boundary conditions. The boundary conditions are: at $x=0$, $\bar{y} = c = y_1$, at $x = x_1$, $\bar{y} = y_0$ and at $x = L$, $\bar{y} = y_1$. Upon substitution, the following expression for the neutral axis depth, except at $x_1=0$ and $x_1=L$ is obtained.

$$\bar{y} = \frac{(y_0 - y_1)}{x_1(L - x_1)}(Lx - x^2) + y_1 \quad (C.5)$$

where, L : length of beam

x_1 : location of load position, measured from left support of beam

Due to the variation in applied load and cracking moment of concrete, the neutral axis depth, y_0 , is not constant and hence the effect of applied load has to be considered. The concept of variations in neutral axis profile due to a change in the applied load is shown in **Fig. C.2**. By considering the variation in y_0 as a quadratic equation, the modified neutral axis depth of the cracked section is expressed as follows.

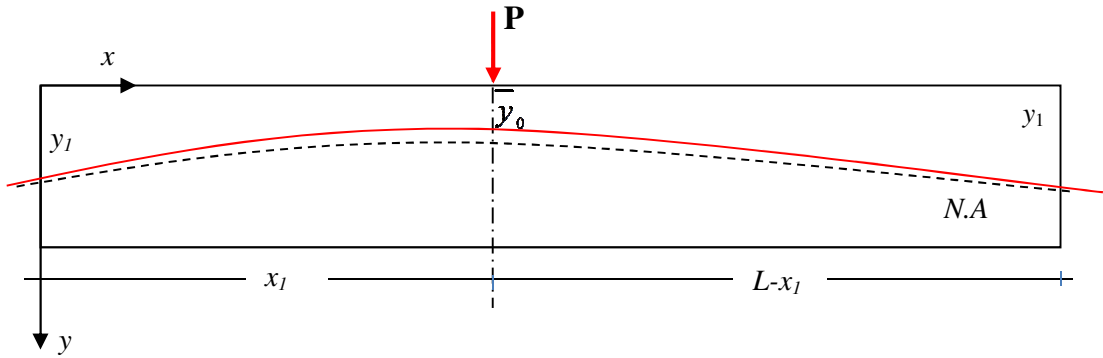


Fig. C.2 Concept of variation in neutral axis depth profile

$$\bar{y}_0 = a_1 \eta^2 + c_1 \quad (C.6)$$

where: a_1, c_1 : constants

\bar{y}_0 : modified neutral axis depth of the cracked section, measured from top fiber (mm)

η : M_a / M_{cr}

The boundary conditions are: at $\eta=0$, $\bar{y}_0 = y_1$ and at $\eta \geq 1$, $\bar{y}_0 = y_0$. Expressions for the modified neutral axis and moment of inertia of the cracked section are given in Eq. (C.7) and Eq. (C.8). The modified neutral axis profile at any section is given in Eq. (C.9).

$$\bar{y}_0 = \eta^2 y_0 + (1 - \eta^2) y_1 \geq y_0 \quad (\text{C.7})$$

$$\bar{I}_{cr} = \eta^2 I_{cr} + (1 - \eta^2) I_{unc} \geq I_{cr} \quad (\text{C.8})$$

$$\bar{y} = \frac{(\bar{y}_0 - y_1)}{x_1(L - x_1)}(Lx - x^2) + y_1 \quad (\text{C.9})$$

where, \bar{I}_{cr} : modified moment of inertia of cracked section corresponding to \bar{y}_0 (mm^4)

A similar method is used to get an expression for moment of inertia at an arbitrary section.

$$I(x) = \frac{(\bar{I}_{cr} - I_{ucr})}{x_1(L - x_1)} x(L - x) + I_{unc} \quad (\text{C.10})$$

where, $I(x)$: moment of inertia

For new RC structures, the neutral axis depth profile is not steady and it moves with the load. In such a case, for the computation of moment of inertia, envelope for neutral axis depth profile is important. For the derivation of NA depth envelope diagram, consider the following RC beam shown in **Fig. C.3**. In the figure, the neutral axis depth envelope is shown in dashed curve.

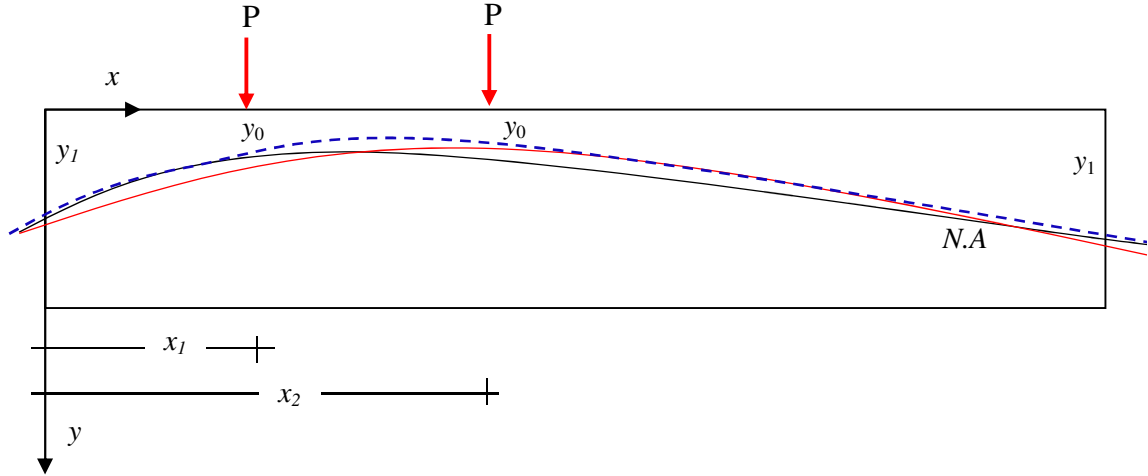


Fig. C.3 Neutral axis depth envelope

Let the neutral axis depth envelope is expressed by a cubic function, given in Eq. (C.11). The constants are determined from boundary conditions. The boundary conditions are: at $x=0$, $\bar{y} = y_1$, at $x=L$, $\bar{y} = y_1$, and at $x = x_1$ and $x = x_2$, $\bar{y} = y_0$.

$$\bar{y} = ax^3 + bx^2 + cx + d \quad (\text{C.11})$$

where, $a = \frac{-(c + bL)}{L^2}$

$$b = \frac{(y_0 - y_1)L^2 - cx_2(L^2 - x_2^2)}{Lx_2^2(L - x_2)}$$

$$c = \frac{[(x_2^3 - x_1^3)(L - x_2) - Lx_1^2(x_2 - x_1)](y_0 - y_1)L}{[L(x_2^2 - x_1^2)(L - x_2) - x_1(L^2 - x_2^2)(x_2 - x_1)](x_1x_2)}$$

$$d = y_1$$

x_1, x_2 - initial and final locations of loads

C.2.2 Neutral Axis Depth Profile for Old Structures

On the other hand, for old structures, for the derivation of neutral axis depth and moment of inertia at a section, the neutral axis depth is assumed to be independent of the location of the load and the section is fully cracked at the mid span. For old structures, in general, the neutral axis depth and the moment of inertia at a section have obtained [C.4]. Consider the longitudinal cross section with symmetrical profile shown in **Fig. C.4**.

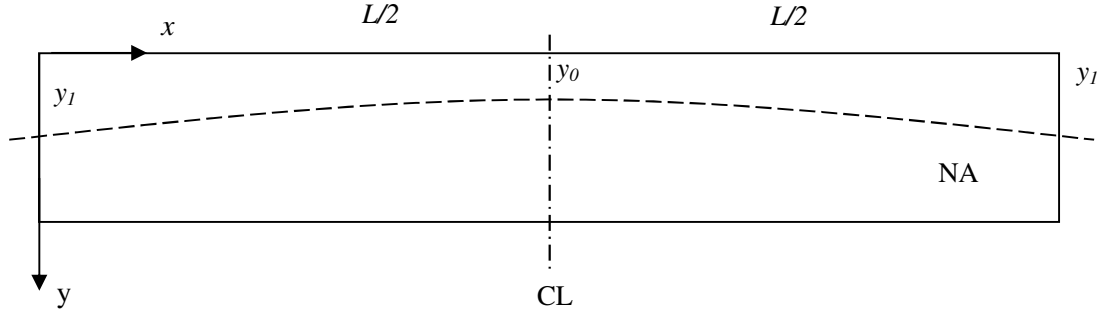


Fig. C.4 Variation of neutral axis depth of existing RC beam

In this case, the boundary conditions are: at $x=0$, and at $x=L$, $\bar{y} = y_1$, at $x = L/2$, $\bar{y} = \bar{y}_0$. Upon substitution and simplification, the expressions for the neutral axis depth and moment of inertia at a section are given in Eqs. (C.12) and (C.13), respectively.

$$\bar{y} = \left(\frac{4x}{L^2} (L-x) \right) \bar{y}_0 + \left(1 - \left(\frac{4x}{L^2} (L-x) \right) \right) y_1 \quad (\text{C.12})$$

$$I(x) = \left(\frac{4x}{L^2} (L-x) \right) \bar{I}_{cr} + \left(1 - \left(\frac{4x}{L^2} (L-x) \right) \right) I_{unc} \quad (\text{C.13})$$

Table C.1 summarizes expressions for neutral axis depth and moment of inertia of different types of beams with different support conditions.

C.3 Moment Distributions for Various Boundary Conditions

Consider the beam fixed at both ends as shown in **Fig. C.5**. Using the method of influence lines, the moment at a section can be obtained. Values of M_a , M_b and M_s (moment ordinates) for different end conditions are given in **Table C.2**.

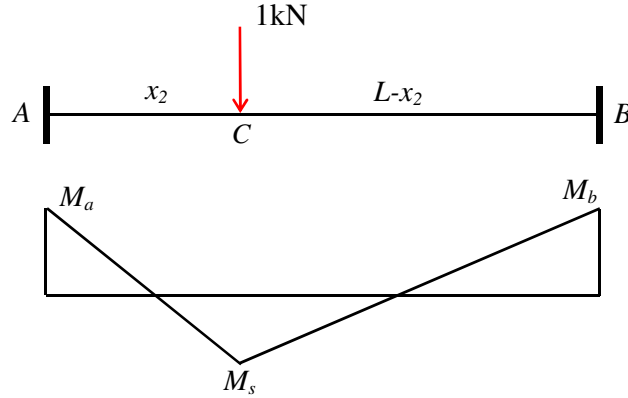


Fig. C.5 Influence Line for Bending Moment at C

Let the moment equation for segment i is expressed by $w_i x + d_i$ and the corresponding moment equations for member AC and CB are given in the following equation.

$$M_x = \begin{cases} w_1 = \frac{(M_s - M_a)}{x_2}, & d_1 = M_a \text{ for } 0 \leq x \leq x_2 \\ w_2 = \frac{(M_b - M_s)}{(L - x_2)}, & d_2 = \frac{(LM_s - x_2 M_a)}{(L - x_2)} \text{ for } x_2 \leq x \leq L \end{cases} \quad (\text{C.14})$$

where, M_a, M_b : moment ordinates at supports A and B , respectively

M_s : span moment (moment ordinate) in member AB

C.4 Slope and Deflection Calculations

The slope and deflection of a beam at any location are calculated using the general beam theory [C.6] and the equations are given as follow:

$$\theta_x = \int \frac{M(x)}{EI(x)} dx \text{ and } \delta_x = \int \theta_x dx \quad (\text{C.15})$$

where, θ_x : slope of beam

δ_x : deflection

Let an expression for moment of inertia at a section $I(x)$ be represented by a quadratic equation, $ax^2 + bx + c$. Upon substitution and integration, equations for slope and deflection of a beam, confirmed by a mathematical operation program, Mathematica [C.7], are obtained. These are given in Eqs. (C.16) - (C.19).

For member interval AC ($0 \leq x \leq x_2$):

$$E\theta_x = \frac{w_1 \log(ax^2 + bx + c)}{2a} + \frac{z_1 \tan^{-1} A}{am} + c_1 \quad (\text{C.16})$$

$$E\delta_x = \frac{1}{2ma^2} \left(2(\tan^{-1} A)(2a^2 d_1 x + a(b(d_1 - w_1 x) + 2cw_1) - b^2 w_1) + m(\log(ax^2 + bx + c)(-ad_1 + aw_1 x + bw_1) + 2ax(ac_1 - w_1)) \right) + c_2 \quad (\text{C.17})$$

For member interval CB ($x_2 \leq x \leq L$):

$$E\theta_x = \frac{w_2 \log(ax^2 + bx + c)}{2a} + \frac{z_2 \tan^{-1} A}{am} + c_3 \quad (\text{C.18})$$

$$E\delta_x = \frac{1}{2ma^2} \left(2(\tan^{-1} A)(2a^2 d_2 x + a(b(d_2 - w_2 x) + 2cw_2) - b^2 w_2) + m(\log(ax^2 + bx + c)(-ad_2 + aw_2 x + bw_2) + 2ax(ac_3 - w_2)) \right) + c_4 \quad (\text{C.19})$$

where, $m = \sqrt{4ac - b^2}$

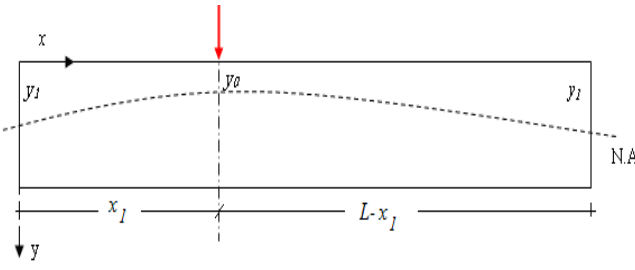
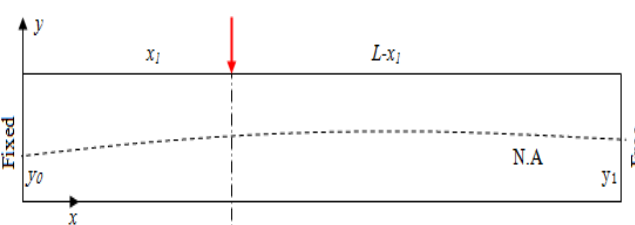
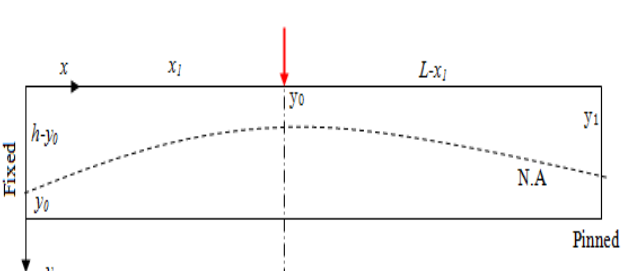
$$z_1 = (2ad_1 - bw_1)$$

$$z_2 = (2ad_2 - bw_2)$$

$$A = (2ax + b)/m$$

The integration constants are to be determined from continuity and boundary conditions. The values of c_1 , c_2 , c_3 and c_4 are given in **Table C.3**.

Table C.1 Variations in neutral axis depth and moment of inertia of different types of beams

No.	Neutral axis depth profile	Expressions for neutral axis depth and moment of inertia
1	 <p style="text-align: center;">Simply supported</p>	$\bar{y} = \frac{(\bar{y}_0 - y_1)}{x_1(L - x_1)}(Lx - x^2) + y_1$ $x_1 = L/2$ <hr/> $I(x) = ax^2 + bx + c$ $a = \frac{4}{L^2}(I_{ucr} - \bar{I}_{cr}), \quad b = \frac{4}{L}(\bar{I}_{cr} - I_{ucr}),$ $c = I_{unc}$
2	 <p style="text-align: center;">Cantilever</p>	$\bar{y} = \bar{y}_0 \left(1 + \left(\frac{x}{L} \right)^2 \right) - y_1 \left(\frac{x}{L} \right)^2$ <hr/> $I(x) = ax^2 + bx + c$ $a = \frac{1}{L^2}(I_{ucr} - \bar{I}_{cr}), \quad b = 0, \quad c = \bar{I}_{cr}$
3	 <p style="text-align: center;">Propped cantilever</p>	$\bar{y} = ax^2 + bx + c$ $a = \frac{[y_1 - (L^2(2\bar{y}_0 - h) - x_1^2 y_1)L]}{x_1 L^3}$ $b = (L^2(2\bar{y}_0 - h) - x_1^2 y_1)/(x_1 L)$ $c = h - \bar{y}_0, \quad x_1 = 5L/8$ <hr/> $I(x) = ax^2 + bx + c$ $a = \frac{2[I_{ucr} - ((2\bar{I}_{cr} - 5I_{ucr}/4))L^3]}{L^4}$ $b = \frac{2}{5}(8\bar{I}_{cr} - 5I_{ucr}), \quad c = I_{ucr} - \bar{I}_{cr}$
4		$\bar{y} = \frac{(2\bar{y}_0 - h)}{x_1(L - x_1)}(Lx - x^2) + (h - \bar{y}_0)$ $x_1 = L/2$

<p style="text-align: center;">Fixed at both ends</p>	$I(x) = ax^2 + bx + c$ $a = \frac{4}{L^2} (2\bar{I}_{cr} - I_{ucr}), \quad b = \frac{4}{L} (2\bar{I}_{cr} - I_{ucr}),$ $c = I_{unc} - \bar{I}_{cr}$
---	---

For all conditions, the modified neutral axis depth and moment of inertia expressions can be obtained from Eq. (C.7) and Eq. (C.8).

Table C.2 Values of M_a , M_s and M_b (moment ordinates) for different types of beams

Type of beam	M_a	M_s	M_b
Simply supported	0	$x_2(L - x_2)/L$	0
Cantilever	$-x_2$	0	0
Propped cantilever	$\frac{-x_2(L - x_2)(2L - x_2)}{2L^2}$	$\frac{x_2^2(L - x_2)(3L - x_2)}{2L^3}$	0
Fixed at both ends	$\frac{-x_2(L - x_2)^2}{L^2}$	$\frac{2x_2^2(L - x_2)^2}{L^3}$	$\frac{-x_2^2(L - x_2)}{L^2}$

Table C.3 Values of c_1 , c_2 , c_3 and c_4 for different types of beams

Type of beam	Constants
Simply supported	$c_1 = \frac{1}{2x_2ma^2} \left(2(\tan^{-1}A)(A_2 - A_1) + m \left(\frac{F(N_2 - N_1)}{2x_2(w_2 - w_1)} \right) \right) + c_3 + \frac{(c_4 - c_2)}{x_2}$ $c_2 = \frac{-1}{2ma^2} (z_1(\tan^{-1}b/m)(E_1) + m \log c(-ad_1 + bw_1))$ $c_3 = \frac{z_1 - z_2}{am} (\tan^{-1}A) + \frac{F}{2a} (w_1 - w_2) + c_1$ $c_4 = -2(\tan^{-1}A)(G + m(\log H)K + 2aL(ac_3 - w_2))$

Cantilever	$c_1 = -\left(\frac{w_1 \log c}{2a} + \frac{z_1 (\tan^{-1} b / m)}{am}\right)$ $c_2 = \frac{-1}{2ma^2} (z_1 (\tan^{-1} b / m)(E_1) + m \log c(-ad_1 + bw_1))$ $c_3 = \frac{z_1 - z_2}{am} (\tan^{-1} A) + \frac{F}{2a} (w_1 - w_2) + c_1$ $c_4 = \frac{1}{2ma^2} \left(2(\tan^{-1} A)(A_1 - A_2) + m \left(\frac{F(N_1 - N_2)}{2x_2(w_2 - w_1)} \right) \right) + x_2(c_1 - c_3) + c_2$
Propped cantilever	$c_1 = -\left(\frac{w_1 \log c}{2a} + \frac{z_1 (\tan^{-1} b / m)}{am}\right)$ $c_2 = \frac{-1}{2ma^2} (z_1 (\tan^{-1} b / m)(E_1) + m \log c(-ad_1 + bw_1))$ $c_3 = \frac{z_1 - z_2}{am} (\tan^{-1} A) + \frac{F}{2a} (w_1 - w_2) + c_1$ $c_4 = -2(\tan^{-1} A)(G + m(\log H)K + 2aL(ac_3 - w_2))$
Fixed at both ends	$c_1 = -\left(\frac{w_1 \log c}{2a} + \frac{z_1 (\tan^{-1} b / m)}{am}\right)$ $c_2 = \frac{-1}{2ma^2} (z_1 (\tan^{-1} b / m)(E_1) + m \log c(-ad_1 + bw_1))$ $c_3 = -\left(\frac{w_2 \log(aL^2 + bL + c)}{2a} + \frac{z_2 \tan^{-1} A}{am}\right)$ $c_4 = -2t(\tan^{-1} A)(G + m(\log H)K + 2aL(ac_3 - w_2))$
	$\left\{ \begin{array}{l} A_1 = x_2 a (2ad_1 - w_1) + E_1, \quad A_2 = x_2 a (2ad_2 - w_2) + E_2, \\ E_1 = a(bd_1 + 2cw_1) - b^2 w_1, \quad F = \log(ax_2^2 + bx_2 + c), \\ H = aL^2 + bL + c, \quad K = -ad_2 + aw_2L + bw_2, \quad E_2 = a(bd_2 + 2cw_2) - b^2 w_2, \\ N_1 = -ad_1 + ax_2 w_1 + bw_1 \quad \text{and} \quad N_2 = -ad_2 + ax_2 w_2 + bw_2. \end{array} \right.$

In actual conditions, structures are subjected to temperature gradient which causes displacements of structures. Thus, during computing deflection of structures, deflections of beams due to temperature gradient and force effects should be added up together. The deflection of a beam due to temperature gradient is computed from the following equation [C.8].

$$\delta_{xT} = \int M_x \frac{\Delta T \alpha_r}{D} dx \quad (C.20)$$

where, δ_{xT} : deflection of a beam due to thermal effect

D : beam depth

ΔT : temperature gradient

α_r : coefficient of thermal expansion

Similarly the values of M_x be obtained from Eq. (C.14). Upon substituting Eq. (C.14) to Eq. (C.20), the deflection of the beam at x_2 , measured from left support, due to thermal effect is calculated as follows. In the derivation, the method of virtual work is used and the moment equation is considered as $w_i x + d_i$.

$$\delta_{xT} = \frac{\Delta T \alpha_r}{D} \int (w_i x + d_i) dx = \frac{\Delta T \alpha_r}{D} \left[\int_0^{x_2} (w_1 x + d_1) dx + \int_{x_2}^L (w_2 x + d_2) dx \right] \quad (C.21)$$

Upon substitution and integration, the equation for deflection of a beam due to temperature gradient is given in Eq. (C.22).

$$\delta_{xT} = \frac{\Delta T \alpha_r}{2D} \left[(L + x_2)(M_s - M_a) + (2L + x_2)M_s - x_2 M_a \right] \quad (C.22)$$

C.5 Summary

- Expressions for the computation of neutral axis depth and moment of inertia of single-span RC beams with different end conditions have been obtained.
- Influence functions for slope and deflection of RC beams by considering the variation in neutral axis depth profile have been proposed.

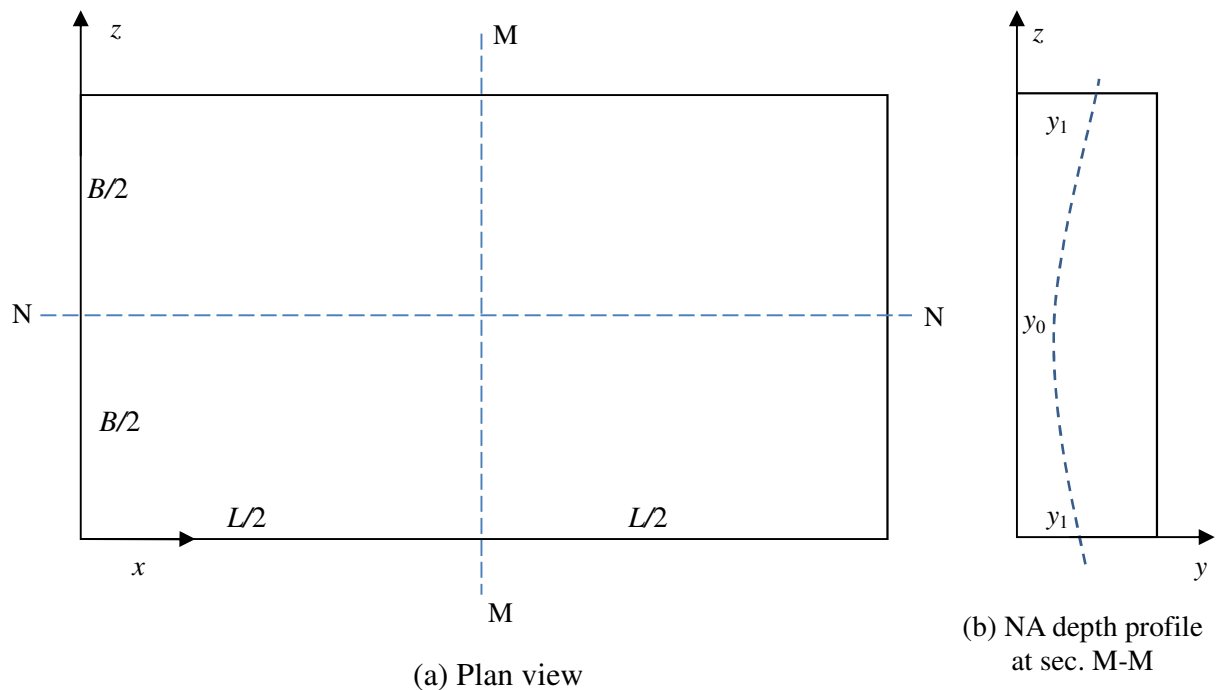
References

- [C.1] İlker Kalkan: Deflection Prediction for Reinforced Concrete Beams through Different Effective Moment of Inertia Expressions, Int. J. Eng. Research & Development, Vol.2, No.1, pp.72-80, January 2010.
- [C.2] AASHTO: American Association of State Highway and Transportation Officials, LRFD Bridge Design Specifications, 4th edition, Washington, 2007.
- [C.3] JSCE: Guidelines for Concrete, No.15, Standard Specifications for Concrete Structures, 2007.
- [C.4] Tarekegn, A.G. and Tsubaki, T.: Restoration Design for RC Slab Bridges by AASHTO LRFD, The 21st PC Symposium on Developments in Prestressed Concrete, JPCA, pp. 29-34, Oct. 2012.
- [C.5] Chen, W.F. and Duan, L.: Bridge Engineering Handbook, CRC Press LLC, Washington, D. C., 2000.
- [C.6] Popov, E.P.: Engineering Mechanics of Solids, Prentice-Hall Inc., New Jersey, 1990.
- [C.7] Wolfram Alpha, Mathematica, Online version.
- [C.8] Deflections, <https://mech.fsv.cvut.cz/homeworks/student/SM3E/deflections.pdf>

APPENDIX D – THREE-DIMENSIONAL INFLUENCE FUNCTION FOR DEFLECTION OF RC SLABS

D.1 Introduction

For three-dimensional members, an expression for the computation of NA depth at any point is of great importance. These points form a NA surface. For the computation of NA, consider the 3D member shown in **Fig. D.1**.



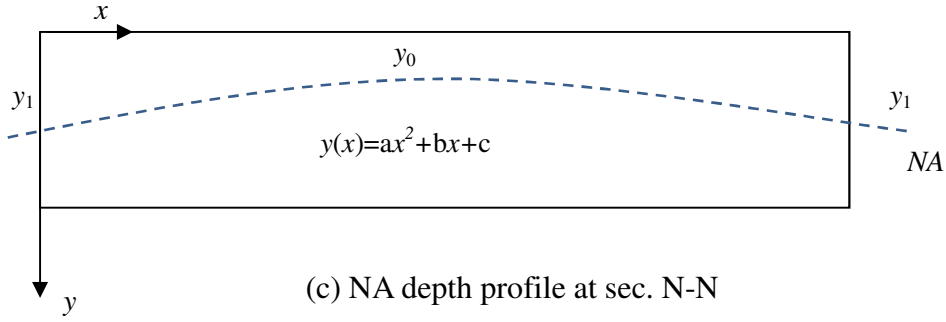


Fig. D.1 Plan view and NA depth profiles

The NA depth profile of the member at section N-N is expressed by the following quadratic equation.

$$\bar{y} = ax^2 + bx + c \quad (D.1)$$

where, $a = \frac{4(y_1 - y_0)}{L^2}$

$$b = \frac{4(y_0 - y_1)}{L}$$

$$c = y_1$$

Assume that the NA surface, $\bar{y}(x, z)$, is expressed by a quadratic equation and it is given in Eq. (D.2).

$$\bar{y}(x, z) = Dx^2 + Ex + F \quad (D.2)$$

The coefficients D , E and F are functions of z and represented by a quadratic equations. These functions are obtained from the boundary conditions (see NA depth profile at sec. M-M). The boundary conditions are: at $z=0$, $\bar{y} = y_1$, at $z = B/2$, $\bar{y} = ax^2 + bx + c$, and at $z = B$, $\bar{y} = y_1$. Thus the coefficients D , E and F become:

$$D = d_1z^2 + d_2z + d_3, \quad E = e_1z^2 + e_2z + e_3, \quad F = f_1 \quad (D.3)$$

Upon substitution, the constants become:

$$d_1 = \frac{-4a}{B^2}, \quad d_2 = \frac{-4a}{B}, \quad d_3 = e_3 = 0, \quad e_1 = \frac{-4b}{B^2}, \quad e_2 = \frac{-4b}{B}, \quad \text{and} \quad f_1 = y_1 \quad (\text{D.4})$$

Upon substituting Eqs. (D.3) and (D.4) to Eq. (D.2), the three-dimensional NA depth profile (surface) is given in Eq. (D.5).

$$\bar{y}(x, z) = \frac{1}{B^2} [2az(B-z)x^2 + 2bz(B-z)x + B^2 y_1] \quad (\text{D.5})$$

D.2 Influence of 3D Deflections of RC Slabs

Consider the following plan view and sections of RC slab shown in **Fig. D.2**. Suppose the load is applied at p_1 and deflection is computed at points p_2, p_3 and p_4 .

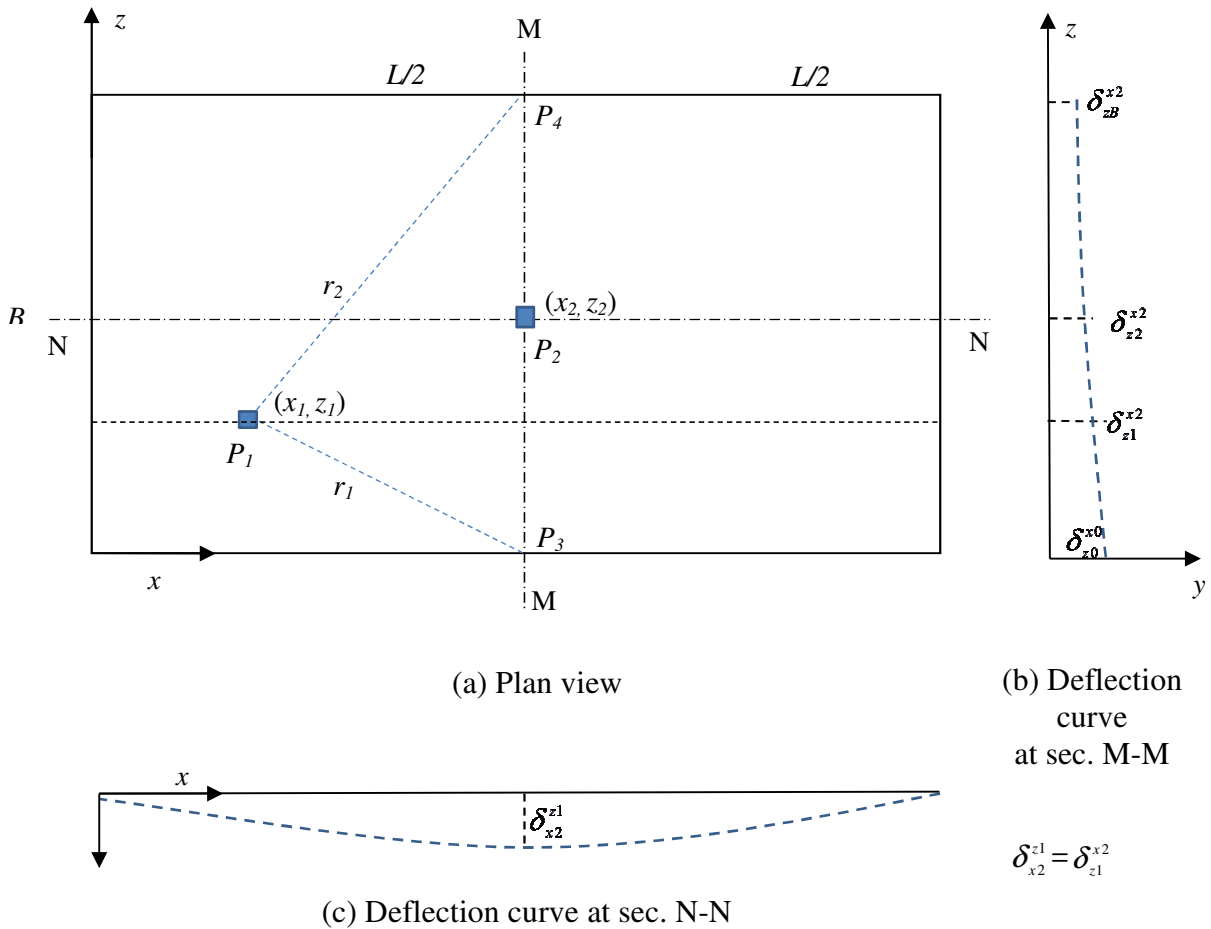


Fig. D.2 Plan view and deflection curves

D.3 Three-Dimensional FEM Simulation

To consider the effect of position of loads along the transverse direction, a standard RC slab bridge is simulated using ATENA 3D [D.1]. Bridge span of 10.40m, effective width of 3.25m, total depth of 540mm, are used. Moreover, diameter 32mm reinforcing bars with *c/c* spacing of 180mm, cover thickness of 35mm, compressive strength of 28MPa and yield strength of steel of 400MPa are used. 3D FEM model of RC slab bridge and load positions considered in the simulation are shown in **Fig. D.3** and **Fig. D.4**, respectively.

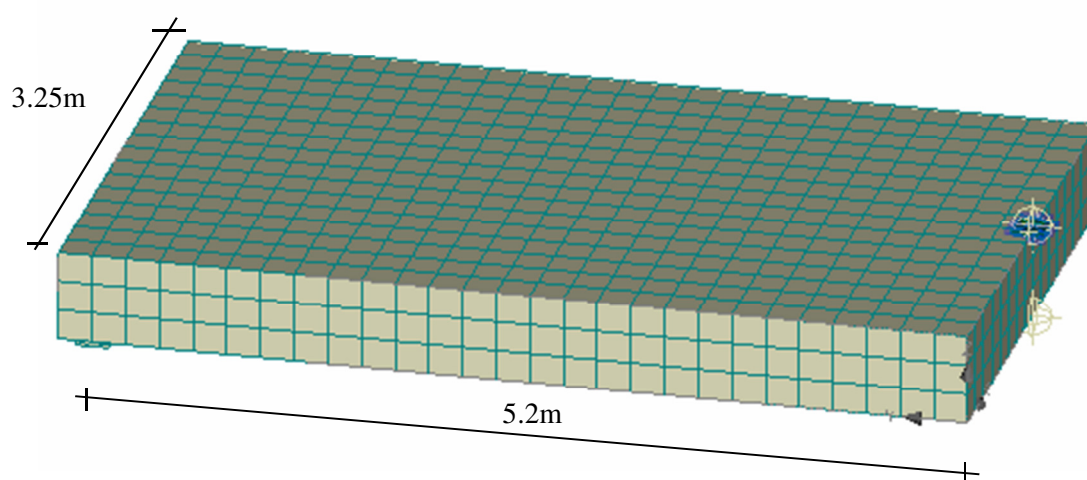


Fig. D.3 3D FEM model of RC slab bridge

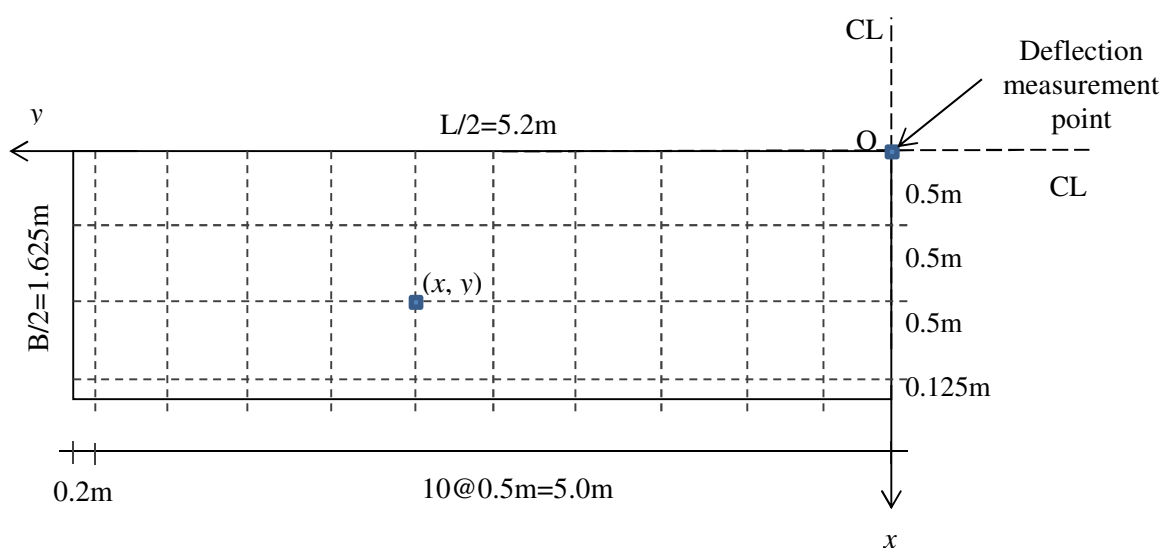


Fig. D.4 Loading grids

To have a steady neutral axis depth profile in the slab bridle, initially the slab is loaded with a uniformly distributed load (two cases are used; loads with low and high magnitudes). Next, a concentrated load is applied at each grid point (at 40 points) and deflection is measured along the longitudinal and transverse directions. At selected loading points, the corresponding deflection diagrams (at $P=75\text{kN}$) are shown in **Fig. D.5** – **Fig. D.8**.

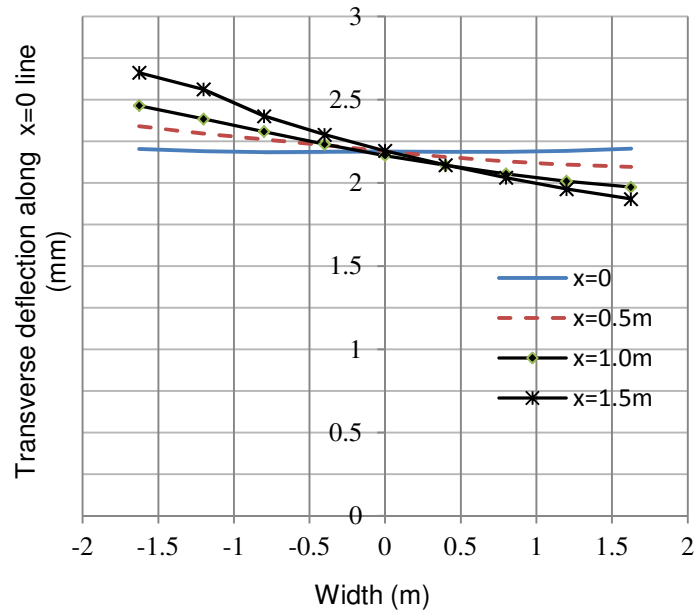


Fig. D.5 Deflection diagram with load applied at $y=0$ line

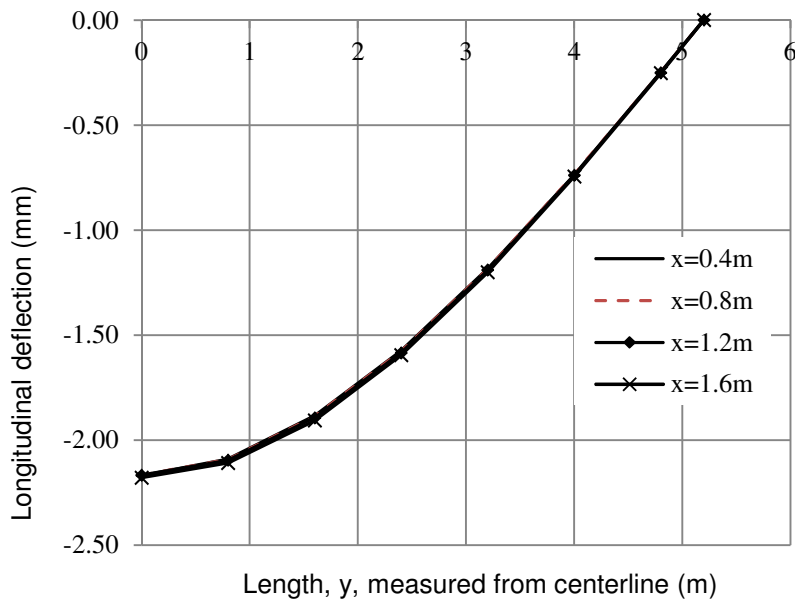


Fig. D.6 Deflection diagram with load applied at $y=0$ line

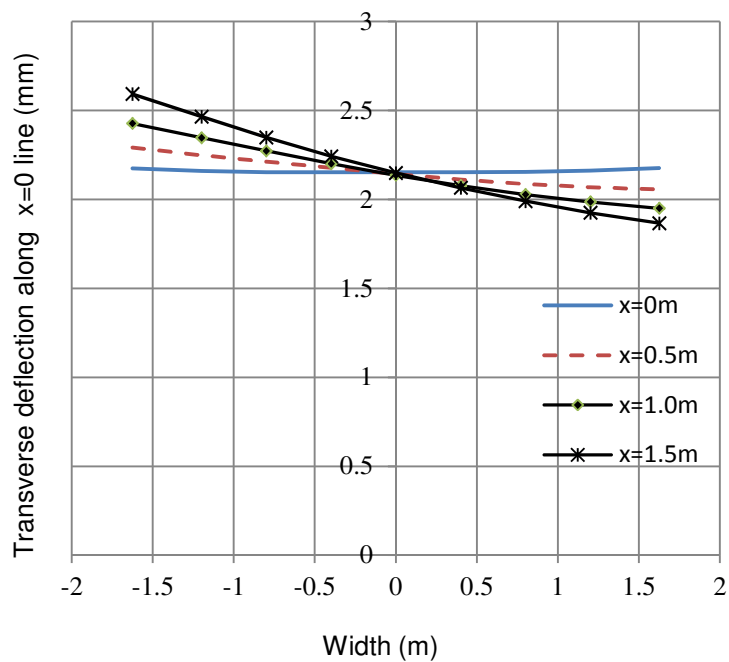


Fig. D.7 Deflection diagram with load applied at $y=1.0$ line

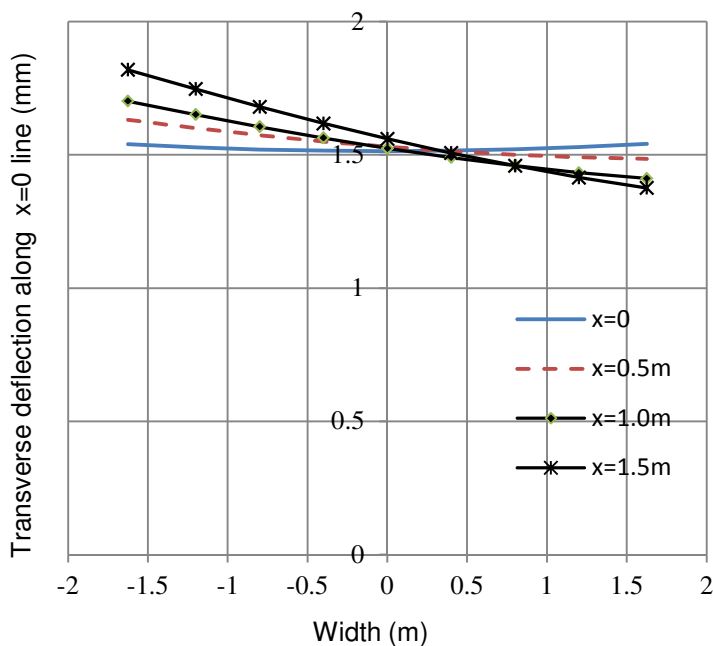


Fig. D.8 Deflection diagram with load applied at $y=2.5$ line

Using regression analysis (deflections due to 40 loading points), the mid-point deflection of the bridge is expressed by the following equation.

$$\delta_o = [-0.8y^2 + (0.27x^3 - 0.6x^2 + 0.43x - 1.7)y + 29.4]P_i \quad (D.6)$$

where, δ_o : midpoint deflection (μm)

x, y : coordinates of load position (m)

P_i : applied load (kN)

D.4 Analysis of Results

Based on the midpoint deflections, the current condition of the bridge is estimated deterministically and summary of design restoration results are shown in **Table D.1**. The position of the load is varying along the transverse line, $y=1.0\text{m}$.

Table D.1 Summary of design restoration results

Random variables	Initial values	Restored values
A_s^a (mm^2/m)	4701.80	4664.06
f_c^a (MPa)	28	28.90
d^a (mm)	489	482.91
f_y^a (MPa)	400	341.55

D.5 Summary

- 3D FEM simulation of RC slab bridge and design restoration results are shown.

References

[D.1] Červenka, V., et al.: ATENA Program Documentation, Part 1-Theory, Prague, March 22, 2010.

APPENDIX E – SUMMARY OF TEST RESULTS OF RC BEAM SPECIMEN - 2

E.1 Introduction

For verification of the design restoration method, a specimen similar to that of RC Beam Specimen-1 with an overall depth of 485mm and different cover thicknesses was prepared. **Fig. E.1** and **Fig. E.2** show the longitudinal profile and cross-section of the beam, respectively. LVDTs are placed at the top, mid-height and bottom surfaces. Strain gauges for steel and concrete at both top and bottom parts are attached. Locations of LVDTs and strain gauges are shown in **Fig. E.3** and **Fig. E.4**, respectively.

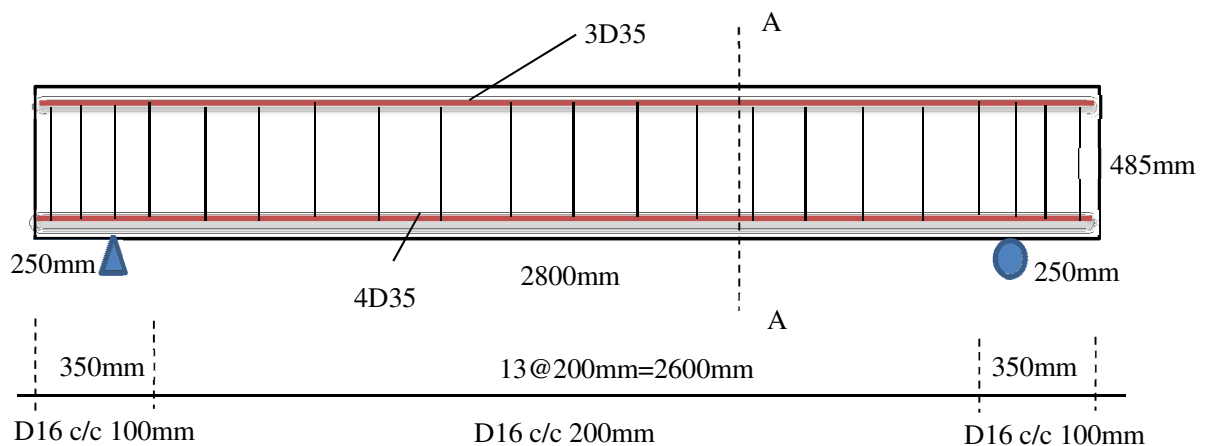


Fig. E.1 Longitudinal section of RC test beam 2

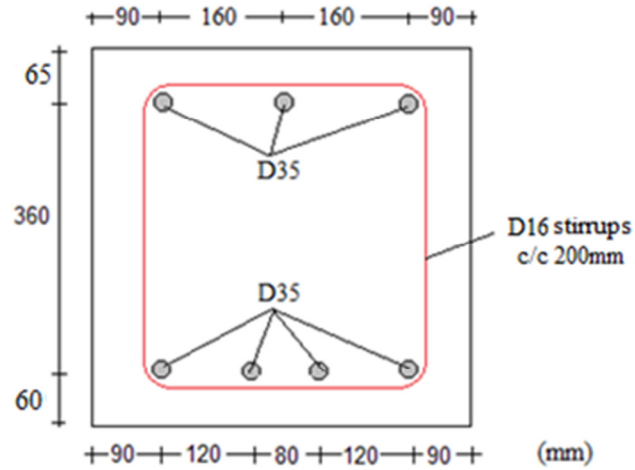


Fig. E.2 Cross section of RC test beam 2

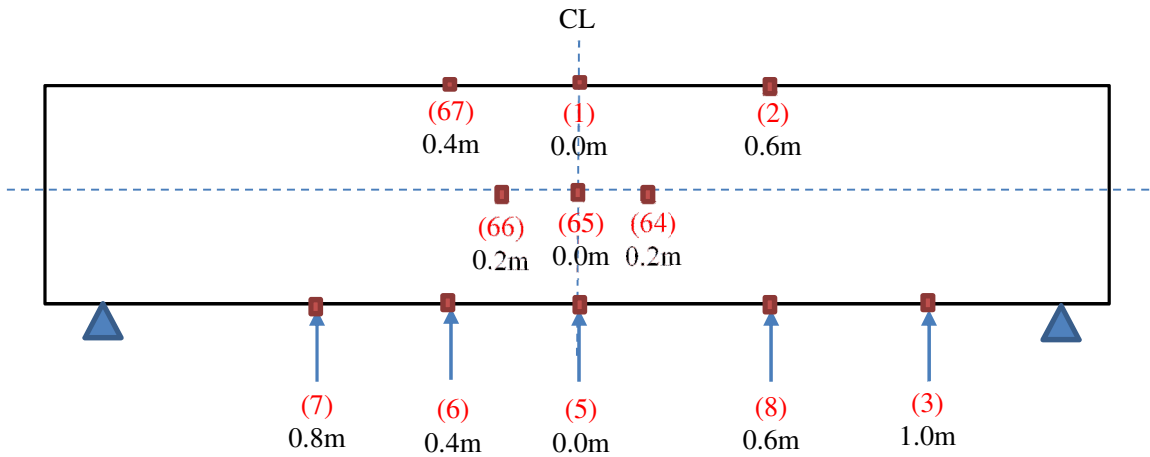


Fig. E.3 Locations of LVDTs

Positions of LVDTs (64) and (66) vary. For load position 1, they are placed at 0.4m apart, for load position 2, they are placed at 1.2m apart and for load position 3, they are placed at 2m apart, all symmetrically.

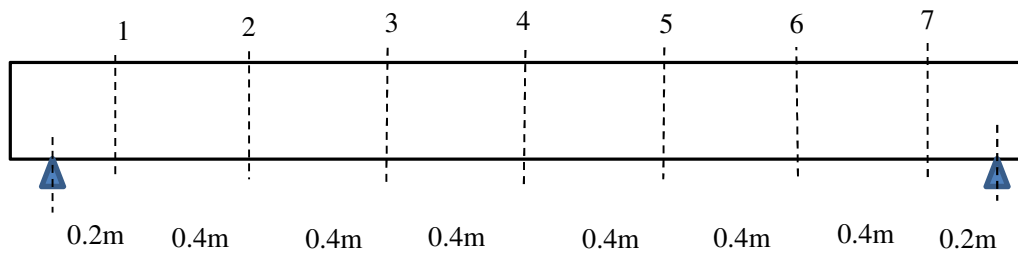


Fig. E.4 Locations of strain gauges

E.2 Loading Pattern

Loads are applied at different positions and they are shown in **Table E.1** Strain gauges for steel bars and concrete are attached at 0.4m intervals. The specimen was simply supported at both ends and tested for two-point loading with loading points symmetrically spaced at 400mm, 1200mm and 2000mm apart. Initially, at the specified load positions, the beam was loaded with 70kN load (below cracking load). This test was repeated twice and subsequently a load beyond cracking load is applied at the same load positions. The maximum load applied was 300kN.

Table E.1 Loading positions of RC beam test specimen

Load position	1 st load from left support (x)	Load spacing (y)
Pos_1	1.2m	0.4m
Pos_2	0.8m	1.2m
Pos_3	0.4m	2.0m

E.3 Load below Cracking Load

The load- displacement diagrams, strain relationships of the test beam specimen loaded with 70kN (load under the cracking load) are shown in **Fig. E.5 - Fig.E.15**.

a) Load Position-1

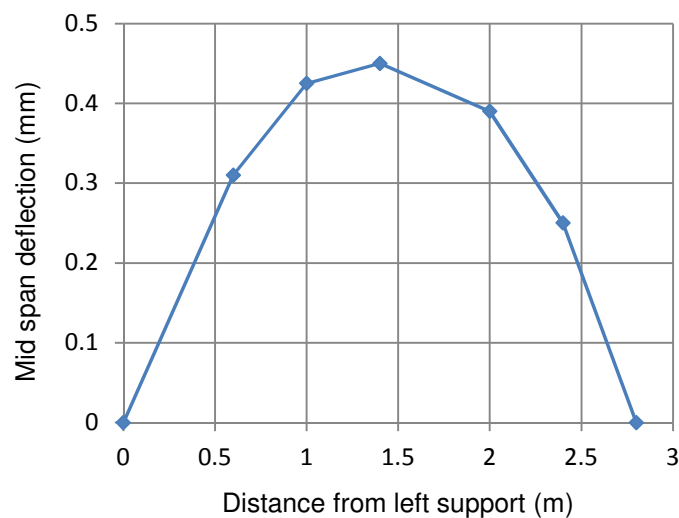


Fig. E.5 Load deflection diagram of Position-1 (bottom surface)

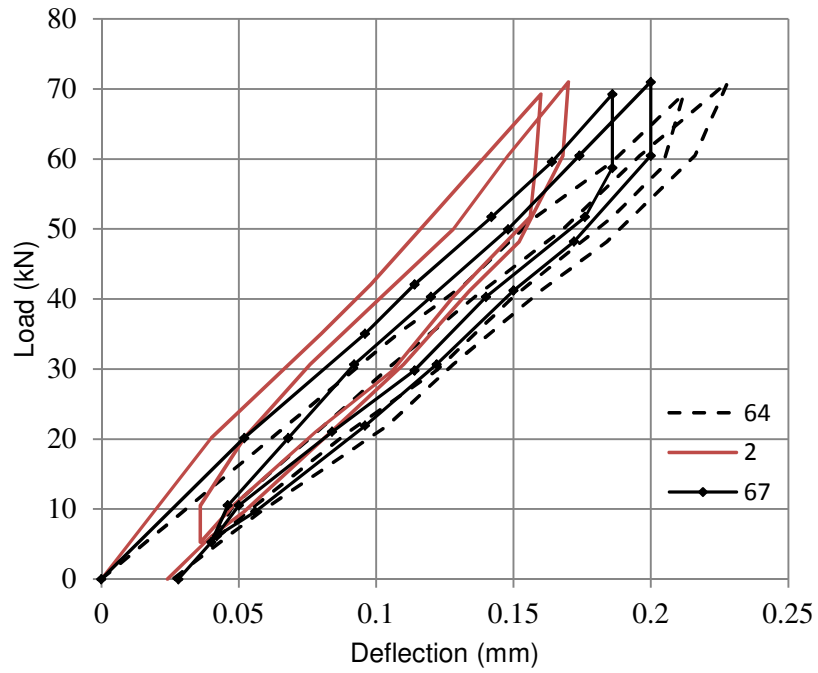


Fig. E.6 Deflection diagrams (at pts. 2, 64 and 67)

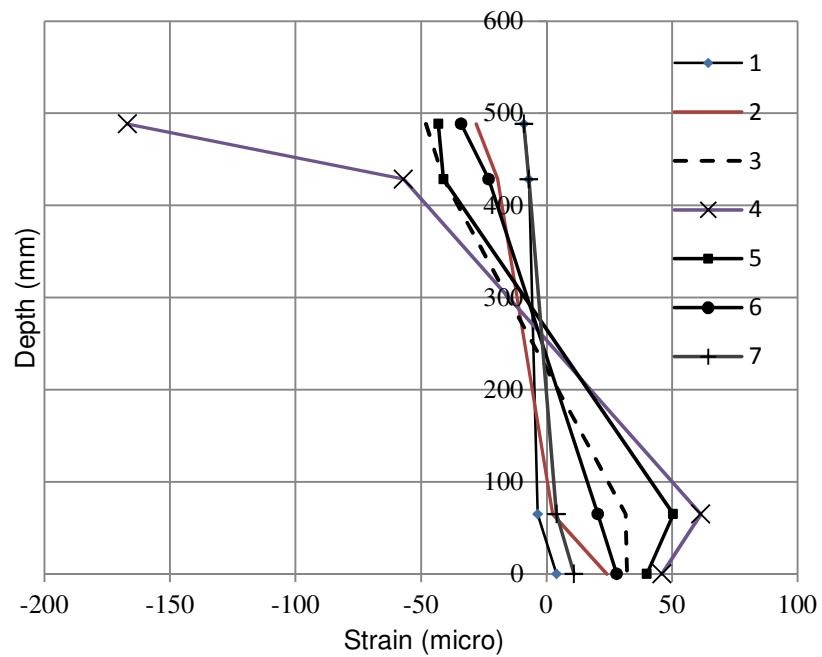
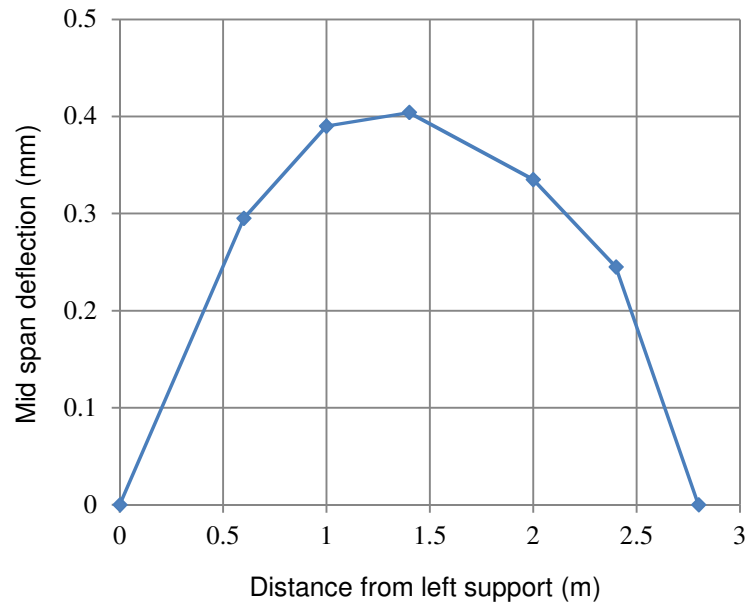
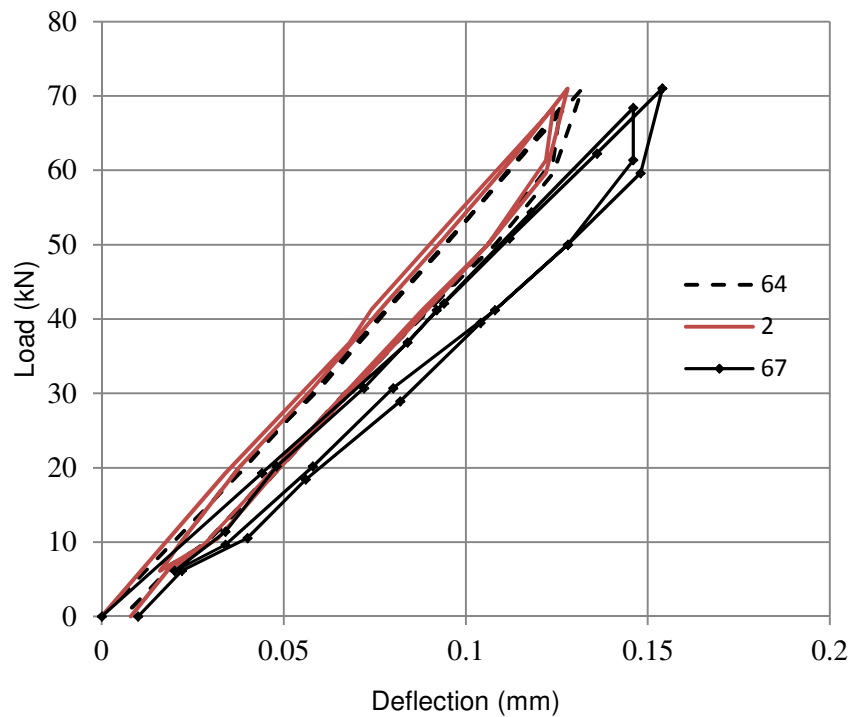


Fig. E.7 Stain distribution (Position-1)

b) Load Position-2**Fig. E.8** Load deflection diagram of Position-2 (bottom surface)**Fig. E.9** Deflection diagrams (at pts. 2, 64 and 67)

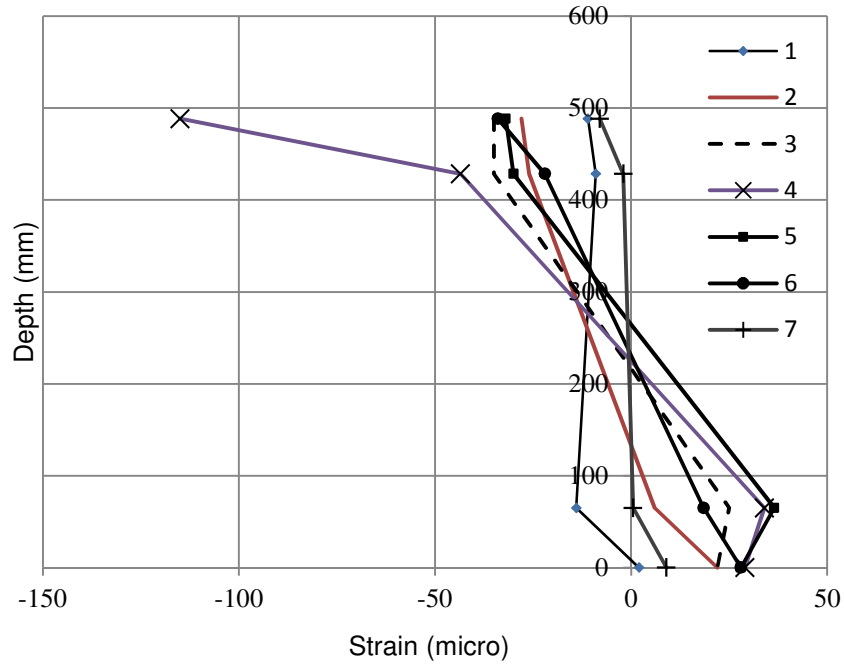


Fig. E.10 Stain distribution (Position-2)

c) Load Position-3

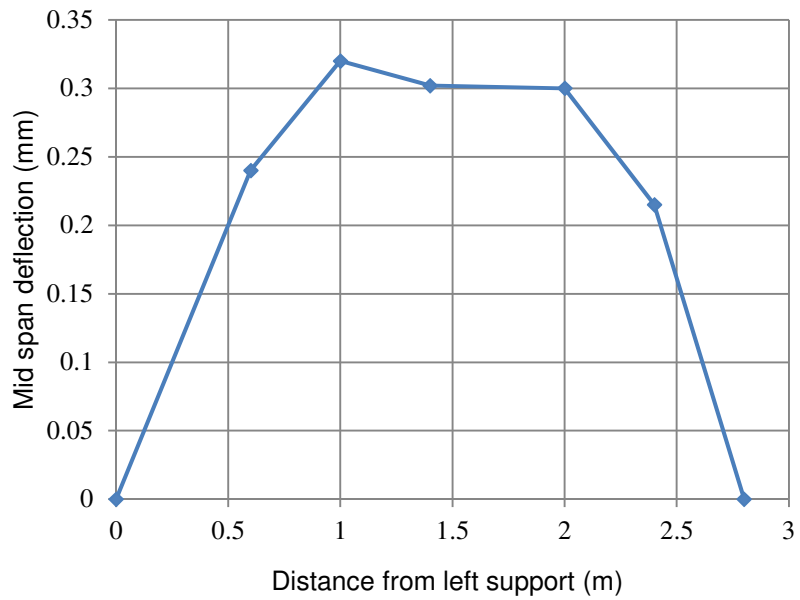


Fig. E.11 Load deflection diagram of Position-3 (bottom surface)

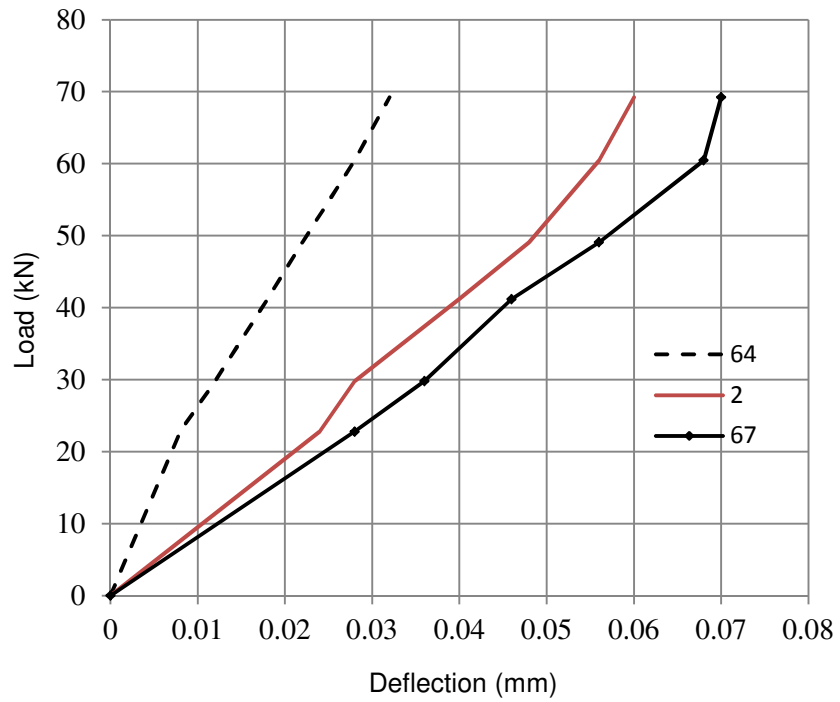


Fig. E.12 Deflection diagrams (at pts. 2, 64 and 67)

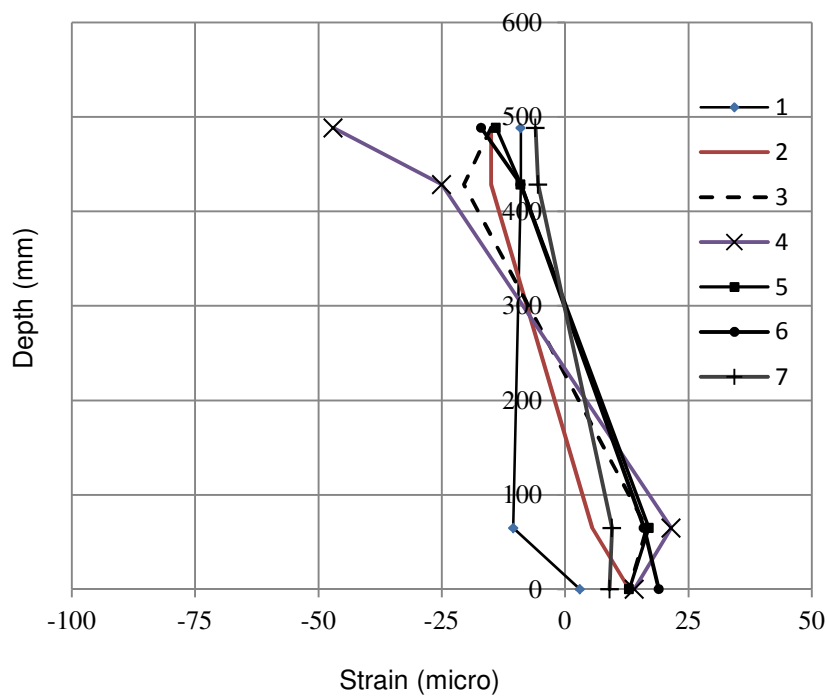


Fig. E.13 Stain distribution (Position-3)

d) Deflection at the top and bottom surfaces

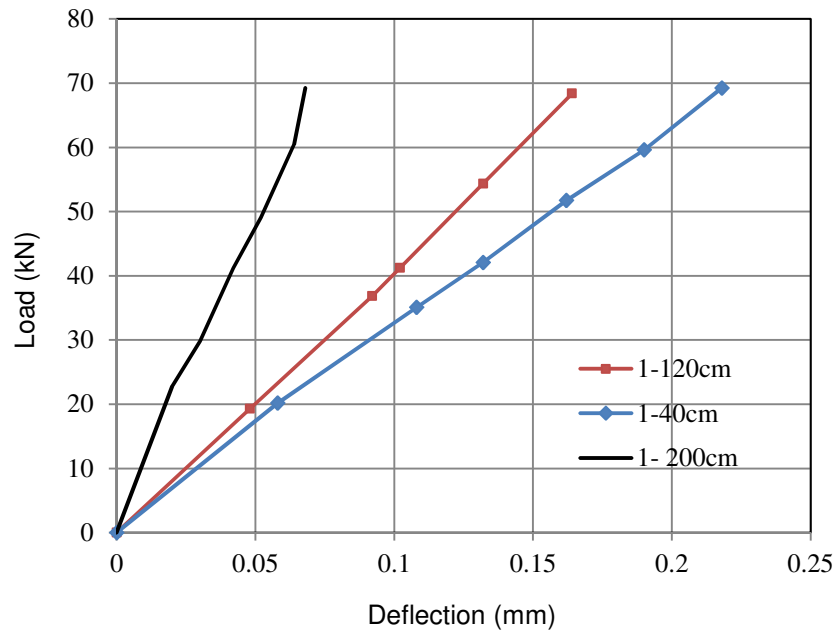


Fig. E.14 Load deflection diagram of pt. 1 (top surface)

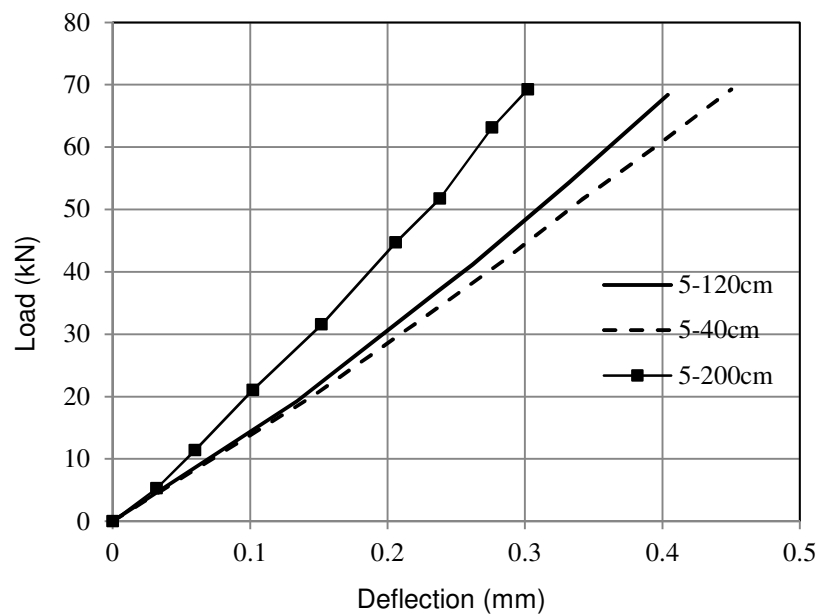


Fig. E.15 Load deflection diagram of pt. 5 (bottom surface)

E.4 Load above Cracking Load

The load-displacement diagrams, strain distributions of the test beam specimen loaded with 300kN (load above the cracking load) are shown in **Fig. E.16 - Fig.E.31**.

a) Load Position-3

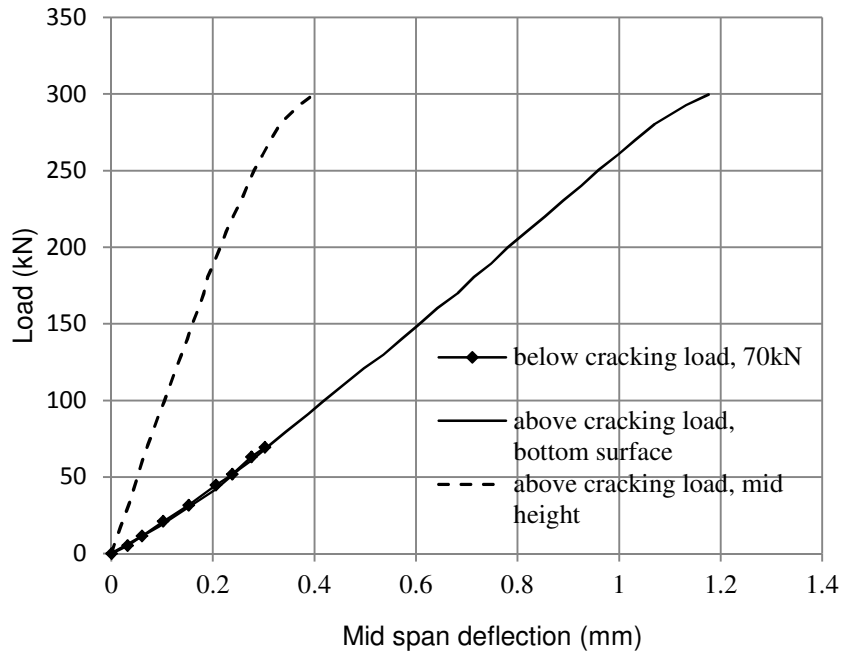


Fig. E.16 Mid span deflection diagram (Position-3)

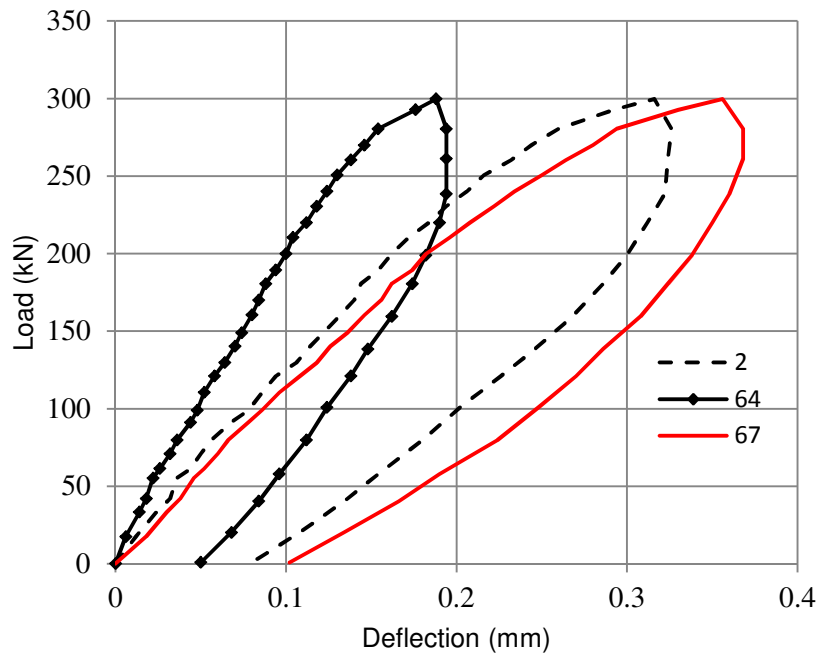


Fig. E.17 Deflection diagrams (at pts. 2, 64 and 67)

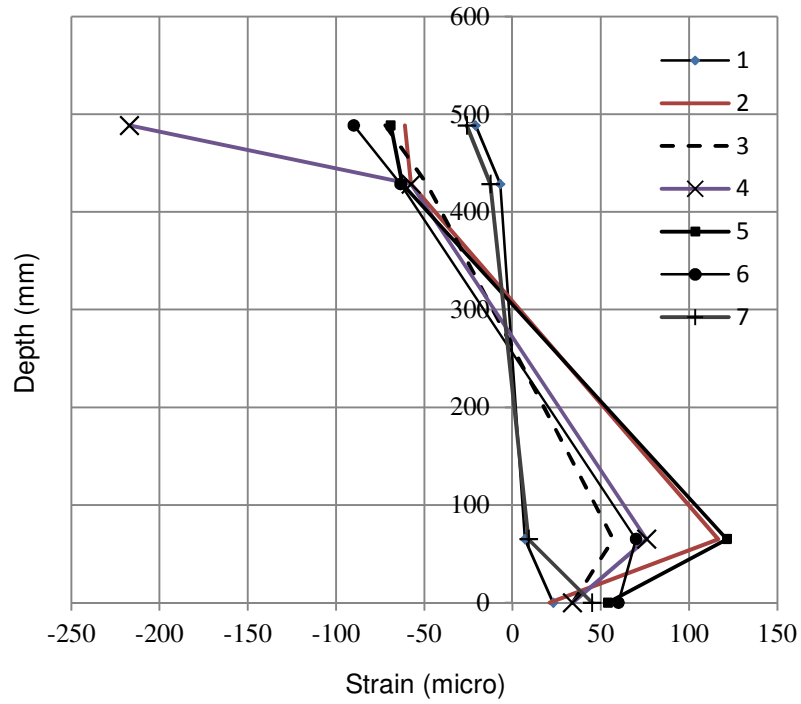


Fig. E.18 Stain distribution at P=300kN (Position-3)

b) Load Position-2

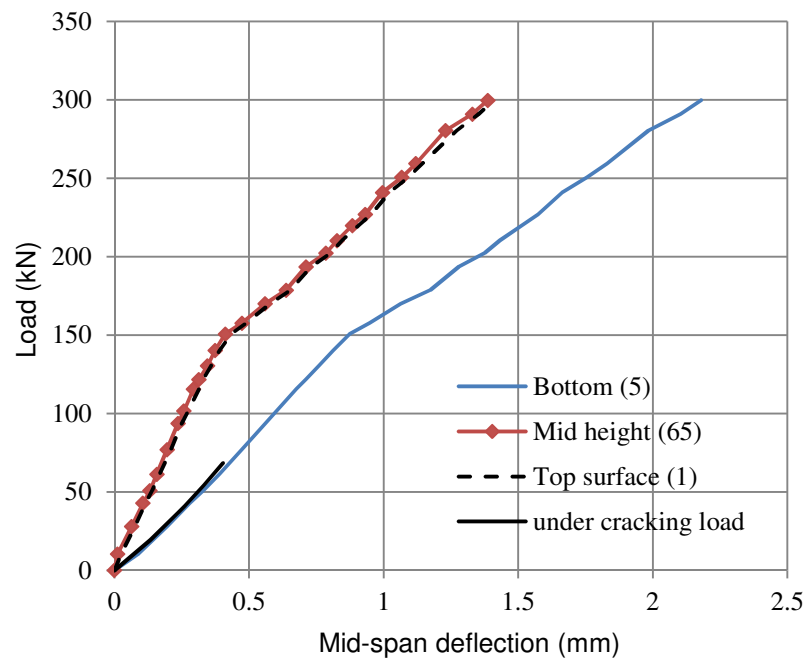


Fig. E.19 Mid span deflection diagram (Position-2)

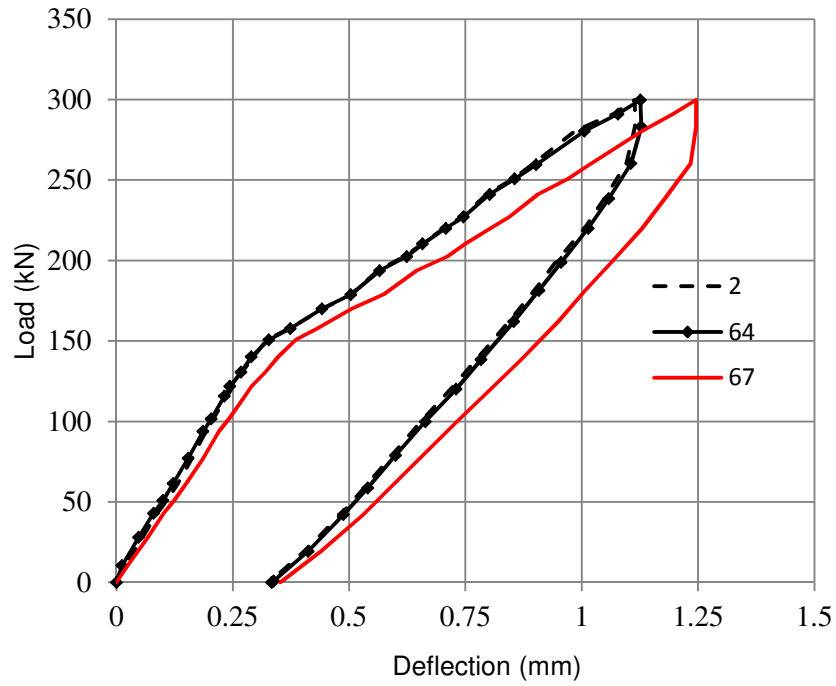


Fig. E.20 Deflection diagrams (at pts. 2, 64 and 67)

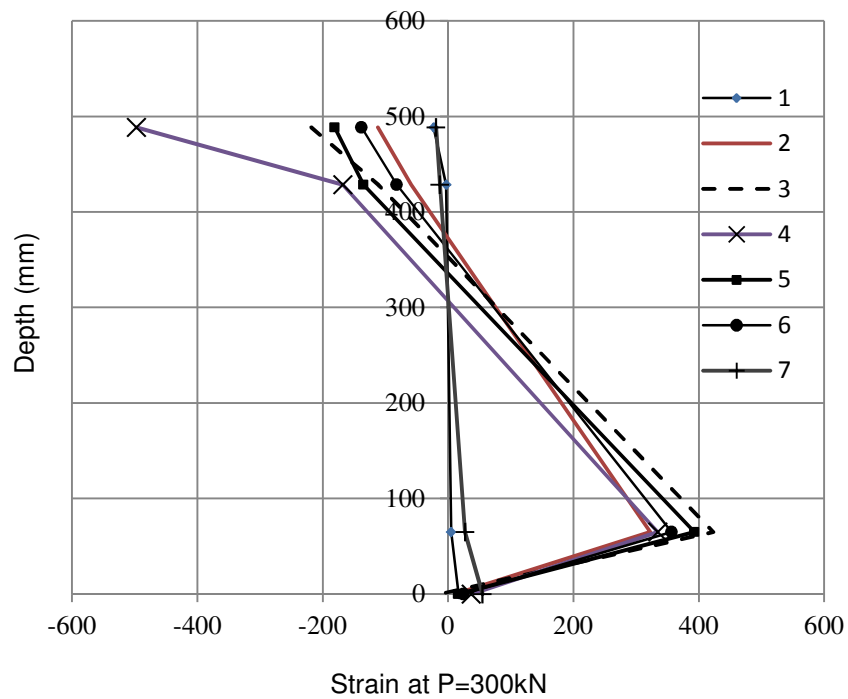


Fig. E.21 Stain distribution at P=300kN (Position-2)

c) Load Position-1

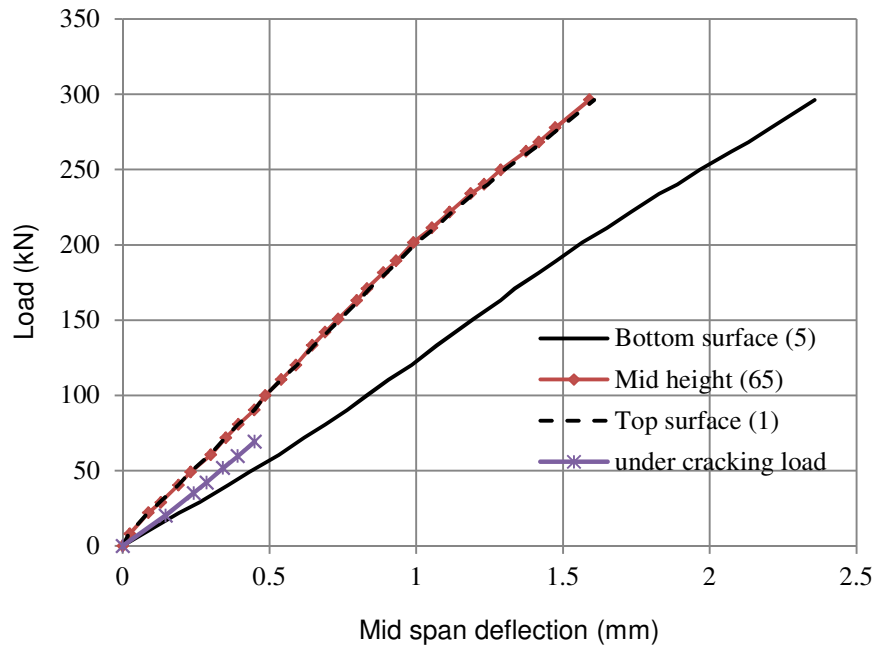


Fig. E.22 Mid span deflection diagram (Position-1)

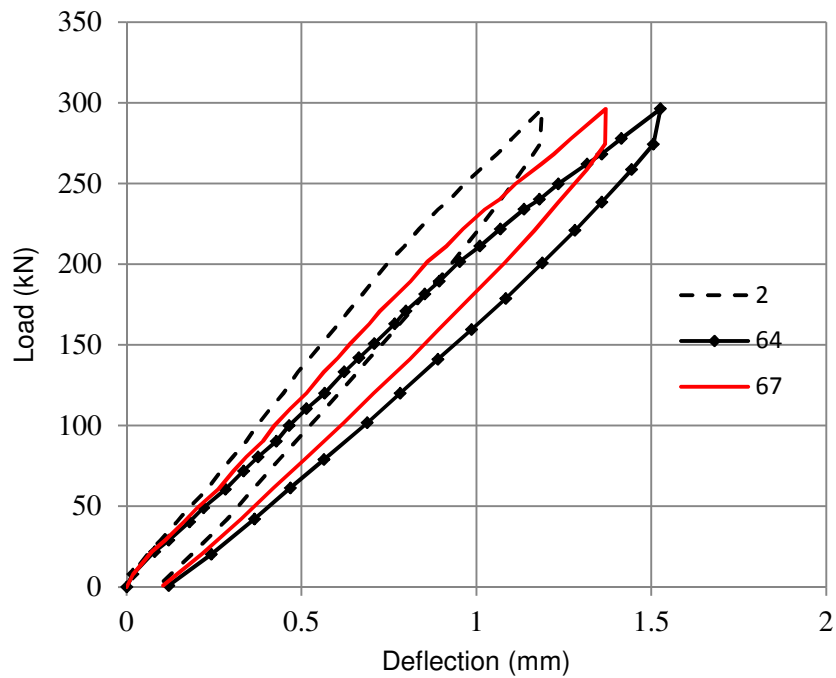


Fig. E.23 Deflection diagrams (at pts. 2, 64 and 67)

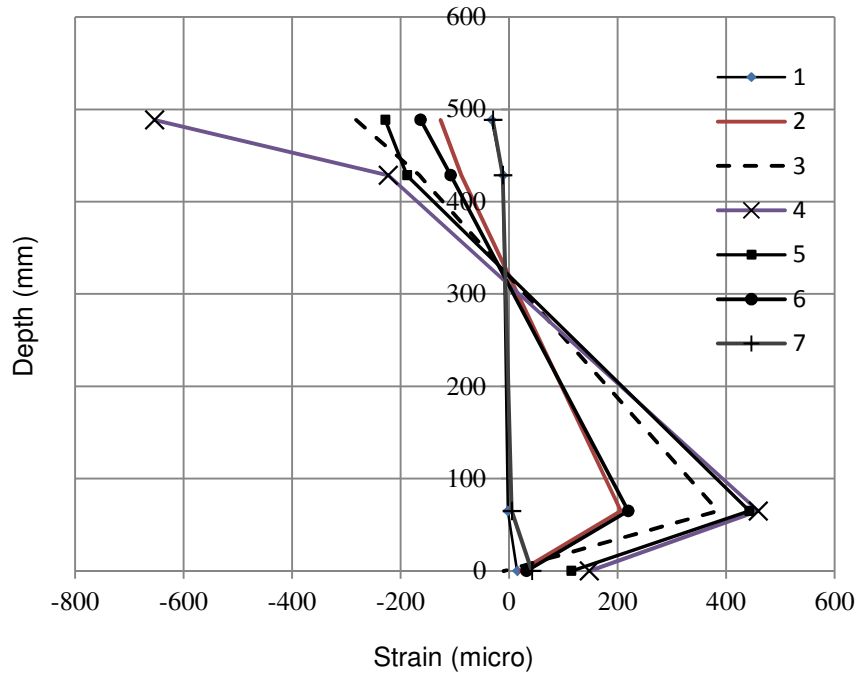


Fig. E.24 Stain distribution at P=300kN (Position-1)

d) Load Position-2 (loaded for the second time)

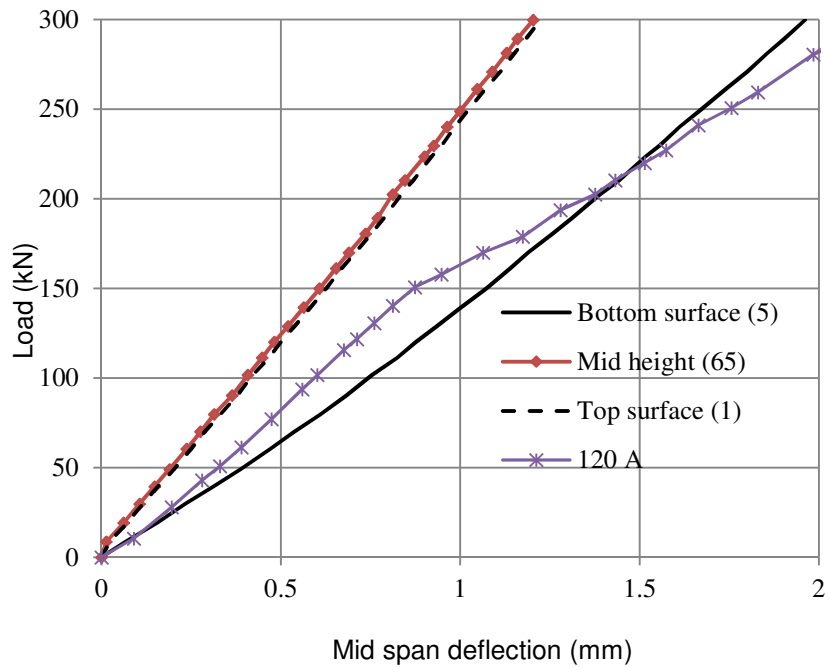


Fig. E.25 Mid span deflection diagram (Position-2)

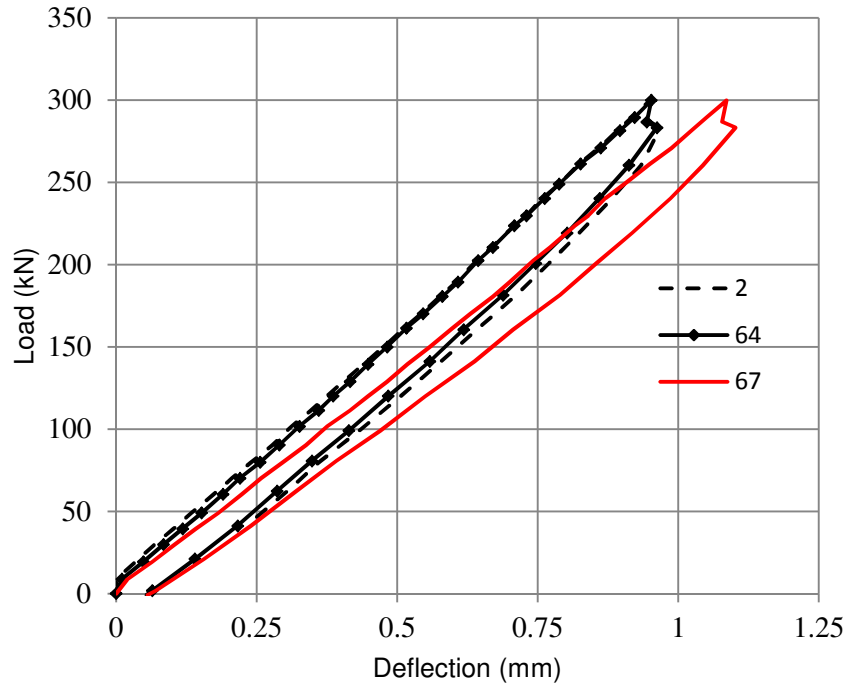


Fig. E.26 Deflection diagram (at pts. 2, 64 and 67)

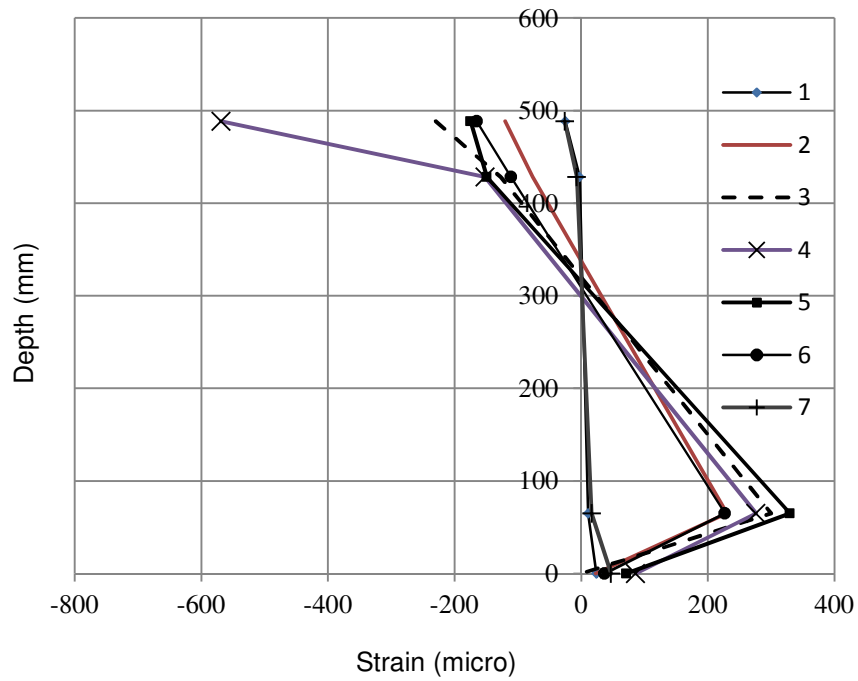


Fig. E.27 Stain distribution at P=300kN (Position-2)

e) Load Position-3 (loaded for the second time)

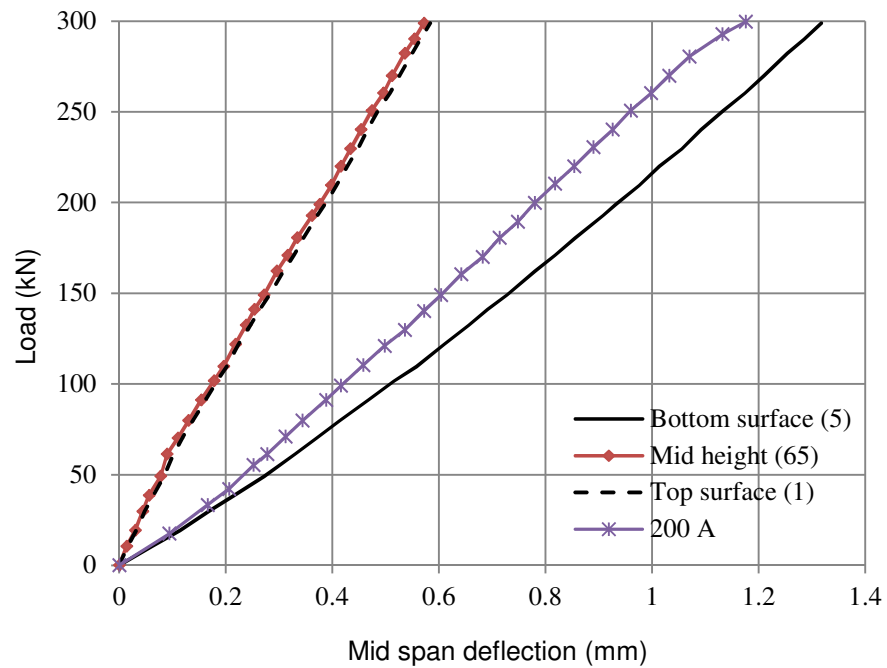


Fig. E.28 Mid span deflection diagram (Position-3)

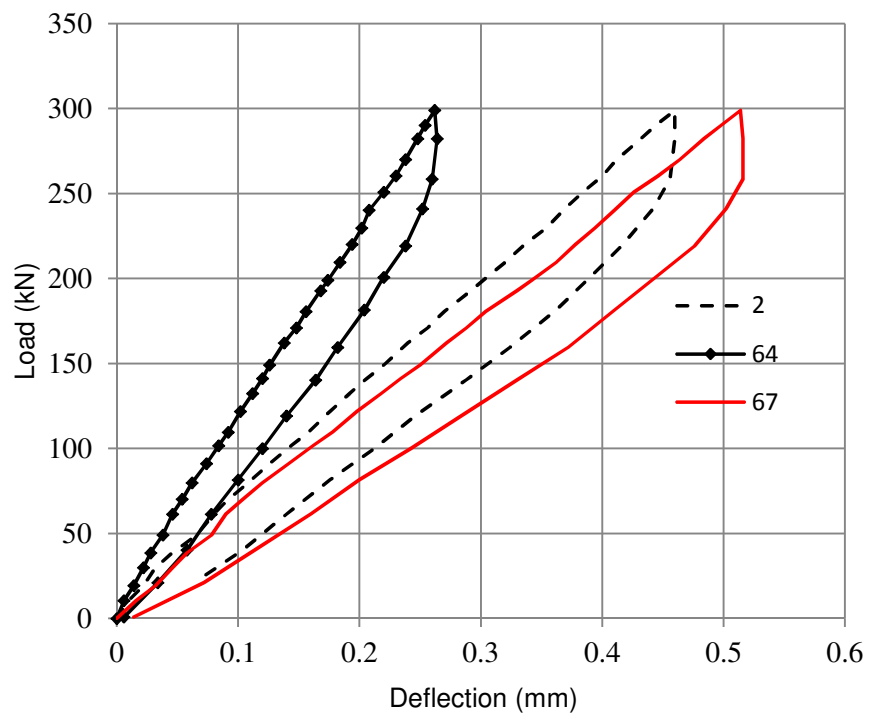


Fig. E.29 Deflection diagram (at pts. 2, 64 and 67)

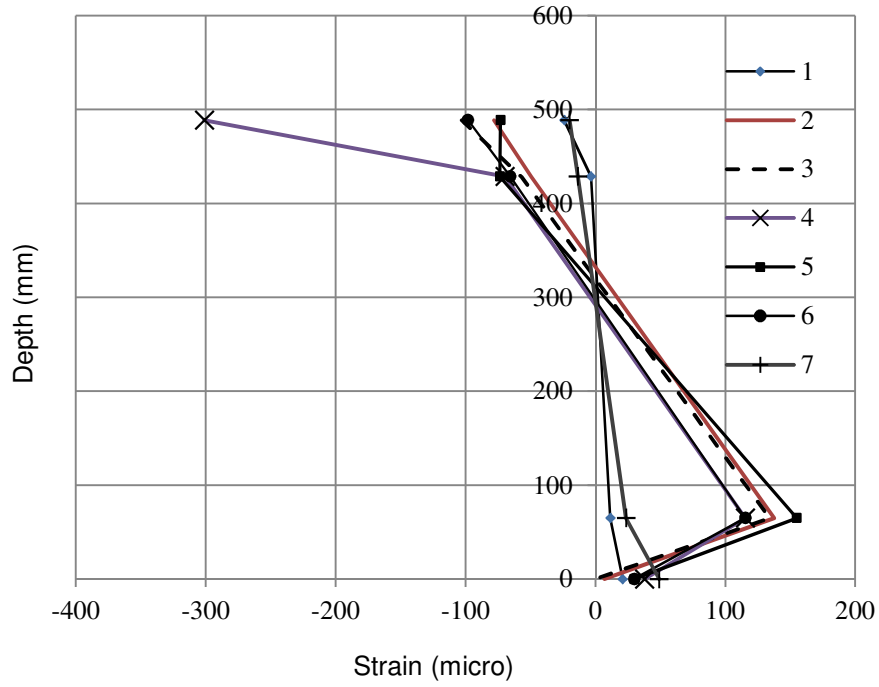


Fig. E.30 Stain distribution at P=300kN (Position-3)

f) Load deflection diagram of the specimen at the last loading case

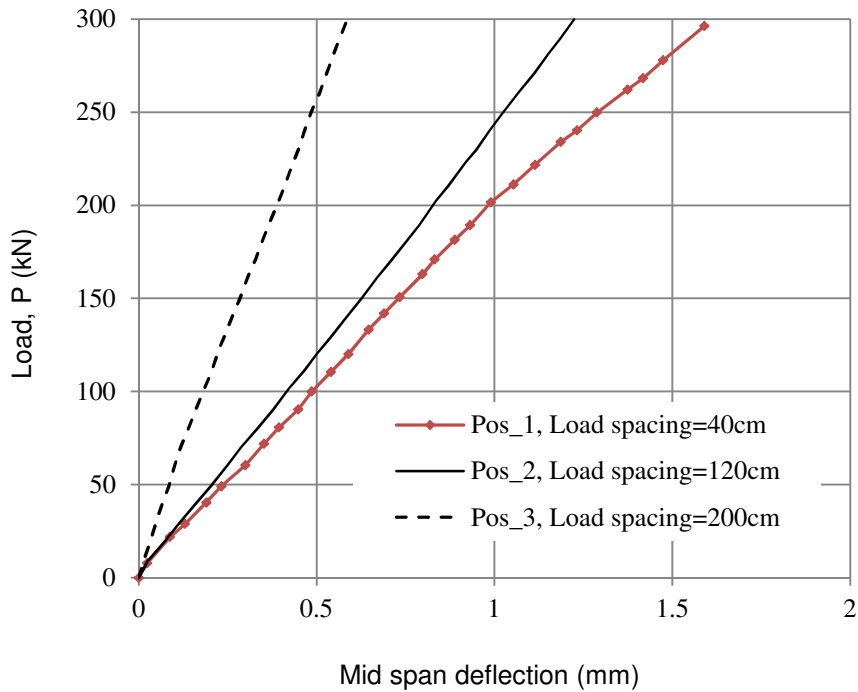


Fig. E.31 Load- mid span deflection diagram (top surface)

E.5 Crack Pattern

The crack pattern of the test beam specimen at the end of loading of 300kN is shown in **Fig. E. 32**, and the total surface crack width, in **Fig. E. 33**.

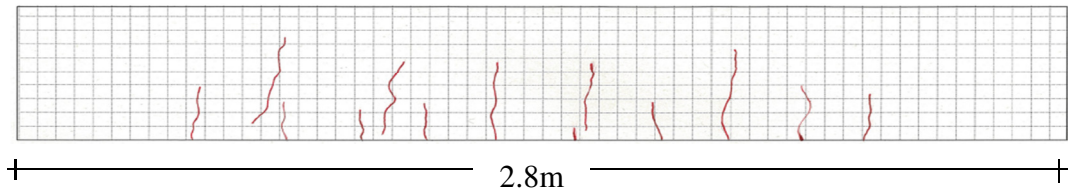


Fig. E.32 Crack pattern at the end of loading of 300kN

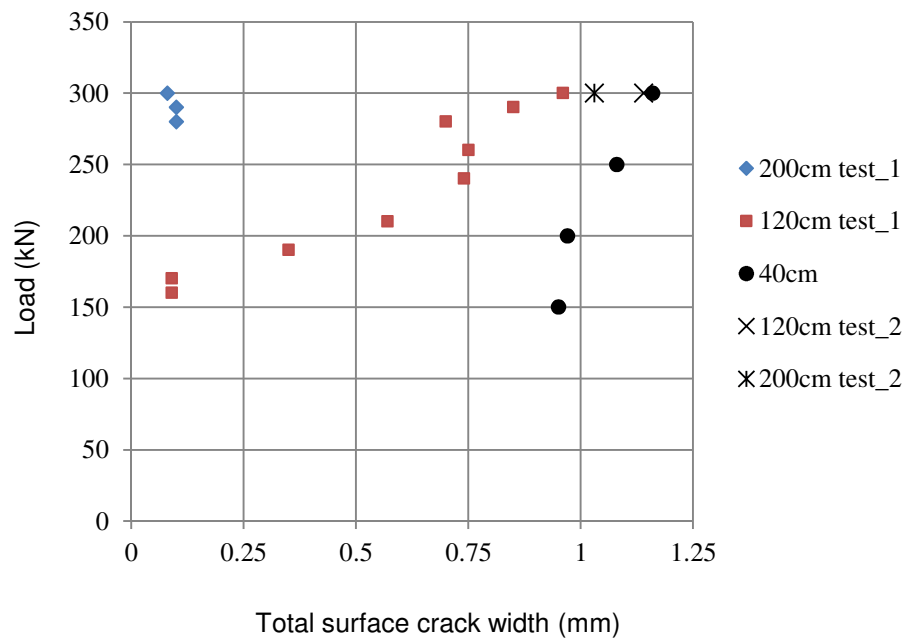


Fig. E.33 Total surface crack width

E.6 Summary

- Experimental investigation of RC beam specimens by varying the load positions has been conducted.
- The experimental results of RC test beam specimen are used to restore the design values and to verify the proposed design restoration method.

APPENDIX F – DESIGN RESTORATION FLOW FOR PRACTICAL APPLICATION

The design restoration flow for practical application is shown in **Fig. F.1**. To apply the proposed method to actual structures, the following steps should be followed.

1. Measure deflection of the bridge, Δ_{1i} , due to the applied load, P_1 , at location x_1 .
2. For other load positions (x_2, x_3, \dots, x_n), repeat step 1 to get $\Delta_{2i}, \Delta_{3i}, \dots, \Delta_{ni}$.
 - i is the number of tests to be repeated at a particular load and position.
3. From each set of data determine the unknown parameters.
4. Repeat steps 1-3 for n times (20-30)
5. Compute mean and confidence intervals.

The computation to determine the unknown parameters will be done by, for example, the nonlinear regression analysis program. The number of repeating the steps 1-3 may vary depending on the bridge condition to get sufficiently accurate design restoration results.

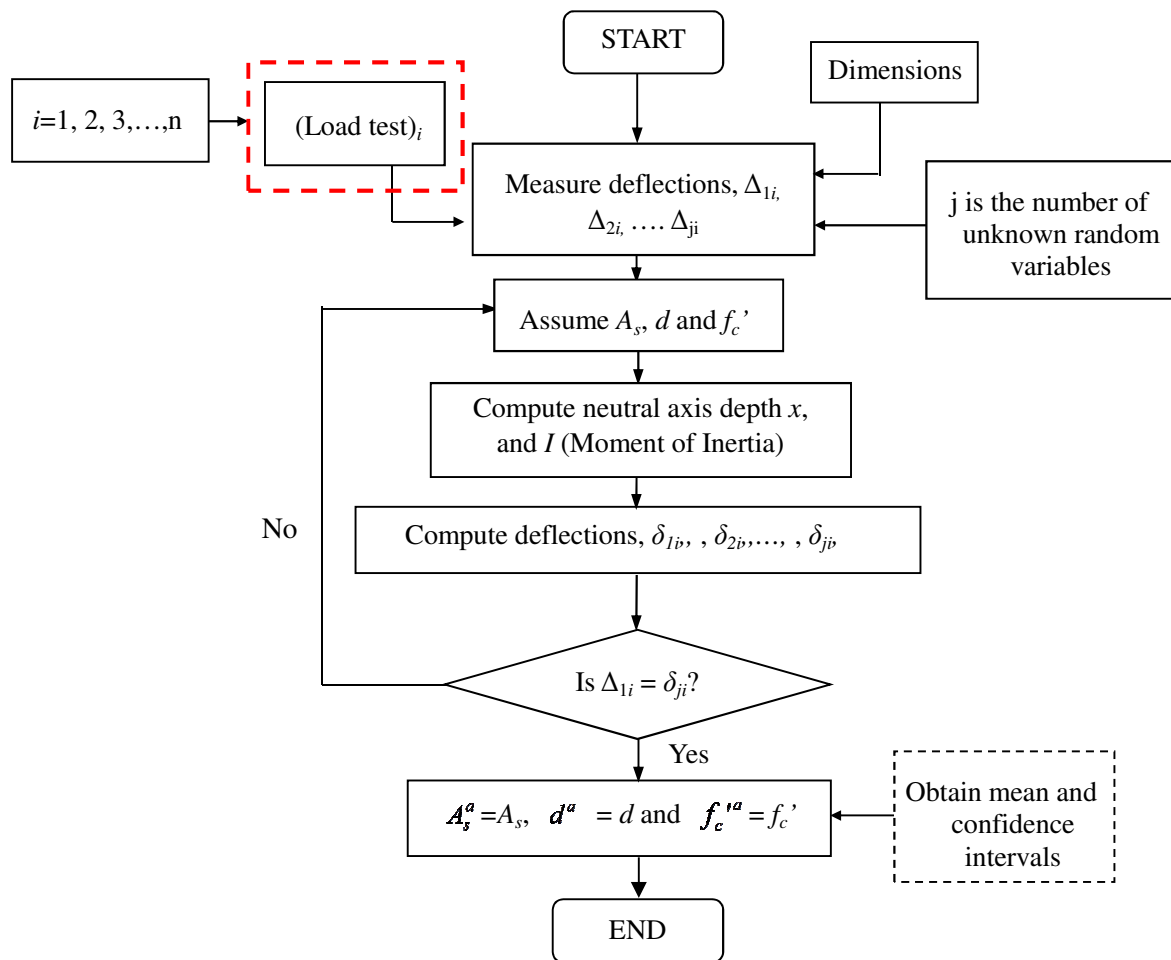


Fig. F.1 Design restoration flow for practical application